Subscription Rates for 2003 Calendar Year: Volume 24

Vol. 24, No. 3 2003

Table of Contents

Publisher's Editorial

Secondary–Undergraduate Articulation: Moving Forward

Solomon A. Garfunkel
Executive Director
COMAP, Inc.
57 Bedford St., Suite 210
Lexington, MA 02420
s.garfunkel@mail.comap.com

The Calls to Change

Several publications in the late 1980s and early 1990s stimulated significant activity aimed at improving mathematics education:

- The National Council of Teachers of Mathematics (NCTM) published the Standards documents for school mathematics (*Curriculum and Evaluation Standards for School Mathematics*, the *Professional Standards for Teaching Mathematics*, the *Assessment Standards for School Mathematics*).

- The Mathematical Association of America (MAA) publication *Calculus for a New Century: A Pump Not a Filter* helped stimulate reform at the undergraduate level in entry-level calculus.

- The Secretary's Commission on Achieving Necessary Skills (SCANS) report *What Work Requires of Schools* suggested that mathematical preparation for success in the workforce extends far beyond basic computation skills.

- Publications such as *Everybody Counts: A Report to the Nation on the Future of Mathematics Education* from the Mathematical Sciences Education Board suggested that large-scale changes would be needed in K–16 mathematics education to prepare our students to meet adequately the challenges of the twenty-first century. Indeed, that publication stresses the need for long-term cooperative effort and planning throughout the school continuum if

we are to meet those needs. "Efforts to change must proceed steadily for many years, on many levels simultaneously, with broad involvement of all constituencies at each stage" (p. 96).

Outlining Specific Changes Needed

Since the late 1980s, there have been multiple efforts to meet the challenges outlined in these and other documents, and we have certainly moved forward. The updated Standards document, the *Principles and Standards for School Mathematics* published in 2000, maintains and clarifies a direction for school mathematics improvement. Among other goals, the objectives of school mathematics include providing the kind of solid foundation students will need

- to be mathematically literate citizens,

- to enter the workplace (broadly determined), or

- to go on to programs of study and professions that use advanced mathematics.

At the post-secondary level, the emerging report from the MAA's Committee on the Undergraduate Program in Mathematics (CUPM) [2003] for two- and four-year colleges and universities is consistent with—and a natural extension of—the Standards vision. It will urge

- giving attention to the educational needs of all students with an updated curriculum and

- providing computational skills, conceptual understanding, and mathematical critical thinking skills.

While earlier CUPM reports focused primarily on the mathematics major, the new report will make broad recommendations for the entire college-level mathematics curriculum, including ones for students taking general education and introductory courses, those majoring in partner disciplines, and those preparing for K–8 teaching.

The original Crossroads document from the American Mathematical Association of Two-Year Colleges (AMATYC), which set standards for college mathematics courses before calculus, and the emerging updated version are in harmony with these documents.

The needs of the business community as reflected in the SCANS report and from other sources are consistent with the directions suggested by NCTM, CUPM, and AMATYC.

The Message Is Strong...

The clear message from policymakers, as reflected in increased accountability measures, mandated testing and other measures of the No Child Left Behind (NCLB) legislation, is:

*We need to raise the mathematical competencies and conceptual understanding of **all** students.*

...But the Medium Is Weak

With the NCTM Standards, new state standards and tests, and the CUPM and Crossroads reports, curricular and pedagogical change continues at both the high school and post-secondary levels. But there is a serious disconnect: the decentralized nature of education in this country, characterized in *Everybody Counts* and in Hiebert and Stigler's *The Teaching Gap* [1999] paradoxically as "no one is in charge—everyone is in charge."

The Dramatic Articulation Disconnect

In contrast to efforts to raise the bar in school mathematics and address the multiple goals in the NCTM vision, the point of view of many of the nation's institutions of higher learning remains fixed on the *belief that the ultimate purpose of pre-college education is to prepare students for calculus*, often reflected in their mathematics placement examinations. So, while the language of the high school documents is mirrored in the emerging CUPM report and similar recommendations, there is still a dramatic articulation problem.

We can no longer tolerate the poor communication and lack of basic understanding between the school and post-secondary mathematics communities. Adding to the problem is the fact that colleges and universities are even more insular and individualistic in developing their mathematics course offerings. Reports such as the one emerging from CUPM seem to carry far less weight in higher education than documents such as the NCTM Standards documents do at the pre-college level.

These problems must be addressed head-on; the emerging of the CUPM report is an ideal time to do so. We feel that it is preferable to deal with articulation issues as the CUPM report is released rather than trying to retrofit solutions later.

What We Don't Know

We need reliable data on a variety of issues:

- How easily do students coming out of reform-based programs move into the undergraduate curricula at both two- and four-year colleges?

- How well do they do?

- Do such students take more mathematics courses, fewer mathematics courses, different (non-major) mathematics courses?

- Can we identify and detail successful transitions? Can we identify real barriers?

There is a different set of articulation questions when we look at the transition from high school to the workplace or to direct workplace-related education programs:

- How well do students perform in the workplace?

- To what extent, for example, do they meet the goals of the SCANS report?

- What do the answers to these questions tell us about changes needed in the college as well as the high school offerings?

A New Role for COMAP

In summary, there is an important research agenda here. We want to do more than document—*we need to facilitate and stimulate articulation* relating to this common vision that bridges secondary and post-secondary education as well as secondary education and the modern workplace. With that in mind, we at COMAP are actively planning to research transitions between high school and college. Similarly, we will look at transitions to workplace environments that epitomize the recommendations of the SCANS report.

Thus, the research focuses on the direction of mathematics education as suggested by the visions of prominent professional organizations involved in the teaching of mathematics, as well as a highly regarded vision of what is needed for success in the workplace. Our study is focused on change and facilitating the implementation of a consistent vision. We cannot afford to have the CUPM report just sit on the shelf. There is too much important work to be done.

References

Assessment Standards Working Group of the National Council of Teachers of Mathematics. 1995. *Assessment Standards for School Mathematics*. Alexandria, VA: National Council of Teachers of Mathematics.

Commission on Standards for School Mathematics of the National Council of Teachers of Mathematics. 1989. *Curriculum and Evaluation Standards for School Mathematics* Alexandria, VA: National Council of Teachers of Mathematics.

Commission on Teaching Standards for School Mathematics of the National Council of Teachers of Mathematics. 1991. *Professional Standards for Teaching Mathematics.* Alexandria, VA: National Council of Teachers of Mathematics.

Committe on the Undergraduate Program in Mathematics of the Mathematical Association of America. 2003. *Undergraduate Programs and Courses in the Mathematical Sciences: A CUPM Curriculum Guide* . Draft 5.2, August 4, 2003. `http://www.maa.org/cupm/` .

Hiebert, James, and James Stigler. 1999. *The Teaching Gap: Best Ideas from the World's Teachers for Improving Education in the Classroom.* Free Press.

Mathematical Sciences Education Board of the National Research Council. 1989. *Everybody Counts: A Report to the Nation on the Future of Mathematics Education.* National Research Council.

National Council of Teachers of Mathematics. 2000. *Principles and Standards for School Mathematics* (with CD-ROM). Alexandria, VA: National Council of Teachers of Mathematics.

Secretary's Commission on Achieving Necessary Skills. 1991. *What Work Requires of Schools: A SCANS Report for America 2000.* DIANE Publishing Co.

Steen, Lynn (ed.). 1987. *Calculus for a New Century: A Pump Not a Filter.* Washington, DC: Mathematical Association of America.

Thompson, Helen M., Susan A. Henley, and Daniel D. Barron. 2000. *Fostering Information Literacy: Connecting National Standards, Goals 2000, and the SCANS Report.* Libraries Unlimited.

Writing Team and Task Force of the Standards for Introductory College Mathematics Project (Don Cohen (ed.)). 1995. *Crossroads in Mathematics: Standards for Introductory College Mathematics Before Calculus.* `http://www.imacc.org/standards/`. Executive summary at `http://www.amatyc.org/Crossroads/CrsrdsXS.html` . Memphis, TN: American Mathematical Association of Two-Year Colleges.

About the Author

Sol Garfunkel received his Ph.D. in mathematical logic from the University of Wisconsin in 1967. He was at Cornell University and at the University of Connecticut at Storrs for 11 years and has dedicated the last 25 years to research and development efforts in mathematics education. He has been the Executive Director of COMAP since its inception in 1980.

He has directed a wide variety of projects, including UMAP (Undergraduate Mathematics and Its Applications Project), which led to the founding of this *Journal*, and HiMAP (High School Mathematics and Its Applications Project), both funded by the NSF. For Annenberg/CPB, he directed three telecourse projects: *For All Practical Purposes* (in which he also appeared as the on-camera host), *Against All Odds: Inside Statistics* (still showing on late-night TV in New York!), and *In Simplest Terms: College Algebra*. He is currently co-director of the Applications Reform in Secondary Education (ARISE) project, a comprehensive curriculum development project for secondary school mathematics.

Modeling Forum

Results of the 2003 Mathematical Contest in Modeling

Frank Giordano, MCM Director
Naval Postgraduate School
1 University Circle
Monterey, CA 93943-5000
frgiorda@nps.navy.mil

Introduction

A total of 492 teams of undergraduates, from 230 institutions in 9 countries—and from varying departments, including an Art Education Center—spent the second weekend in February working on applied mathematics problems in the 18th Mathematical Contest in Modeling (MCM).

The 2003 MCM began at 8:00 P.M. EST on Thursday, Feb. 6 and ended at 8:00 P.M. EST on Monday, Feb. 10. During that time, teams of up to three undergraduates were to research and submit an optimal solution for one of two open-ended modeling problems. Students registered, obtained contest materials, downloaded the problems at the appropriate time, and entered completion data through COMAP'S MCM Website.

Each team had to choose one of the two contest problems. After a weekend of hard work, solution papers were sent to COMAP on Monday. Eleven of the top papers appear in this issue of *The UMAP Journal*.

Results and winning papers from the first sixteen contests were published in special issues of *Mathematical Modeling* (1985–1987) and *The UMAP Journal* (1985–2002). The 1994 volume of *Tools for Teaching*, commemorating the tenth anniversary of the contest, contains all of the 20 problems used in the first ten years of the contest and a winning paper for each. Limited quantities of that volume and of the special MCM issues of the *Journal* for the last few years are available from COMAP.

This year's Problem A teams were asked to determine the size, location, and number of cardboard boxes needed to cushion a stunt person's fall using

different combined weights (stunt person and motorcycle) and different jump heights.

Problem B dealt with the use of a gamma knife in the treatment of tumor cells in brain tissue. Teams were asked to design a model to provide the fewest and most direct doses in order to treat the tumor without going outside the target tumor itself.

In addition to the MCM, COMAP also sponsors the Interdisciplinary Contest in Modeling (ICM) and the High School Mathematical Contest in Modeling (HiMCM). The ICM, which runs concurrently with MCM, offers a modeling problem involving concepts in operations research, information science, and interdisciplinary issues in security and safety. Results of this year's ICM are on the COMAP Website at `http://www.comap.com/undergraduate/contests`; results and Outstanding papers appeared in Vol. 24 (2003), No. 2. The HiMCM offers high school students a modeling opportunity similar to the MCM. Further details about the HiMCM are at `http://www.comap.com/highschool/contests`.

Problem A: The Stunt Person

An exciting action scene in a movie is going to be filmed, and you are the stunt coordinator! A stunt person on a motorcycle will jump over an elephant and land in a pile of cardboard boxes to cushion their fall. You need to protect the stunt person, and also use relatively few cardboard boxes (lower cost, not seen by camera, etc.).

Your job is to:

- determine what size boxes to use,

- determine how many boxes to use,

- determine how the boxes will be stacked,

- determine if any modifications to the boxes would help, and

- generalize to different combined weights (stunt person and motorcycle) and different jump heights.

Note that in the 1997 film "Tomorrow Never Dies," the James Bond character, on a motorcycle, jumps over a helicopter.

Problem B: Gamma Knife Treatment Planning

Stereotactic radiosurgery delivers a single high dose of ionizing radiation to a radiographically well-defined, small intracranial 3D brain tumor without

delivering any significant fraction of the prescribed dose to the surrounding brain tissue. Three modalities are commonly used in this area; they are the gamma knife unit, heavy charged particle beams, and external high-energy photon beams from linear accelerators.

The gamma knife unit delivers a single high dose of ionizing radiation emanating from 201 cobalt-60 unit sources through a heavy helmet. All 201 beams simultaneously intersect at the isocenter, resulting in a spherical (approximately) dose distribution at the effective dose levels. Irradiating the isocenter to deliver dose is termed a "shot." Shots can be represented as different spheres. Four interchangeable outer collimator helmets with beam-channel diameters of 4, 8, 14, and 18 mm are available for irradiating different size volumes. For a target volume larger than one shot, multiple shots can be used to cover the entire target. In practice, most target volumes are treated with 1 to 15 shots. The target volume is a bounded, three-dimensional digital image that usually consists of millions of points.

The goal of radiosurgery is to deplete tumor cells while preserving normal structures. Since there are physical limitations and biological uncertainties involved in this therapy process, a treatment plan needs to account for all those limitations and uncertainties. In general, an optimal treatment plan is designed to meet the following requirements.

1. Minimize the dose gradient across the target volume.

2. Match specified isodose contours to the target volumes.

3. Match specified dose-volume constraints of the target and critical organ.

4. Minimize the integral dose to the entire volume of normal tissues or organs.

5. Constrain dose to specified normal tissue points below tolerance doses.

6. Minimize the maximum dose to critical volumes.

   In gamma unit treatment planning, we have the following constraints:

1. Prohibit shots from protruding outside the target.

2. Prohibit shots from overlapping (to avoid hot spots).

3. Cover the target volume with effective dosage as much as possible. But at least 90% of the target volume must be covered by shots.

4. Use as few shots as possible.

Your tasks are to formulate the optimal treatment planning for a gamma knife unit as a sphere-packing problem, and propose an algorithm to find a solution. While designing your algorithm, you must keep in mind that your algorithm must be reasonably efficient.

The Results

The solution papers were coded at COMAP headquarters so that names and affiliations of the authors would be unknown to the judges. Each paper was then read preliminarily by two "triage" judges at either Appalachian State University (Problem A) or at the National Security Agency (Problem B). At the triage stage, the summary and overall organization are the basis for judging a paper. If the judges' scores diverged for a paper, the judges conferred; if they still did not agree on a score, a third judge evaluated the paper.

This year, an additional Regional Judging site was created at the U.S. Military Academy to support the growing number of contest submissions.

Final judging took place at Harvey Mudd College, Claremont, California. The judges classified the papers as follows:

	Outstanding	Meritorious	Honorable Mention	Successful Participation	Total
Stunt Person	6	36	97	128	267
Gamma Knife Treatment	5	34	56	130	225
	11	70	153	258	492

The 11 papers that the judges designated as Outstanding appear in this special issue of *The UMAP Journal*, together with commentaries. We list those teams and the Meritorious teams (and advisors) below; the list of all participating schools, advisors, and results is in the **Appendix**.

Outstanding Teams

Institution and Advisor   **Team Members**

Stunt Person Papers

"Safe Landings"
California Institute of Technology   Chad T. Kishimoto
Pasadena, CA   Justin C. Kao
Darryl H. Yong   Jeffrey A. Edlund

"A Time-Independent Model of Box Safety
      for Stunt Motorcyclists"
Harvard University   Ivan Corwin
Cambridge, MA   Sheel Ganatra
Clifford H. Taubes   Nikita Rozenblyum

"Thinking Outside the Box
    and Over the Elephant"

Harvey Mudd College   Melissa J. Banister

Claremont, CA   Matthew Macauley

Jon Jacobsen   Micah J. Smukler

"You Too Can Be James Bond"

Southeast University   Deng Xiaowei

Nanjing, China   Xu Wei

Chen Enshui   Zhang Zhenyu

"Cardboard Comfortable When It Comes
    to Crashing"

University of Washington   Jeffrey Giansiracusa

Seattle, WA   Ernie Esser

James Allen Morrow   Simon Pai

"Fly With Confidence"

Zhejiang University   Hu Yuxiao

Hangzhou, China   Hua Zheng

Tan Zhiyi   Zhou Enlu

Gamma Knife Treatment Papers

"The Genetic Algorithm-Based Optimization
    Approach for Gamma Unit Treatment"

Donghua University   Sun Fei

Shanghai, China   Yang Lin

Ding Yongsheng   Wang Hong

"A Sphere-Packing Model for the
    Optimal Treatment Plan"

Peking University   Long Yun

Beijing, China   Ye Yungqing

Liu Xufeng   Wei Zhen

"The Gamma Knife Problem"

University of Colorado   Darin W. Gillis

Boulder, CO   David R. Lindstone

Anne M. Dougherty   Aaron T. Windfield

"Shelling Tumors with Caution and Wiggles"
University of Washington   Luke Winstrom
Seattle, WA   Sam Coskey
James Allen Morrow   Mark Blunk

"Fly With Confidence"
Youngstown State University   Sarah Grove
Youngstown, OH   Chris Jones
Angela Spalsbury   Joel Lepak

Meritorious Teams

Stunt Person Papers (36 teams)
Asbury College, Wilmore, KY (Ken Rietz)
California Polytechnic State University, San Luis Obispo, CA (Jonathan E. Shapiro)
Central Washington University, Ellensburg, WA (Stuart F. Boersma)
City Univ. of Hong Kong, China (Jonathan J. Wylie)
Duke University, Durham, NC (David Kraines)
Earlham College, Richmond, IN (Charlie Peck) (two teams)
Harvey Mudd College, Claremont, CA (Ran Libeskind-Hadas) (two teams)
James Madison University, Harrisonburg, VA (Joseph W. Rudmin)
Kansas State University, Manhattan, KS (Dave Auckly, Mikil Foss, and Marianne Korten)
Luther College, Decorah, IA (Reginald D. Laursen)
Maggie Walker Governor's School, Richmond, VA (John, A. Barnes)
Massachusetts Institute of Technology, Cambridge, MA (Martin Z. Bazant)
Mesa State College, Grand Junction, Colorado (Edward K. Bonan-Hamada)
Messiah College, Grantham, PA (Lamarr C. Widmer)
N.C. School of Science and Mathematics, Durham, NC (Dot Doyle)
National University of Defence Technology, China (Ziyang Mao)
Rose-Hulman Institute of Technology, Terre Haute, IN (David J. Rader)
Southeastern Oklahoma State University, Durant, OK (Brett M. Elliott)
Southern Oregon University, Ashland, OR (Kemble R. Yates)
State University of West Georgia, Carrollton, Georgia (Scott Gordon)
Tri-State University, Angola, IN (Steven A. Schonefeld)
Truman State University, Kirksville, MO (Steve J. Smith)
United States Air Force Academy, USAF Academy, CO (James S. Rolf)
United States Military Academy, West Point, NY (Frank A. Wattenberg)
University College Cork, Ireland (James Gleeson)
University College Cork, Ireland (Donal J. Hurley)
University of Alaska Fairbanks, Fairbanks, AK (Chris M. Hartman)
University of New South Wales, Sydney, Australia (James W. Franklin)
University of Puget Sound, Tacoma, WA (Michael S. Casey)
University of San Diego, San Diego, CA (Jeffrey H. Wright)
University of Science and Technology of China, China (Li Yu)

Worcester Polytechnic Institute, Worcester, MA (Suzanne L. Weekes)
Xidian University, China (Zhou Shui-Sheng)
York University, Toronto, Ontario, Canada (Huaxiong Huang)

Gamma Knife Treatment Papers (34 teams)
Bethel College, St. Paul, MN (William, M, Kinney) (two teams)
Boston University, Boston, MA (Glen, R, Hall)
California Polytechnic State University, San Luis Obispo, CA (Jonathan E. Shapiro)
Dalhousie University, Canada (Dorothea A. Pronk)
Hangzhou University of Commerce, China (Ding Zhengzhong)
Harvey Mudd College, Claremont, CA (Jon Jacobsen)
Hong Kong Baptist University, China (Chong-Sze Tong)
Kenyon College, Gambier, OH (Keith E. Howard)
Lawrence Technological University, Southfield, MI (Ruth G. Favro)
Northwestern Polytechnical University, China (Peng Guohua)
Rensselaer Polytechnic Institute, Troy, NY (Peter R. Kramer)
Rowan University, Glassboro, NJ (Hieu D. Nguyen)
Saint Louis University, St. Louis, MO (James E. Dowdy)
Science Institution of Northeastern University, China (Sun Ping)
Shanghai Jiaotong University, China (Baorui Song)
Shanghai Jiaotong University, China (Jianguo Huang)
Simpson College, Indianola, Iowa (Werner Kolln)
South China University of Technology, China (Jianliang Lin)
Southeast Missouri State University, Cape Girardeau, MO (Robert W. Sheets)
Tianjin University, China (Zeyi Liu)
Trinity University, San Antonio, TX (Robert W. Laird)
Tsinghua University, China (Jun Ye)
University College Dublin (Maria G. Meehan)
University of Arizona, Tucson, AZ (Bruce J. Bayly)
University of Colorado at Boulder, Boulder, CO (Anne M. Dougherty)
University of Delaware, Newark, DE (Louis F. Rossi)
University of Richmond, Richmond, VA (Kathy W. Hoke)
University of Saskatchewan, Canada (Rainer Dick)
University of Saskatchewan, Canada (James A. Brooke)
Washington University, St. Louis, MO (Hiro Mukai)
Westminster College, New Wilmington, PA (Barbara T. Faires)
Wuhan University of Technology, China (Peng Sijun)
Xidian University, China (Zhang Zhuo-kui)

Awards and Contributions

Each participating MCM advisor and team member received a certificate signed by the Contest Director and the appropriate Head Judge.

INFORMS, the Institute for Operations Research and the Management Sciences, recognized the teams from Zhejiang University (Stunt Person Problem)

and University of Washington (Gamma Knife Treatment Problem) as INFORMS Outstanding teams and provided the following recognition:

- a letter of congratulations from the current president of INFORMS to each team member and to the faculty advisor;

- a check in the amount of $300 to each team member;

- a bronze plaque for display at the team's institution, commemorating their achievement;

- individual certificates for team members and faculty advisor as a personal commemoration of this achievement;

- a one-year student membership in INFORMS for each team member, which includes their choice of a professional journal plus the *OR/MS Today* periodical and the INFORMS society newsletter.

- a one-year subscription access to the COMAP modeling materials Website for the faculty advisor.

The Society for Industrial and Applied Mathematics (SIAM) designated one Outstanding team from each problem as a SIAM Winner. The teams were from Calfiornia Institute of Technology (Stunt Person Problem) and University of Colorado (Gamma Knife Treatment Problem). Each of the team members was awarded a $300 cash prize and the teams received partial expenses to present their results in a special Minisymposium at the SIAM Annual Meeting in Montreal, Canada in June. Their schools were given a framed, hand-lettered certificate in gold leaf.

The Mathematical Association of America (MAA) designated one Outstanding team from each problem as an MAA Winner. The teams were from University of Washington (Stunt Person Problem) and Youngstown State University (Gamma Knife Treatment Problem). With partial travel support from the MAA, both teams presented their solutions at a special session of the MAA Mathfest in Boulder, CO in August. Each team member was presented a certificate by Richard S. Neal, Co-Chair of the MAA Committee on Undergraduate Student Activities and Chapters.

Judging

Director
Frank R. Giordano, Naval Postgraduate School, Monterey, CA

Associate Directors
Robert L. Borrelli, Mathematics Dept., Harvey Mudd College, Claremont, CA
Patrick Driscoll, Dept. of Mathematical Sciences, U.S. Military Academy,
    West Point, NY

Contest Coordinator
Kevin Darcy, COMAP Inc., Lexington, MA

Stunt Person Problem

Head Judge
Marvin S. Keener, Executive Vice-President, Oklahoma State University,
    Stillwater, OK (MAA)

Associate Judges
William C. Bauldry, Chair, Dept. of Mathematical Sciences,
        Appalachian State University, Boone, NC (Triage)
Kelly Black, Mathematics Dept., University of New Hampshire,
    Durham, NH (SIAM)
Courtney Coleman, Mathematics Dept., Harvey Mudd College,
    Claremont, CA
Lisette De Pillis, Mathematics Dept., Harvey Mudd College, Claremont, CA
Ben Fusaro, Mathematics Dept., Florida State University,
    Tallahassee, FL (SIAM)
Mario Juncosa, RAND Corporation, Santa Monica, CA
Michael Moody, Mathematics Dept., Harvey Mudd College, Claremont, CA
John L. Scharf, Mathematics Dept., Carroll College, Helena, MT
    (COMAP HiMCM)
Dan Solow, Mathematics Dept., Case Western Reserve University,
    Cleveland, OH (INFORMS)
Michael Tortorella, Lucent Technologies, Holmdel, NJ
Daniel Zwillinger, Newton, MA (author)

Gamma Knife Treatment Problem

Head Judge
Maynard Thompson, Mathematics Dept., University of Indiana,
    Bloomington, IN

Associate Judges
Peter Anspach, National Security Agency, Ft. Meade, MD (Triage)
Karen D. Bolinger, Mathematics Dept., Ohio State University, Columbus, OH
James Case, Baltimore, MD (SIAM)
J. Douglas Faires, Youngstown State University, Youngstown, OH (MAA)
William P. Fox, Mathematics Dept., Francis Marion University, Florence, SC
    (MAA)
Jerry Griggs, Mathematics Dept., University of South Carolina, Columbia, SC
    (author rep)
John Kobza, Mathematics Dept., Texas Tech University, Lubbock, TX
    (INFORMS)
Veena Mendiratta, Lucent Technologies, Naperville, IL
Don Miller, Mathematics Dept., St. Mary's College, Notre Dame, IN (SIAM)

Kathleen Shannon, Mathematics Dept., Salisbury State University,
    Salisbury, MD
Marie Vanisko, Dept. of Mathematics, Engineering, Physics, and
    Computer Science, Carroll College, Helena, MT (MAA)

Regional Judging Session

Head Judge
Patrick Driscoll, Dept. of Mathematical Sciences

Associate Judges
Edward Pohl, Dept. of Systems Engineering
Michael Jaye, Dept. of Mathematical Sciences
Darrall Henderson, Dept. of Mathematical Sciences
Steven Horton, Dept. of Mathematical Sciences
                    —all of the U.S. Military Academy, West Point, NY

Triage Sessions:

Stunt Person Problem

Head Triage Judge
William C. Bauldry, Chair, Dept. of Mathematical Sciences,
     Appalachian State University, Boone, NC

Associate Judges
Terry Anderson, Dept. of Mathematical Sciences
Anthony Calamai, Physics Dept.
Mark Ginn, Dept. of Mathematical Sciences
Andrew Graham, Physics Dept.
Rick Klima, Dept. of Mathematical Sciences
                    —all from Appalachian State University, Boone, NC
Dan Warner, Dept. of Mathematical Sciences, Clemson University,
     Clemson, SC
Richard West, Mathematics Dept., Francis Marion University, Florence, SC

Gamma Knife Treatment Problem

Head Triage Judge
Peter Anspach, National Security Agency (NSA), Ft. Meade, MD

Associate Judges
James Case, Baltimore, Maryland
Antonia Bluher, Stuart Gott, Blair Kelly, Dean McCullough (retired), Craig Orr,
    Brian Pilz, and other members of NSA.

Sources of the Problems

The Stunt Person Problem was contributed by Dan Zwillinger, Newton, MA. The Gamma Knife Treatment Problem was contributed by Jie Wang.

Acknowledgments

Cautions

To the reader of research journals:

Usually a published paper has been presented to an audience, shown to colleagues, rewritten, checked by referees, revised, and edited by a journal editor. Each of the student papers here is the result of undergraduates working on a problem over a weekend; allowing substantial revision by the authors could give a false impression of accomplishment. So these papers are essentially au naturel. Editing (and sometimes substantial cutting) has taken place: Minor errors have been corrected, wording has been altered for clarity or economy, and style has been adjusted to that of *The UMAP Journal*. Please peruse these student efforts in that context.

To the potential MCM Advisor:

It might be overpowering to encounter such output from a weekend of work by a small team of undergraduates, but these solution papers are highly atypical. A team that prepares and participates will have an enriching learning experience, independent of what any other team does.

COMAP's Mathematical Contest in Modeling and Interdisciplinary Contest in Modeling are the only international modeling contests in which students work in teams. Centering its educational philosophy on mathematical modeling, COMAP uses mathematical tools to explore real-world problems. It serves the educational community as well as the world of work by preparing students to become better-informed and better-prepared citizens.

Appendix: Successful Participants

KEY:

P = Successful Participation   A = Stunt Person Problem

H = Honorable Mention   B = Gamma Knife Treatment Problem

M = Meritorious

O = Outstanding (published in this special issue)

INSTITUTION	CITY	ADVISOR	A	B
ALASKA				
University of Alaska	Fairbanks	Chris M. Hartman	M	
ARKANSAS				
Arkansas Schl for Math. & Sci.	Hot Springs	Bruce E. Turkal	H,P	
Hendrix College	Conway	Duff Gordon Campbell		P
CALIFORNIA				
California Institute of Tech.	Pasadena	Darryl H. Yong	O	
California Polytech. State Univ.	San Luis Obispo	Jonathan E. Shapiro	M	M
Calif. State Univ., Monterey Bay	Seaside	Hongde Hu	H	
Calif. State Univ., Bakersfield	Bakersfield	David Gove	H	
Calif. State Univ., Northridge	Northridge	Gholam Ali Zakeri	H,P	
Calif. State Univ., Stanislaus	Turlock	Brian Jue	P	
Harvey Mudd College	Claremont	Jon Jacobsen	O	M
		Ran Libeskind-Hadas	M,M	
Monta Vista High School	Cupertino	I-Heng McComb	H,P	
Pomona College	Claremont	Ami E. Radunskaya		P
Sonoma State University	Rohnert Park	Elaine T. McDonald	P	
University of San Diego	San Diego	Jeffrey H. Wright	M,P	
COLORADO				
Colorado College	Colorado Springs	Peter L. Staab	H	P
Colorado State University	Fort Collins	Michael J. Kirby		P
	Pueblo	Bruce N. Lundberg	P	
U.S. Air Force Academy	USAF Academy	James S. Rolf	M	
University of Colorado	Boulder	Anne M. Dougherty		O,M
Mesa State College	Grand Junction	Edward K. Bonan-Hamada	M	
CONNECTICUT				
Sacred Heart University	Fairfield	Peter Loth	H	
Western Conn. State Univ.	Danbury	Charles F. Rocca jr	P	
DELAWARE				
University of Delaware	Newark	Louis F. Rossi	H	M
DISTRICT OF COLUMBIA				
Georgetown University	Washington	Andrew Vogt	P	
FLORIDA				
Embry-Riddle Aeronaut. Univ.	Daytona Beach	Greg Scott Spradlin	H	
Florida Gulf Coast University	Fort Myers	Charles Lindsey		H
Jacksonville University	Jacksonville	Paul R. Simony	H,P	

INSTITUTION	CITY	ADVISOR	A	B
ILLINOIS				
Greenville College	Greenville	Galen R. Peters	H	P
		Hugh E. Siefken	P	
Monmouh College	Monmouth	Christopher G. Fasano	P	
Wheaton College	Wheaton	Paul Isihara		P
INDIANA				
Earlham College	Richmond	Timothy J. McLarnan		P
		Charlie Peck	M,M	
		Jennifer Joy Ziebarth		H
Goshen College	Goshen	David Housman	H	
Rose-Hulman Inst. of Tech.	Terre Haute	David J. Rader	M	P
		Cary Laxer		P
Saint Mary's College	Notre Dame	Joanne R. Snow	H	P
Tri-State University	Angola	Steven Schonefeld	M	
IOWA				
Grand View College	Des Moines	Sergio Loch	P,P	
Grinnell College	Grinnell	Alan R. Wolf	P,P	
		Mark Montgomery		H,P
Luther College	Decorah	Reginald D. Laursen	M,H	
Simpson College	Indianola	Bruce F. Sloan	H	P
		Werner Kolln		M
Wartburg College	Waverly	Mariah Birgen	H	
KANSAS				
Kansas State University	Manhattan	Dave Auckly, Mikil Foss,		
		and Marianne Korten	M	P
KENTUCKY				
Asbury College	Wilmore	Ken Rietz	M	P
Bellarmine University	Louisville,	William J. Hardin	H	
Northern Kentucky Univ.	Highland Heights	Gail S. Mackin		H
MAINE				
Colby College	Waterville	Jan Holly	H,P	
MARYLAND				
Goucher College	Baltimore	Robert E. Lewand	H,P	
Hood College	Frederick	Betty Mayfield		P
Loyola College	Baltimore	Christos Xenophontos	H,H	
Mount St. Mary's College	Emmitsburg	Fred J. Portier	H,P	
Salisbury University	Salisbury	Steven M. Hetzler	H	
Towson University	Towson	Mike P. O'Leary	H,P	
Washington College	Chestertown	Eugene P. Hamilton	P,P	
MASSACHUSETTS				
Boston University	Boston	Glen R. Hall	H	M
Harvard University	Cambridge	Clifford H. Taubes	O	
Massachusetts Inst. of Tech.	Cambridge	Martin Z. Bazant	M	
Olin College of Engineering	Needham	Burt S. Tilley		P

INSTITUTION	CITY	ADVISOR	A	B
MICHIGAN				
Calvin College	Grand Rapids	Gary W. Talsma	P	
Eastern Michigan University	Ypsilanti	Christopher E. Hee	P	P
Hillsdale College	Hillsdale	John P. Boardman	H	
Hope College	Holland	Aaron C. Cinzori	P	
Lawrence Tech. Univ.	Southfield	Ruth G. Favro	H	M
		Valentina Tobos	P	
Siena Heights University	Adrian	Toni Carroll	H,P	
		Timothy H. Husband	P	
University of Michigan	Dearborn	David James		P
MINNESOTA				
Augsburg College	Minneapolis	Nicholas Coult		P
Bemidji State University	Bemidji	Colleen G. Livingston	P	H
Bethel College	St. Paul	William M, Kinney		M,M
College of St. Benedict and St. John's University	Collegeville	Robert J. Hesse	H,P	
Gustavus Adolphus College	St. Peter	Thomas P. LoFaro	H	
Macalester College	St. Paul	Daniel T. Kaplan	H	P
		Elizabeth G. Shoop		P
MISSOURI				
NW Missouri State Univ.	Maryville	Russell N. Euler	P,P	
Saint Louis University	St. Louis	David Jackson	P	
		Stephen Blythe	H	
		James E. Dowdy		M
SE Missouri State Univ.	Cape Girardeau	Robert W. Sheets		M
Truman State University	Kirksville	Steve J. Smith	M,H	
Washington University	St. Louis	Hiro Mukai		M,H
MONTANA				
Carroll College	Helena	Holly S. Zullo	H	
NEBRASKA				
Hastings College	Hastings	David Cooke	H,H	
NEVADA				
Sierra Nevada College	Incline Village	Charles Levitan	P	
NEW JERSEY				
Rowan University	Glassboro	Hieu D. Nguyen		M
William Paterson Univ.	Wayne	Donna J. Cedio-Fengya	P	
NEW MEXICO				
New Mexico State Univ.	Las Cruces	Caroline P. Sweezy		P
NEW YORK				
Cornell University	Ithaca	Alexander Vladimirsky	H	
Hobart & William Smith Coll.	Geneva	Scotty L. Orr	H,P	
Manhattan College	Riverdale	Kathryn W. Weld		P
Marist College	Poughkeepsie	Tracey McGrail	P	
Nazareth College	Rochester	Nelson G. Rich	H	
Rensselaer Polytechnic Inst.	Troy	Peter R. Kramer		M,H

INSTITUTION	CITY	ADVISOR	A	B
NORTH CAROLINA				
Appalachian State University	Boone	Eric S. Marland		P
Brevard College	Brevard	C. Clarke Wellborn	P	
Davidson College	Davidson	Laurie J. Heyer	H	H
Duke University	Durham	David Kraines	M	
Elon University	Elon	Todd Lee		H
Meredith College	Raleigh	Cammey E. Cole	P	
N.C. School of Sci. and Math.	Durham	Dot Doyle	M	
North Carolina State Univ.	Raleigh	Jeffrey S. Scroggs		P
OHIO				
Kenyon College	Gambier	Keith E. Howard		M
Miami University	Oxford	Stephen E. Wright		P
Mount Vernon Nazarene Univ.	Mount Vernon	John T. Noonan	H	
Wright State University	Dayton	Thomas P. Svobodny	P	
Youngstown State University	Youngstown	Angela Spalsbury	H	O
		Michael Crescimanno	H	
		Scott Martin		P
Xavier University	Cincinnati	Michael Goldweber	H	
OKLAHOMA				
Southeastern Okla. State Univ.	Durant	Brett M. Elliott	M	
OREGON				
Eastern Oregon University	La Grande	Anthony Tovar	H	
Lewis and Clark College	Portland	Robert W. Owens	H	H
		Thomas Olsen		P
Southern Oregon University	Ashland	Kemble R. Yates	M	
PENNSYLVANIA				
Bloomsburg University	Bloomsburg	Kevin K. Ferland		P
Bucknell University	Lewisburg	Sally Koutsoliotas		P
Clarion Univ. of Pennsylvania	Clarion	Paul G. Ashcraft	P,P	
		Steve I. Gendler	P	
Gettysburg College	Gettysburg	James P. Fink and		
		Sharon Stephenson	H	
Juniata College	Huntingdon	John F. Bukowski		P
Lafayette College	Easton	Thomas Hill	H	
Messiah College	Grantham	Lamarr C. Widmer	M	
University of Pittsburgh	Pittsburgh	Jonathan E. Rubin		H
Westminster College	New Wilmington	Barbara T. Faires	H	M
SOUTH CAROLINA				
Benedict College	Columbia	Balaji S. Iyangar	P	
Francis Marion University	Florence	Thomas Fitzkee	P	
SOUTH DAKOTA				
Mount Marty College	Yankton	Jim Miner	P,P	
		Shane K. Miner		P
SD School of Mines and Tech.	Rapid City	Kyle Riley	P	H

INSTITUTION	CITY	ADVISOR	A	B
VERMONT				
Johnson State College	Johnson	Glenn D. Sproul	P	
VIRGINIA				
Chesterfield County				
Math. and Sci. HS	Midlothian	Zorica Skoro	H	
Eastern Mennonite University	Harrisonburg	John L. Horst	P	P
		Charles D. Cooley		P
James Madison University	Harrisonburg	Dorn W. Peterson	H	
		Joseph W. Rudmin	M	
Maggie Walker Governor's Schl	Richmond	John A. Barnes	M	P
Mills E. Godwin High School	Richmond	Ann W. Sebrell	P	
Randolph-Macon College	Ashland	Bruce F. Torrence	H,P	
Roanoke College	Salem	Jeffrey L. Spielman		H
		Roland Minton		P
University of Richmond	Richmond	Kathy W. Hoke		M
U. of Virginia's College at Wise	Wise	George W. Moss	P	
Virginia Western	Roanoke	Ruth Sherman	H	
		Dawn Reinhard	H	
WASHINGTON				
Central Washington Univ.	Ellensburg	Stuart F. Boersma	M	
Gonzaga University	Spokane	Thomas M. McKenzie	P	
Heritage College	Toppenish	Richard W. Swearingen	P	P
Pacific Lutheran Uinversity	Tacoma	Mei Zhu	H,H	
University of Puget Sound	Tacoma	Michael S. Casey	M,P	
		John E. Riegsecker	H	
University of Washington	Seattle	James Allen Morrow	O	O
Western Washington Univ.	Bellingham	Tjalling J. Ypma	H,H	
		Saim Ural	H	
WISCONSIN				
Beloit College	Beloit	Paul J. Campbell	P	
Edgewood College	Madison	Steven Post	H	
St. Norbert College	De Pere	John Frohliger	H	
University of Wisconsin	River Falls	Kathy Tomlinson	H,H	
AUSTRALIA				
Univ. of New South Wales	Sydney	James W. Franklin	M	H
CANADA				
Dalhousie University	Halifax, NS	Dorothea Pronk		M
University of Western Ontario	London, ON	Martin H. Muser	H	
University of Saskatchewan	Saskatoon, SK	Rainer Dick		M
		James Brooke		M
York University	Toronto, ON	Huaxiong Huang	M	H
CHINA				
Anhui University	Hefei	Zhang Quanbing	P	H
BeiHang University	Beijing	Liu Hongying	H	
Beijing Institute of Technology	Beijing	Zhang Bao Xue	P	
		Cui Xiao Di		P

INSTITUTION	CITY	ADVISOR	A	B
Beijing Univ. of Chemical Tech.	Beijing	Yuan Wenyan	H	
		Shi Xiaoding	P	
		Jiang Guangfeng	P	
		Cheng Yan		P
Beijing Univ. of Posts and Tel.	Beijing	He Zuguo		H
		Sun Hongxiang		H
		Wang Xiaoxia		P
		Luo Shoushan	H	
Beijing Univ. of Technology	Beijing	Yi Xue		P
		Gao Luduan	H,P	
Central South University	Changsha	Chen Xiaosong		H
		Zheng Zhoushun	P,P	
		Qin Xuanyun		H
China Univ. of Mining Tech.	Xuzhou	Zhang Xingyong		P
		Zhou Shengwu		P
		Wu Zongxiang		P
Chongqing University	Chongqing	Shu Yonglu	P	
		Yang Dadi	P	
		Gong Qu		H
		Duan Zhengmin		H
		Zhang Xingyou		H
Dalian University	Dalian	Tan Xinxin	P	H
Dalian Univ. of Tech.	Dalian	He Mingfeng		P,P
		Wang Yi		P
		Zhao Lizhong		P
Dong Hua University	Shanghai	Ding Yongsheng		O
		Feng Yili		P
		He Guoxing		H
		You Surong		H
East China U. of Sci. and Tech.	Shanghai	Su Chunjie		P,P
		Lu Yuanhong	H,P	
Fudan University	Shanghai	Cai Zhijie		H
		Cao Yuan		P
Guangxi University	Nannng	Lu Yuejin	P	P
		Huang Xinming	P	
Hangzhou Univ. of Commerce	Hangzhou	Ding Zhengzhong	P	M
		Zhao Heng		P,P
Harbin Engineering Univ.	Harbin	Zhang Xiaowei	P	P
		Gao Zhenbin	P	
Harbin Institute of Tech.	Harbin	Shang Shouting	H,P	
		Zhang Chiping	P	
		Wang Xuefeng		P
Harbin Univ. of Sci. and Tech.	Harbin	Li Dongmei	H	P
		Tian Guangyue	P	
Hebei University	Baoding	Ma Guodong		P
		Fan TieGang		P
		Hua Qiang		H
		Wang XiZhao	P	

INSTITUTION	CITY	ADVISOR	A	B
Institute of Theoretical Physics	Beijing	Jiang Daquan	H	
Jiamusi University	Jiamusi	Bai Fengshan		P
		Wei Fan	P	
		Gu Lizhi		P
Jilin University	Changchun	Fang Peichen		P,P
		Huang Qingdao		P,P
Jinan University	Guangzhou	Fan Suohai		H
		Ye Shiqi	P	
		Luo Shizhuang	P	
		Hu Daiqiang		P
Nanchang University	Nanchang	Ma Xinsheng		H,P
		Chen Tao	P	
Nanjing Normal University	Nanjing	Fu Shitai		P
		Hu Yong	P	
		Qu Weiguang	P	
		Chen Xin		P
Nanjing University	Nanjing	Wu Zhaoyang		P
		Hao Pan	P	
Nanjing Univ. of Sci. & Tech.	Nanjing	Huang Zhenyou		P
		Wang Pingling		P
		Wu XinMin	P	
		Zhang Zhengjun		P
Nankai University	Tianjin	Huang Wuqun	P,P	
″ , School of Math.	Tianjin	Ruan Jishou		P,P
National U. of Defence Tech.	Changsha	Mao Ziyang	M,P	
		Wu Mengda		H,P
Northeast Agricultural Univ.	Harbin	Li Fangge	P	P
		Hu Xiaobing	P	
Northeastern University	Shenyang	Hao Peifeng		P
		Zhang Shujun		H,P
″ , Info. Sci. and Eng. Inst.	Shenyang	Hao Peifeng	P	
″ , Mechanical Inst.	Shenyang	He XueHong	H	H
		Jing YuanWei		P,P
″ , Science Inst.	Shenyang	Han Tiemin	P	P
		Sun Ping		M,H
Northern Jiaotong Univ.	Beijing	Wang Bingtuan		P,P
		Wang Xiaoxia	P	
		Gui Wenhao	H	
Northwestern Polytech. Univ.	Xián	Xu Wei	P	
		Peng Guohua		M
		Zhang Lining		P
		Nie Yufeng	H	
Peking University	Beijing	Wang Ming		P,P
		Liu Xufeng		O,P
Shandong University	Jinan	Cui Yuquan		P
		Liu Bao dong		P
Shanghai Foreign Lang. Schl	Shanghai	Sun Yu	P,P	
		Li Qun Pan		H
Shanghai Jiading No. 1 HS	Shanghai	Xie Xilin		P

INSTITUTION	CITY	ADVISOR	A	B
Shanghai Normal Univ.	Shanghai	Cong Yuhao		
		and Guo Shenghuan	P	
		Zhang Jizhou		H
		Tang Yincai		P
		Liu Rongguan	P	
Shanghai Univ. of				
Finance and Econ.	Shanghai	Yang Xiaobin		P
South China Normal University	Guangzhou	Wang Henggeng	H,P	
″, Art Ed. Ctr	Guangzhou	Yi Lou		P
South China Univ. of Tech.	Guangzhou	Yi Hong		P
		Lin Jianliang		M
		Zhu Fengfeng		P
		Liang Manfa		P
Southeast University	Nanjing	Chen Enshui	O	P
		Zhang Zhiqiang		P,P
Tianjin Polytechnic University	Tianjin	Zhou Junming		P
		Huang Dongwei		H
Tianjin University	Tianjin	Liu Zeyi		M
		Dan Lin	P	
		Rong Ximin		P
		Liang Fengzhen		P
Tsinghua University	Beijing	Jiang Qiyuan		H
		Jun Ye		M,P
		Hu Zhiming	H	P
U. of Electronic Sci. and Tech.	Chengdu	Qin Siyi		P,P
		Du Hongfei		P,P
Univ. of Sci. and Tech. of China	Hefei	Yang Zhouwang		H
		Li Yu	M	
		Le Xuli	P	
Wuhan University	Wuhan	Hu Yuanming	H,H	
		Zhong Liuyi		P,H
		Chen Shihua		H
Wuhan Univ. of Tech.	Wuhan	Peng Sijun		M
		Huang Zhangcan	P	
		Wang Zhanqing	P	
		Jin Shengping		P
Xián Jiaotong University	Xián	Zhou Yicang		H
		Dai Yonghong		H
Xián Univ. of Tech.	Xián	Qin XinQiang		P
		Cao Maosheng		P
Xiamen University	Xiamen	Sun Hongfei		P
Xidian University	Xián	Zhang Zhuo-kui		M,H
		Zhou Shui-Sheng	M	
		Liu Hong-Wei	H	
Xuzhou Inst. of Tech.	Xuzhou	Li Subei	P	H
Zhejiang University	Hangzhou	Yang Qifan	P	
		Yong He		H
		Tan Zhiyi	O	

INSTITUTION	CITY	ADVISOR	A	B
FINLAND				
Päivölä College	Tarttila	Merikki Lappi	H	P
Mathematical HS of Helsinki	Helsinki	Esa Ilmari Lappi	H,P	
HONG KONG				
City Univ. of Hong Kong	Hong Kong	Kei Shing	P,P	
		Jonathan J. Wylie	M	
		Yiu-Chung Hon	P	
Hong Kong Baptist Univ.	Hong Kong	Wai Chee Shiu	P	
		Chong-Sze Tong		M
INDONESIA				
Institut Teknologi Bandung	Bandung	Rieske Hadianti		H
		Kuntjoro Adji Sidarto	H	
IRELAND				
University College Cork	Cork	James Gleeson	M	
		Donal J. Hurley	M,H	
University College Dublin	Belfield	Maria G. Meehan	P	M
		Ted Cox	H	H
SINGAPORE				
National Univ. of Singapore	Singapore	Victor Tan	P	
SOUTH AFRICA				
University of Stellenbosch	Stellenbosch	Jan H. van Vuuren	H	P

Editor's Note

For team advisors from China, we have endeavored to list family name first.

Safe Landings

Chad T. Kishimoto
Justin C. Kao
Jeffrey A. Edlund
California Institute of Technology
Pasadena, California 91125

Advisor: Darryl H. Yong

Abstract

We examine the physical principles of stunt crash pads made of corrugated cardboard boxes and build a mathematical model to describe them. The model leads to a computer simulation of a stunt person impacting a box catcher. Together, the simulation and model allow us to predict the behavior of box catchers from physical parameters and hence design them for maximum safety and minimum cost.

We present two case studies of box-catcher design, a motorcyclist landing after jumping over an elephant and David Blaine's televised Vertigo stunt. These demonstrate the ability of our model to handle both high-speed impacts and large weights. For each case, we calculate two possible box-catcher designs, showing the effects of varying design parameters. Air resistance is the dominant force with high impact speeds, while box buckling provides greater resistance at low speeds. We also discuss other box-catcher variations.

Basic Concept

Requirements

A falling stunt person has a large amount of kinetic energy,

$$U_\mathrm{s} = \tfrac{1}{2}\, m_\mathrm{s} u_\mathrm{s}^2.$$

To land safely, most of it must be absorbed by a catcher before the performer hits the ground. Therefore, following Newton's Second Law, the catcher must exert a force to decelerate the performer,

$$F = m\, \frac{du_\mathrm{s}}{dt}.$$

The total energy absorbed should equal the performer's initial energy (kinetic and potential),

$$\int F \, dz = U_{s_0} + V_{s_0}.$$

However, the catcher itself cannot exert too large a force or it would be no better than having the performer hit the ground in the first place. We therefore set a maximum force, F_{max}. The smaller we make F, the larger (and more expensive) the box catcher has to be. Therefore, to save both money and life, we would like to have

$$F \approx (1 - \delta)F_{max},$$

where δ is a safety margin ($0 < \delta < 1$).

The Box Catcher

A box catcher consists of many corrugated cardboard boxes, stacked in layers, possibly with modifications such as ropes to keep the boxes together or inserted sheets of cardboard to add stability and distribute forces. When the stunt person falls into the box catcher, the impact crushes boxes beneath. As a box collapses, not only does the cardboard get torn and crumpled, but the air inside is forced out, providing a force resisting the fall that is significant but not too large. As the performer passes though the layers, each layer takes away some kinetic energy.

Modeling the Cardboard Box

We examine in detail the processes involved when a stunt person vertically impacts a single cardboard box. This analysis allows us to predict the effect of varying box parameters (shape, size, etc.) on the amount of energy absorbed by the box.

Assumptions: Sequence of Events

Although the impact involves many complex interactions—between the performer's posture, the structure of the box, the air inside the box, the support of the box, the angle and location of impact, and other details—modeling thin-shell buckling and turbulent compressible flow is neither cost-effective for a movie production nor practical for a paper of this nature. We therefore assume and describe separately the following sequence of events in the impact.

1. A force is applied to the top of the cardboard box.

2. The force causes the sides of the box to buckle and lose structural integrity.

3. Air is pushed out of the box as the box is crushed.

4. The box is fully flattened.

We now consider the physical processes at play in each of these stages.

Table 1.

Nomenclature.

Property	Symbol	Units
Potential energy density	v	J/m^3
Young's modulus	Y	Pa
Strain in box walls	ϵ	none
Stress in box walls	S	Pa
Tensile strength	T_S	Pa
Total kinetic energy	U	J
Total potential energy	V	J
Volume of cardboard in box walls	$\mathcal{V}$	m^3
Distance scale over which buckling is significant	ΔH	m
Width of box	w	m
Thickness of box walls	τ	m
Height of box	ℓ	m
Surface area of the top face of the box	A	m^2
Proportion of top face through which air escapes	α	—
Velocity of stunt person	u_s	m/s
Mean velocity of expelled air	u_a	m/s
Mass of stunt person (and vehicle, if any)	m	kg
Density of air	ρ	kg/m^3
Acceleration due to gravity, $g = 9.8\,\text{m/s}^2$	g	m/s^2

Stage 1: Force Applied

A force $F(t)$ is applied uniformly over the top surface. The walls of the box expand slightly, allowing the box to compress longitudinally (along the direction of the force). While this applied force is small enough (less than the force necessary to cause buckling), the box absorbs little of the force and transmits to the ground (or next layer of the box catcher) a large fraction of the applied force. The applied force increases until it is on the order of the buckling force ($F(t) \sim F_B$). At this point, the box begins to buckle.

Stage 2: Box Buckles

The walls crumple, the box tears, and the top of the box is pressed down. Once the box has lost structural integrity, although the action of deforming the box may present some resistance, the force that the box itself can withstand is greatly diminished.

Consider the pristine box being deformed by a force applied to its upper face. To counteract this force, the walls of the box expand in the transverse

directions (perpendicular to the force), creating a strain in the walls. For a given strain ϵ, the potential energy density v stored in the walls of the box is

$$v = \tfrac{1}{2} Y \epsilon^2 + \mathcal{O}(\epsilon^4),$$

where Y is the Young's modulus for boxboard. For this calculation, the effects of longitudinal (along the direction of the force) contractions in the box walls are negligible compared to the transverse expansion.

A stress S is created in the box walls as a result of the battle between the wall's pressure to expand and its resistance to expansion,

$$S = Y\epsilon + \mathcal{O}(\epsilon^2).$$

Only a small strain ($\epsilon \ll 1$) is necessary to cause the box to buckle, so we neglect higher-order terms. There is a point where the box stops expanding and begins to give way to the increasing stress placed on it. When the stress in the box walls reaches its tensile strength T_S, it loses its structural integrity and the box bursts as it continues to buckle. Thus, we can set a limit on the maximum strain that the box walls can endure,

$$\epsilon_{\max} = \frac{T_S}{Y}.$$

The typical tensile strength of cardboard is on the order of a few MPa, while the Young's modulus is on the order of a few GPa. Thus, we may assume that $\epsilon \ll 1$. The maximum energy density allowed in the walls of the box is now

$$v_{\max} = \tfrac{1}{2} Y \epsilon_{\max}^2 = \frac{1}{2} \frac{T_S^2}{Y}.$$

The total energy stored in the walls just before the box bursts is

$$V_{\max} = \frac{1}{2} \frac{T_S^2}{Y} \mathcal{V},$$

where $\mathcal{V} = $ (lateral surface area) $\times$ (thickness) is the volume of cardboard in the box walls. If we assume that the force to deform the box is constant over the deformation distance, then by conservation of energy, we have

$$\frac{dU_s}{dt} + \frac{dV_s}{dt} = -\frac{dU_{\text{box}}}{dt} = -\frac{dU_{\text{box}}}{dt}\frac{dz}{dt} = -\frac{\Delta U_{\text{box}}}{\Delta H}\frac{dz}{dt} = \frac{u_s}{2\Delta H}\frac{T_S^2}{Y}\mathcal{V},$$

where ΔH is the change in height of the box over the course of the buckling process. Since

$$m_s u_s \frac{du_s}{dt} = \frac{dU_s}{dt},$$

the change in velocity of the falling stunt person due to buckling the box is

$$\frac{du_s}{dt} = \frac{1}{2m_s\Delta H}\frac{T_S^2}{Y}\mathcal{V}. \tag{1}$$

To determine ΔH, we assume an average force $F \approx F_B$, where F_B is the buckling force of the cardboard walls. The **Appendix** shows that the buckling force is related to the Young's modulus and other physical parameters by

$$F_B = Y \frac{\pi^2}{12} \frac{w\tau^3}{\ell^2}. \tag{2}$$

In this case, $\mathcal{V} = 4\ell w\tau$ for a square box. Then ΔH can be estimated by

$$F_B \Delta H = \frac{1}{2} \frac{T_S^2}{Y} \mathcal{V},$$

$$Y \frac{\pi^2}{12} \frac{w\tau^3}{\ell^2} \Delta H = 2\ell w\tau \frac{T_S^2}{Y},$$

$$\Delta H = \frac{24}{\pi^2} \left(\frac{T_S}{Y}\right)^2 \left(\frac{\ell}{\tau}\right)^2 \ell.$$

For a typical box, ΔH is on the order of a few centimeters.

Stage 3: Box is Crushed

Without structural integrity, the box is crushed by the applied force. However, in crushing the box, the air inside must be pushed out.

Let A be the surface area of the top of the box. We make the ad hoc assumption that when the box buckled, it is torn such that air can escape through an area αA. Provided $\alpha \sim \mathcal{O}(1)$, we can assume incompressible flow, since the area of opening in the box is of the same order of magnitude as the area being pushed in. By conservation of mass, we obtain the the velocity of the air moving out of the box in terms of α and the velocity of the stunt person:

$$-u_s A = u_a(\alpha A) \qquad \Longrightarrow \qquad u_a = -u_s/\alpha.$$

Using conservation of energy, we equate the change in energy of the stunt person and the air leaving the box,

$$\frac{dU_s}{dt} + \frac{dV_s}{dt} = -\left(\frac{dU_a}{dt} + \frac{dV_a}{dt}\right).$$

The potential energy of the air does not change significantly as it is ejected, so the energy equation simplifies to

$$\frac{dU_s}{dt} + \frac{dV_s}{dt} = -\frac{dU_a}{dt}. \tag{3}$$

The energy gain of air outside the box is due to air carrying kinetic energy out of the box:

$$\frac{dU_a}{dt} = \frac{1}{2} \frac{dm_a}{dt} u_a^2 = \tfrac{1}{2} \left(\rho\alpha A u_a\right) u_a^2, \tag{4}$$

while the energy loss of the stunt person is from deceleration and falling:

$$\frac{dU_s}{dt} + \frac{dV_s}{dt} = m_s u_s \frac{du_s}{dt} + m_s g u_s. \tag{5}$$

Combining **(3–5)**, substituting for u_a, and rearranging, we obtain

$$\frac{du_s}{dt} = \frac{1}{2} \frac{\rho A}{m_s} \frac{u_s^2}{\alpha^2} - g. \tag{6}$$

Stage 4: Box Is Flattened

Once the cardboard box is fully compressed and all the air is pushed out, we assume that the box no longer has any effect on the stunt person.

Summary

In stages 1 and 4, the box is essentially inert—little energy goes into it. Therefore in our mathematical description, we ignore these and concentrate on stages 2 and 3. Stage 2 occurs in the top ΔH of box deformation, while stage 3 occurs in the remainder of the deformation. Combining **(1)** and **(6)**, we get

$$\frac{du_s}{dt} = \begin{cases} \dfrac{1}{2m_s \Delta H} \dfrac{T_S^2}{Y} \mathcal{V}, & |z| < |\Delta H|; \\[2ex] \dfrac{1}{2} \dfrac{\rho A}{m_s} \dfrac{u_s^2}{\alpha^2} - g, & |z| \geq |\Delta H|, \end{cases} \tag{7}$$

where z is measured from the top of the box.

Modeling the Box Catcher

Cardboard Properties

We assume that each cardboard box is made of corrugated cardboard with uniform physical properties, using the data shown in **Table 2**.

Table 2.

Properties of corrugated cardboard [Bever 1986].

Property	Symbol	Value
Tensile strength	T_S	12.2 MPa
Thickness	τ	5 mm
Young's modulus	Y	1.3 GPa

Assumptions

- Layers of boxes are comprised of identical boxes laid side-by-side over the entire area of the box catcher.

- The box catcher is large enough compared to the stunt person that edge effects are negligible.

- The boxes are held together so that there is no relative horizontal velocity between them.

- Loose cardboard is placed between layers of cardboard boxes, so that any force transmitted through the top layer of boxes is well distributed to lower boxes, ensuring that only one layer is crushed at a time. In other words, we treat each layer of boxes independently and the box catcher as a sequence of layers.

Equations of Motion

Since each layer is independent, the equations of motion for the box catcher look similar to the equation of motion for a single box **(7)**. The equations depend on the dimensions of the boxes in each level, so we solve numerically for the motion of the stunt person. At each level of the box catcher, the performer impacts several boxes (approximately) at once. The number of boxes that act to decelerate the stunt person is the ratio A_s/A of the performer's cross-sectional area to the surface area of the top face of a cardboard box. Thus, we alter the equations of motion by this ratio, getting

$$
\frac{du_{\mathrm{s}}}{dt} =
\begin{cases}
\dfrac{1}{2m_{\mathrm{s}}\Delta H}\dfrac{T_S^2}{Y}\mathcal{V}\dfrac{A_{\mathrm{s}}}{A} & |z - z_{\mathrm{top}}| < |\Delta H|; \\[2ex]
\dfrac{1}{2}\dfrac{\rho A_{\mathrm{s}}}{m_{\mathrm{s}}}\dfrac{u_{\mathrm{s}}^2}{\alpha^2} - g, & |z - z_{\mathrm{top}}| \geq |\Delta H|,
\end{cases}
\tag{8}
$$

where

z is the vertical distance measured from the top of the stack,

z_{top} is the value of z at the top of the current box, and

A_{s} is the cross sectional area of the stunt person.

Now, given a suggested stack of boxes, we can integrate the equations of motion to see whether or not the stack successfully stops the falling stunt person, and if so, where in the stack.

Analysis

Our model allows us to predict a stunt person's fall given parameters for the box catcher. Now we would like to find analytic results to guide box-catcher design.

Using the equations of motion **(8)**, we determine the force that the stunt person feels falling through the box catcher:

$$F = m_s \frac{du_{\mathrm{s}}}{dt} = \begin{cases} \dfrac{1}{2\Delta H} \dfrac{T_{\mathrm{S}}^2}{Y} \mathcal{V} \dfrac{A_{\mathrm{s}}}{A}, & |z - z_{\mathrm{top}}| < |\Delta H|; \\[2ex] \dfrac{1}{2} \rho A_{\mathrm{s}} \dfrac{u_{\mathrm{s}}^2}{\alpha^2} - m_{\mathrm{s}}g, & |z - z_{\mathrm{top}}| \geq |\Delta H|. \end{cases}$$

We want to make this force large enough to stop but not harm the performer. Therefore, we demand that

$$F \leq (1 - \delta)F_{\mathrm{max}}. \tag{9}$$

However, we wish to find solutions that both minimize cost (fewest boxes) and conform to spatial constraints (we don't want the box catcher to be taller than the obstacle that the stunt person is jumping over). Thus, it is in our best interest to maximize the force applied to the performer subject to **(9)**.

We are faced with two independent equations with three unknowns; we solve for two of them in terms of the third. With the simplifying assumption that the top face of each box is a square ($A = w^2$), we can solve for the optimal dimensions of the box given the stunt person's impact velocity:

$$\frac{\pi^2}{12} Y \tau^3 \frac{w}{\ell^2} \frac{A_{\mathrm{s}}}{A} = F_{\mathrm{max}}(1 - \delta) = F_{\mathrm{thresh}},$$

$$\frac{1}{2} \frac{\rho}{\alpha^2} A_{\mathrm{s}} \tilde{u}^2 - m_s g = F_{\mathrm{thresh}},$$

where $\tilde{u}^2$ is the stunt person's velocity after causing the box to buckle (but before expelling all the air). So we have

$$\tilde{u}^2 = u_o^2 - 4\tau \frac{T_{\mathrm{S}}^2}{m_s Y} w\ell \frac{A_{\mathrm{s}}}{A}.$$

Define γ, the maximum number of gees of acceleration felt by the stunt person, by $F_{\mathrm{thresh}} = (1 - \delta)F_{\mathrm{max}} = \gamma m_{\mathrm{s}}g$. We get

$$\ell^3 = \frac{\pi^2}{48\gamma} \left(\frac{Y}{T_{\mathrm{S}}}\right)^2 \frac{\tau^2}{g} \left(u_0^2 - 2(\gamma + 1)\alpha^2 \frac{m_{\mathrm{s}}g}{\rho A_{\mathrm{s}}}\right) \tag{10}$$

and

$$\frac{A(w)}{w} = w = \frac{\pi^2}{12\gamma} \frac{A_{\mathrm{s}}Y}{m_{\mathrm{s}}g} \frac{\tau^3}{\ell^2}. \tag{11}$$

Thus, we could write a routine that would integrate the equations of motion of the stunt person falling through each level of boxes and for each layer use the incoming velocity to calculate the optimal dimensions for the next layer of boxes. This would yield a box-catcher structure that would safely stop the stunt person in the fewest levels of boxes, minimizing the cost of the box catcher.

General Solutions

The most difficult aspect of finding a general solution is the need to know the speed of the stunt person at impact, which depends on the height of the box catcher. Given sufficient computing time, we could solve the equations with condition that the height above the ground at impact is the height of the box catcher. However, this is unnecessary for a paper of this scope.

Instead, we use the model to shed light on the qualitative aspects of building a box catcher. Equation **(10)** tells us that for higher speeds of the stunt person, we need taller boxes (larger ℓ) to keep the force on the stunt person at its maximum allowable level. This means that it is necessary to place the tallest boxes at the top of the stack, followed by shorter ones, for both cost effectiveness and safety. Inspecting **(11)** shows that the optimal width of the box is inversely proportional to the height ($w \propto \ell^{-2}$). Thus, the box catcher should have the thinnest boxes on top and the widest ones on the bottom.

It follows that

the optimal box catcher has short, wide boxes at the bottom and tall, narrow boxes at the top.

Furthermore, the equations of motion **(8)** contain u^2 in the air expulsion stage but no velocity-dependent term in the buckling stage. Hence, for high impact speeds, air expulsion provides the dominant deceleration, while for smaller impacts, box buckling is the more important stage.

Results

Motorcycle Stunt

A stunt person on a motorcycle is preparing to jump over an elephant for the filming of a blockbuster movie. What should be going through a stunt coordinator's mind?

The average height of an African elephant is 4 m; the mass of a top-of-the-line motorcycle is 230 kg [Encyclopedia Britannica Online 2003].

We assume that the stunt person clears the elephant by about 2 m, so the impact velocity is 8 m/s. Choosing the parameters $\ell = \frac{1}{3}$ m and $w = \frac{1}{2}$ m, a 3 m-tall homogeneous box catcher stops the stunt person and motorcycle after they fall about 2.33 m (**Figure 1**).
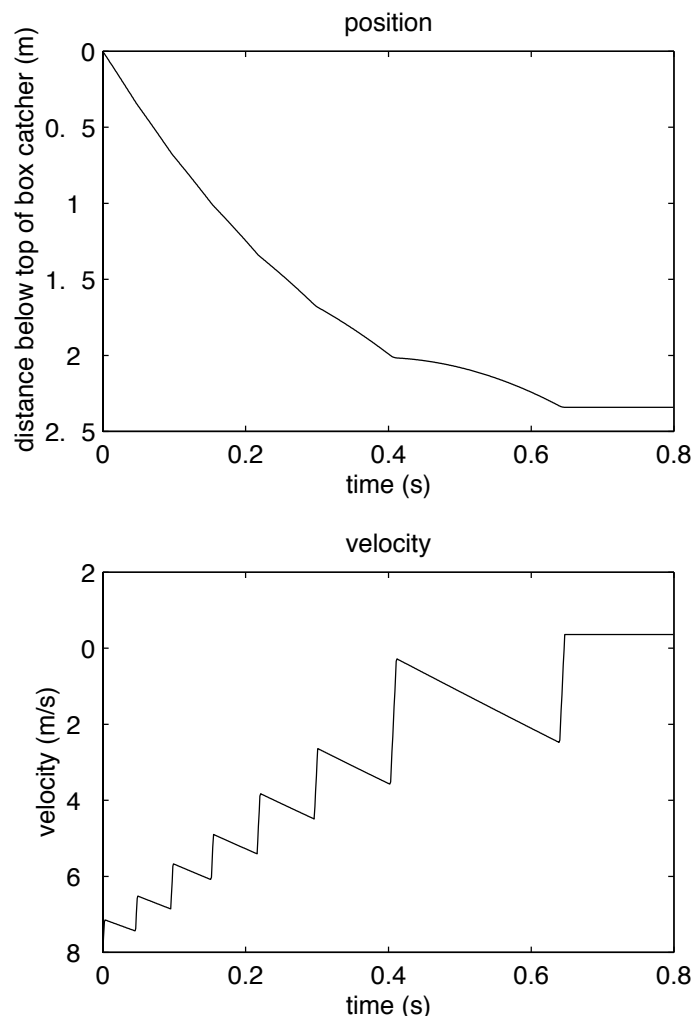
Figure 1. Simulation of box catcher stopping stunt person and motorcycle.

However, we can do better. We take our previous solution, remove one layer of boxes, and change the top layer to boxes with height $\frac{1}{6}$ m and width $\frac{2}{3}$ m (for a $\gamma \sim 1.3$). We've removed a row without compromising the safety of the stunt person. In this way, we can make changes until we arrive at an optimal arrangement, one with the fewest boxes necessary.

David Blaine's Vertigo

On May 22, 2002, David Blaine leaped from a ten-story pole onto a cardboard box catcher below. We consider his fall of more than 25 m onto approximately 4 m of boxes. His impact velocity was approximately 36.5 m/s (using the approximation $v_f = \sqrt{2gh}$, which is valid since the terminal velocity for a person falling in air is about 60 m/s [Resnick et al. 1992]).

Viewing his fall in the TV special [David Blaine's Vertigo 2002], we estimate the boxes to have height $\ell = \frac{1}{3}$ m and width $w = \frac{2}{3}$ m, with 12 layers of boxes in

the catcher. According to our simulation, Blaine's momentum is finally stopped by the last box. A larger margin of safety could be accomplished by decreasing the value of either ℓ or w. By changing the width of the boxes to $w = \frac{1}{2}$ m, our simulation shows that Blaine would be stopped 1 m from the ground.

Other Factors

Landing Zone Considerations

The stunt person must land on the box catcher for it to be of any use. We suggest a probabilistic calculation of the landing zone; but since the principles involved are so dependent on the fall setup and conditions, we do not attempt this.

Box and Box Catcher Construction

We made a few key assumptions about design:

- *The boxes in the box catcher are held together so that there is no relative horizontal velocity between the boxes. This assumption is essential.* If the boxes could shift horizontally, they would likely shift out of the way of the falling stunt person. The catcher must also be large enough so that the structure that holds the boxes together doesn't interfere with energy dissipation.

- *Loose cardboard forms intervening layers between the different levels of cardboard boxes.* This assumption is necessary so that any force retransmitted by the top-level box does not cause another box to buckle; requiring one layer of boxes to buckle at a time allows us to optimize box parameters at each layer independently. A layer of cardboard on top of the catcher is essential to guarantee that the impact force of the falling stunt person is well-distributed.

Following these principles, and using a variety of sizes of boxes (as in equations **(10)** and **(11)**), we can tailor the box catcher to each stunt situation.

Conclusion

We present a model of energy dissipated by the collapse of a single box, noting two key stages:

- The walls of the box buckle and give way to the overwhelming force applied to it. Shearing forces cause tears in the walls, eventually leading to collapse.

- The air within the box is expelled, absorbing kinetic energy of the falling stunt person in the process.

We consider each mechanism acting independently of the other. By solving the equations of motion in each stage, we predict the trajectory of a stunt person moving through a single box, and by extension, through the box catcher as a whole.

Whether or not the performer is stopped before reaching the bottom (and being injured) depends on the structure of the box catcher and the size of the boxes. Taller is safer but shorter is cheaper (and may be necessary to remain off-camera); we must balance safety with cost and size.

We present a solution where 9 layers of boxes are used to break the fall of the elephant-leaping motorcyclist, each with a height of $\frac{1}{3}$ m and a width of $\frac{1}{2}$ m. This is a poor solution, for the force on the falling stunt person is not optimized. We also present a slightly better solution with only 8 layers of boxes and outline the principles for continued optimization.

Finally, we observe that air resistance is the dominant force with high speeds, while box deformation provides greater resistance at low speeds.

Strengths of the Model

- All parameters in the program are flexible. Whether humid weather tends to weaken the cardboard (and lower both the tensile strength and Young's modulus), or the height of the jump changes, the stunt coordinator can test the safety of the box catcher with our program.

- The algorithm is robust, in that small changes in initial conditions do not cause drastic changes in the end result. We have seen results for extreme cases, such as extreme impact velocities (falling from great heights) or extreme weight considerations (a person on a motorcycle).

- Our algorithm takes just a few seconds to compute the trajectory of the stunt person through the box catcher, so it is practical for a stunt coordinator to test a variety of box-catcher configurations.

Weaknesses of the Model

- We were unable to derive an optimal box configuration.

- We could not get a good estimate of the magnitude of the force experienced by the stunt person. We present a plausible mechanism for dissipation of energy by a box catcher, but the force function that we use is discontinuous between box layers, though the actual physics of the situation has a continuous force.

Future Research

Future research on this project should develop an algorithm that not only tests the safety of a configuration of boxes but suggests an optimal configuration

of boxes.   Another challenge is that cardboard boxes probably have a cost
proportional to the surface area of cardboard used, not to the number of boxes.

Appendix: On Buckling

We derive **(2)**,

$$F_B = Y \frac{\pi^2}{12} \frac{w\tau^3}{\ell^2}.$$ **(2)**

Consider one wall of a cardboard box with external forces acting on both
ends. Considering the effects of shearing and inertial dynamical acceleration,
the displacement of the box wall from its equilibrium (unstressed) position
obeys the equation of motion

$$-D \frac{\partial^4 \eta}{\partial z^4} - F \frac{\partial^2 \eta}{\partial z^2} = \Lambda \frac{\partial^2 \eta}{\partial t^2},$$

where $\Lambda \equiv W/g_e$ is the mass per unit length of the box wall [Thorne and
Blandford 2002].

Table A1.

Nomenclature.

Property	Symbol	Units
Horiz. displacement from equilibrium (unstressed) location	η (z, t)	m
Flexural rigidity of the box wall	D	J $\cdot$ m
Young's modulus of the box wall	Y	Pa
Length of the box wall in z-direction	ℓ	m
Width of the box wall	w	m
Thickness of the box wall	τ	m
Force applied to each end of the box wall	F	N
Weight per unit length of the box wall	W	N/m
Acceleration due to gravity	g_e	m/s^2
Buckling force	F_B	N

We seek solutions for which the ends of the box wall remain fixed. This is
a good assumption for our model, since we require the box catcher to be held
together so that the boxes remain horizontally stationary with respect to one
other. Thus, we set the boundary conditions to be $\eta(0, t) = \eta(\ell, t) = 0$. Using
the separation ansatz $\eta(z, t) = \zeta(z)T(t)$, we get the linear ordinary differential
equations

$$-D \frac{d^4 \zeta}{dz^4} - F \frac{d^2 \zeta}{dz^2} = \kappa_n \zeta \qquad \text{and} \qquad \Lambda \frac{d^2 T}{dt^2} = \kappa_n T,$$

where κ_n is the separation constant. The normal-mode solutions are thus

$$\eta_n(z, t) = A \sin \left(\frac{n\pi}{\ell} z \right) e^{-i\omega_n t},$$

where $\omega_n \in \mathbb{C}$ satisfies the dispersion relation

$$\omega_n^2 = \frac{1}{\Lambda} \left(\frac{n\pi}{\ell}\right)^2 \left[\left(\frac{n\pi}{\ell}\right)^2 D - F\right].$$

Consider the lowest-order normal mode ($n = 1$). For $F < F_{\text{crit}} \equiv \pi^2 D/\ell^2$, we have $\omega_1^2 > 0$, so $\omega_1 \in \mathbb{R}$, and the normal mode just oscillates in time, giving stable solutions. However, if $F > F_{\text{crit}}$, then $\omega_1^2 < 0$ and $\omega = \pm i\varpi$, $\varpi \in \mathbb{R}$, i.e. there are exponentially growing solutions ($\propto e^{\varpi t}$), and the normal-mode solution becomes unstable. Thus, the box wall buckles for applied forces $F > \pi^2 D/\ell^2$. The buckling force is

$$F_B = \frac{\pi^2 D}{\ell^2} = Y \frac{\pi^2}{12} \frac{wt^3}{\ell^2},$$

which is **(2)**.

References

Bever, Michael B. (ed.) 1986. *Encyclopedia of Materials Science and Engineering.* Vol. 2. Cambridge, MA: MIT Press.

Blaine, David. 2002 . David Blaine's Vertigo. Television special, May 2002.

Encyclopaedia Britannica Online. 2003. `http://search.eb.com/`.

Polking, John C. 2002. ODE Software for MATLAB. 4th order Runge-Kutta demonstration `rk4.m`. `http://math.rice.edu/~dfield/` .

Resnick, Robert, David Halliday, and Kenneth S. Krane. 1992. *Physics.* New York: John Wiley and Sons.

Thorne, Kip S., and Roger D. Blandford. 2002. *Ph136: Applications of Classical Physics.* Unpublished lecture notes. Pasadena, CA: California Institute of Technology. `http://www.pma.caltech.edu/Courses/ph136/yr2002/index.html` .

A Time-Independent Model of Box Safety for Stunt Motorcyclists

Ivan Corwin
Sheel Ganatra
Nikita Rozenblyum
Harvard University
Cambridge, MA

Advisor: Clifford H. Taubes

Abstract

We develop a knowledge of the workings of corrugated fiberboard and create an extensive time-independent model of motorcycle collision with one box, our Single-Box Model. We identify important factors in box-to-box and frictional interactions, as well as several extensions of the Single-Box Model.

Taking into account such effects as cracking, buckling, and buckling under other boxes, we use the energy-dependent Dual-Impact Model to show that the "pyramid" configuration of large 90-cm cubic boxes—a configuration of boxes in which every box is resting equally upon four others—is optimal for absorption of the most energy while maintaining a reasonable deceleration. We show how variations in height and weight affect the model and calculate a bound on the number of boxes needed.

General Assumptions

- The temperature and weather are assumed to be "ideal conditions"—they do not affect the strength of the box.

- The wind is negligible, because the combined weight of the motorcycle and the person is sufficiently large.

- The ground on which the boxes are arranged is a rigid flat surface that can take any level of force.

- All boxes are cubic, which makes for the greatest strength [Urbanik 1997].

Table 1.

Variables.

Variable	Definition	Units
l	Box edge length	cm
$V(t)$	Velocity as a function of time (v_0 is velocity of impact)	cm/s
A_T	Energy change due to the top of the box	kg-cm^2/s^2
A_B	Energy change due to the buckling of the box	kg-cm^2/s^2
A_{NET}	Total energy including gravity for top	kg-cm^2/s^2
$A_{\text{CD-EDGE}}$	Energy absorbed by CD springs in modelled buckling	kg-cm^2/s^2
$A_{\text{MD-EDGE}}$	Energy absorbed by MD springs in modelled buckling	kg-cm^2/s^2
x_{NET}	Total depression of the top	cm
Δx	Change in a distance	cm
x_{DOWN}	Component of edge's depression in the z-direction	cm
$x(t)$	Downward displacement of the top of the box ($x_0 = 0$)	cm
x_F	Final depression before top failure.	cm
δL	Offset from top center.	cm
M	Motorcycle and stuntman combined mass	kg
P_{CD}	Tensile strength in the cross-machine direction	kg/(s^{2}cm)
P_{MD}	Tensile strength in the machine direction	kg/(s^{2}cm)
P_{ECT}	Maximum strength as measured with the Edge Crush Test	kg/s^2
P_{ML}	Maximum strength as measured with the Mullen Test	kg/(s^{2}cm)
F_{CD}	Force in the cross-machine direction	kg-cm/s^2
F_{CDMAX}	Maximum force in the cross-machine direction	kg-cm/s^2
F_{MD}	Force in the machine direction	kg-cm/s^2
F_{MDMAX}	Maximum force in the machine direction	kg-cm/s^2
F_{UP}	Net dampening force the box exerts on the motorcycle	kg-cm/s^2
F_{UPMAX}	Maximum dampening force the box exerts on the motorcycle	kg-cm/s^2
F_{ECT}	Force box exerts on the frame	kg-cm/s^2
F_{ECTMAX}	Maximum force the box exerts on the frame before yielding	kg-cm/s^2
F_{NET}	Total force	kg-cm/s^2
x_{MD}	Depression at which MD tensile strength is exceeded	cm
x_{CD}	Depression at which CD tensile strength is exceeded	cm
x_{ECT}	Depression at which a buckle occurs	cm
x_{ML}	Depression at which a puncture occurs	cm
V_x	Velocity in the x-direction	cm/s
V_y	Velocity in the y-direction	cm/s
V_{ix}	Initial velocity in the x-direction	cm/s
V_{iy}	Initial velocity in the y-direction	cm/s
V_{fx}	Final velocity in the x-direction	cm/s
V_{fy}	Final velocity in the y-direction	cm/s
M_B	Mass of boxes displaced	kg
t	Time	s
A_x	Energy in the x-direction	kg-cm^2/s^2
A_y	Energy in the y-direction	kg-cm^2/s^2
A_z	Energy in the z-direction	kg-cm^2/s^2
d	Distance	cm

Table 2.

Constants.

Variable	Definition	Value
E_{MD}	Young's modulus in the machine direction	3000000 kg/(s^2-cm)
E_{CD}	Young's modulus in the cross-machine direction	800000 kg/(s^2-cm)
E	Sum of E_{MD} and E_{CD}	3800000 kg/(s^2-cm)
L_{MD}	Tire rect. length in the machine direction	7cm front, 10cm back
L_{CD}	Tire rect. length in the cross-machine direction	10 cm
P_{CD}	Tensile strength in the cross-Machine direction	2000 kg/(s^2-cm)
P_{MD}	Tensile strength in the machine direction	2500 kg/(s^2-cm)
P_{ECT}	Max. strength as measured with the edge crush test	10000 kg/s^2
P_{ML}	Max. strength as measured with the Mullen test	25000 kg/(s^2-cm)
g	Gravitational Constant	980 cm/s^2
μ	Coefficient of kinetic friction	0.4
w	Cardboard thickness	0.5 cm
δv	Speed variation	200 cm/s
$\delta \phi$	Angle variation away from y-axis leaving the ramp	$\pi/36$
M	Mass of rider and motorcycle	300 kg
v_i	Initial velocity leaving ramp	1500 cm/s
θ	Ramp angle of elevation	$\pi/6$

Definitions and Key Terms

- **Buckling** is the process by which a stiff plane develops a crack due to a stress exceeding the yield stress.

- **Compressive strength** is the maximum force per unit area that a material can withstand, under compression, prior to yielding.

- **Corrugation** is the style found in cardboard of sinusoidal waves of liner paper sandwiched between inner and outer papers. We use boxes with the most common corrugation, *C-flute corrugation* (see below for definition of a flute).

- **Cracking** is a resulting state when the tensile force exceeds the tensile strength.

- **Cross-machine direction** is the direction perpendicular to the sinusoidal wave of the corrugation.

- **Depression** is when, due to a force, a section of a side or edge moves downwards.

- **ECT** is the acronym for a common test of strength, the *edge crush test*.

- **Fiberboard** is the formal name for cardboard.

- **Flute** is a single wavelength of a sinusoidal wave between the inner and outer portion papers that extends throughout the length of the cardboard. A C-flute has a height of 0.35 cm and there are 138 flutes per meter [Packaging glossary n.d.].

- **Machine direction** is parallel to the direction of the sinusoidal waves.

- **Motorcycle** We use the 1999 BMW R1200C model motorcycle for structural information; it has a 7.0-cm front wheel and a 10-cm back wheel, with radii 46 and 38 cm. It is 3 m long and has 17 cm ground clearance. The weight is 220 kg (dry) and 257 kg (fueled) [Motorcycle specs n.d.].

- **Mullen test** is a common measurement of the maximum force that a piece of cardboard can stand before bursting or puncturing.

- **Puncturing** is when a force causes an area to burst through the cardboard surface.

- **Pyramid configuration** is a configuration of boxes in which each box is resting equally on four others.

- **Strain** is the dimensionless ratio of elongation to entire length.

- **Stress** is the force per unit area to which a material is subject.

- **Tensile strength** is the maximum force per unit area which a material can withstand while under tension prior to yielding.

- **Young's modulus of elasticity** is the value of stress divided by strain and relates to the ability of a material to stretch.

Developing the Single-Box Model

Expectations

- Given sufficiently small impact area, the surface plane either punctures or cracks before the frame buckles.

- Given sufficiently large impact area, the frame should buckle and no puncturing occurs.

- During buckling, corners are more resistive to crushing than edges.

Preliminary Assumptions

- The force is exerted at or around the center of the top.

- The top of the box faces upward. This assumption allows us to use ECT (Edge Crush Test) results. This orientation also ensures that the flutes along the side are oriented perpendicular to the ground, so they serve as columns.

The Conceptual Single-Box Model

During the puncturing or cracking of the top of the box:

- The frame stays rigid.

- The cardboard can be modeled as two springs with spring constants equal to the length of board times its modulus of elasticity [Urbanik 1999] (**Figure 1**).
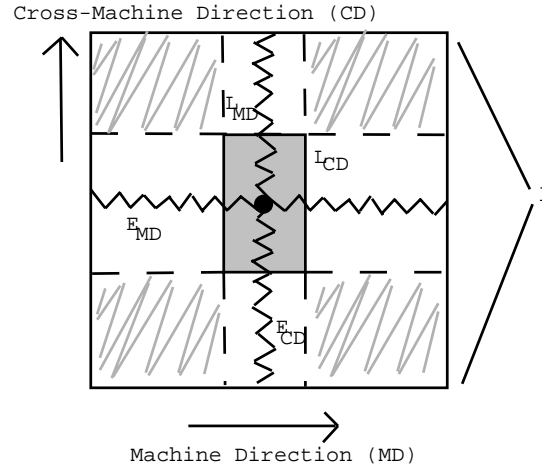
Figure 1. Our model for a tire hitting the top of one box. We treat the portions of the box directly vertical or horizontal from the edges of the motorcycle tire (the rectangle in the middle) as ideal springs, neglecting the effect of the rest of the box.

- The surface of the motorcycle tire that strikes the box is approximated as a rectangle with dimensions L_{MD} (the wheel's width) and L_{CD} (the length of the wheel in contact with the cardboard surface). We neglect the spin and tread of the tire.

- The part of the spring beneath the tire does not undergo any tension. In reality, this is not the case; but with this assumption, cracking and puncturing occur along the edges of the tire. The force still comes from the rigid frame, and the springs have the same constant; therefore, we believe this assumption affects only the position of the cracking and puncturing, not when it occurs or how much energy is dissipated.

- There is no torque on the box during this first process. This assumption can be made since the force is at the center of the top.

The top of the cardboard box can fail in several ways:

- If the resistive upwards force from the top, F_{UP}, exceeds $P_{ML} \cdot L_{MD} \cdot L_{CD}$ (the Mullen maximum allowable pressure over this area), then puncturing occurs.

- If the force F_{MD} on the machine direction spring exceeds $P_{MD} \cdot w \cdot (3L_{CD} - l)/2$ (the tensile strength in the machine direction times cross-sectional area perpendicular to the force), then a crack occurs in the cross-machine direction. We assume that this force that causes cracking is evenly distributed over a section larger than the actual edge of the tire rectangle, because of the solid nature of cardboard.

- If the force F_{CD} on the cross machine direction spring exceeds $P_{CD} \cdot w \cdot (3L_{MD} - l)/2$, then a crack occurs in the machine direction, for the same reasons as above.

- If the force on the edges exceeds $P_{ECT} \cdot 4l$ (the compression strength of the edges times the total edge length), then buckling occurs first. Here we assume that even though we model the top as two springs, the force is evenly distributed over the edges, taking advantage of the high spring constant and solid behavior of cardboard.

There are several ways in which boxes can fail:

- Puncture: The wheel enlarges the hole, and only when the hull of the motorcycle hits the edge does buckling occur.

- Crack: The tire does not break through the material, and buckling eventually occurs.

- Buckling: Can occur without a puncture or crack first.

We assume that at most one puncture or crack occurs per box, followed inevitably by buckling.

Calculations for the Box Top

[EDITOR'S NOTE: We do not give all the details of the following calculations.] Refer to **Figure 2**. We solve for F_{CD}, getting

$$F_{CD} = E_{CD}L_{MD}\left(\sqrt{\left(\frac{l - L_{CD}}{2}\right)^2 + [x(t)]^2} - \frac{l - L_{CD}}{2}\right). \tag{1}$$

We apply the results to solve for F_{MD} and combine them to get F_{UP}. After obtaining the vertical component of F_{CD},

$$x(t)E_{CD}L_{MD}\left(\frac{\sqrt{\left(\frac{l-L_{CD}}{2}\right)^2 + [x(t)]^2} - \frac{l-L_{CD}}{2}}{\sqrt{\left(\frac{l-L_{CD}}{2}\right)^2 + [x(t)]^2}}\right),$$
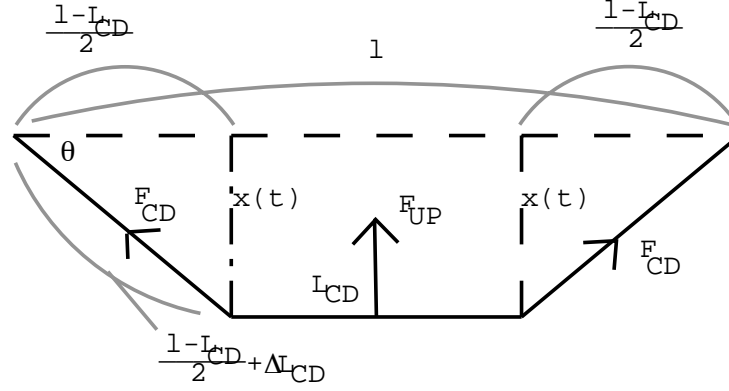
Figure 2. Side view of the depression of the motorcycle tire into the top of the box.

and the analogue by symmetry for F_{MD}, we have F_{UP}, namely:

$$
F_{\mathrm{UP}} = x(t) \left[2E_{\mathrm{CD}}L_{\mathrm{MD}} \left(1 - \frac{\frac{l-L_{\mathrm{CD}}}{2}}{\sqrt{\left(\frac{l-L_{CD}}{2}\right)^2 + [x(t)]^2}} \right) + \right.
$$
$$
\left. 2E_{\mathrm{MD}}L_{\mathrm{MD}} \left(1 - \frac{\frac{l-L_{\mathrm{MD}}}{2}}{\sqrt{\left(\frac{l-L_{\mathrm{CD}}}{2}\right)^2 + [x(t)]^2}} \right) \right]. \quad \textbf{(2)}
$$

The force F_{UP} is the resistive force that the top exerts on the motorcycle's wheel. Balancing the force and taking into effect gravity (in the form of the normal force), we get the force equation of the motion of the motorcycle's wheel on the box prior to puncture, crack, or buckle:

$$
F_{\mathrm{NET}} = F_{\mathrm{UP}} + mg.
$$

We use this expression to calculate the energy as a function of depression into the box. We use our initial force calculation to determine the level of depression and the type of failure that the top incurs. This depression is the minimum depression for which any failure occurs.

If the force F_{CD} on the cross-machine direction spring (contributed by both sides of the spring) exceeds $2P_{CD}L_{MD}w$, then a crack occurs in the machine direction. Solving for the depression, we get

$$
x_{\mathrm{CD}} = \sqrt{\left(\frac{P_{\mathrm{CD}}w}{E_{\mathrm{CD}}}\right)^2 + \frac{P_{\mathrm{CD}}w}{E_{\mathrm{CD}}} (l - L_{\mathrm{CD}})}
$$

Likewise, if the force F_{MD} on the machine direction spring (contributed by both sides of the spring) exceeds $2P_{\mathrm{MD}}L_{\mathrm{CD}}w$, then a crack occurs in the cross-machine direction, with the analogous formula for the depression.

If the resistive upwards force F_{UP} from the top exceeds $P_{ML}L_{\mathrm{MD}}L_{\mathrm{CD}}$, puncturing occurs. Similarly, if the net force on the edges, $2F_{\mathrm{CD}} + 2F_{\mathrm{MD}}$, exceeds $4P_{ECT}l$, buckling occurs first. We find the respective depressions in the next section.

We can use the x-position in energy calculations to determine the new speed of the motorcycle.

Energy is a distance integral of net force, so using **(2)** we can find energy A_T absorbed by the top:

$$A_T(x) = \int_0^x F_{NET}ds = E_{\mathrm{CD}}L_{\mathrm{MD}}\left(x^2 - (l - L_{\mathrm{CD}})\sqrt{\left(\tfrac{l-L_{\mathrm{CD}}}{2}\right)^2 + x^2} + \tfrac{(l-L_{\mathrm{CD}})^2}{2}\right)$$

$$+ E_{\mathrm{MD}}L_{\mathrm{CD}}\left(x^2 - (l - L_{\mathrm{MD}})\sqrt{\left(\tfrac{l-L_{\mathrm{MD}}}{2}\right)^2 + x^2} + \tfrac{(l-L_{\mathrm{MD}})^2}{2}\right) + mgx.$$

Extensions of Top Model

Testing the model shows that not all the force and dissipative energy comes from the top of the box springs. We make the following further assumptions:

- Since the deflection is small compared to the edge lengths, $x \ll l - L_{\mathrm{CM}}/2$ and $x \ll l/2$.

- The boxes have two layers coming together at the top that are corrugated in different directions, hence the cardboard on the top really is of width $2w$.

- Since the flutes in one top piece are perpendicular to the flutes of the other, the resulting combined modulus of elasticity is the sum of the two original values in both directions. This means that we can define $E = E_{\mathrm{MD}} + E_{\mathrm{CD}}$ and modify all equations accordingly.

The equations for the forces F_{CD} **(1)** and F_{MD} are of the form

$$f(x) = k(a^2 + x^2)^{1/2} - a,$$

with $a = (l - L_{\mathrm{CD}})/2$. For small deflections x, such a function can be approximated well by its second-degree Taylor expansion around $x = 0$:

$$f(x) \approx \frac{x^2}{2a}.$$

The resulting equations are

$$F_{\mathrm{CD}} = 2EL_{\mathrm{MD}}\left(\frac{x^2}{l - L_{\mathrm{CD}}}\right), \qquad F_{\mathrm{MD}} = 2EL_{\mathrm{CD}}\left(\frac{x^2}{l - L_{\mathrm{MD}}}\right),$$

$$F_{\mathrm{UP}} = x(t)\left(2EL_{\mathrm{MD}}\frac{x(t)}{l - L_{\mathrm{CD}}} + 2EL_{\mathrm{CD}}\frac{x(t)}{l - L_{\mathrm{MD}}}\right)$$

We deal briefly with the position of the rectangle on the box. The ECT deflection should not depend on the position of the rectangle, since ECT depends only on the net force. The other three deflections become less as the force moves away from the center, so we can model them with a standard linear decrease factor of $1 - \delta L(l/2)$, where δL is the distance radially from the center.

Now we solve equations for x, taking the δ factor into account, as well as $F_{\text{ECT}} = 2(F_{\text{CD}} + F_{\text{MD}})$, getting

$$x_{\text{CD}} = \left(1 - \frac{2\delta L}{l}\right)\sqrt{\frac{F_{\text{CDMAX}}(l - L_{\text{CD}})}{2EL_{\text{MD}}}}, \qquad x_{\text{MD}} = \left(1 - \frac{2\delta L}{l}\right)\sqrt{\frac{F_{\text{MDMAX}}(l - L_{\text{MD}})}{2EL_{\text{CD}}}},$$

$$x_{\text{ML}} = \left(1 - \frac{2\delta L}{l}\right)\sqrt{\frac{F_{\text{UPMAX}}}{\left(\frac{2EL_{\text{MD}}}{l - L_{\text{CD}}} + \frac{2EL_{\text{CD}}}{l - L_{\text{MD}}}\right)}}, \qquad x_{\text{ECT}} = \sqrt{\frac{F_{\text{ECTMAX}}}{\left(\frac{2EL_{\text{MD}}}{l - L_{\text{CD}}} + \frac{2EL_{\text{CD}}}{l - L_{\text{MD}}}\right)}}.$$

To obtain energy, we integrate the Taylor-expanded version of $F_{\text{UP}} + mg$:

$$A_T(x) = 2E\frac{x_F^3}{3}\left(\frac{L_{\text{MD}}}{l - L_{\text{CD}}} + \frac{L_{\text{CD}}}{l - L_{\text{MD}}}\right) + mgx_F,$$

where $x_F = \min\{x_{\text{CD}}, x_{\text{MD}}, x_{\text{ML}}, x_{\text{ECT}}\}$.

Now we can substitute the maximum values of the respective forces and solve for the x-values. We use the same values of $F_{\text{UP}} = P_{\text{ML}}L_{\text{MD}}L_{\text{CD}}$ and $F_{\text{ECT}} = 4P_{\text{ECT}}l$. For the cracking forces, we double their values to take into account both springs on the side of the tire. So this gives

$$F_{\text{CD}} = 2(P_{\text{CD}} + P_{\text{MD}})wL_{\text{CD}}, \qquad F_{\text{MD}} = 2(P_{\text{CD}} + P_{\text{MD}})wL_{\text{MD}}.$$

We make one last change. Energy is absorbed not only from the elasticity of the top but also from that of the edges. We determine the average force on this edge spring and the change in the depression x that occurs for this spring. It is reasonable to use average force, because this is over a small distance, and a parabolic function is reasonably linear in such an interval. Using modulus of elasticity E and first-order Taylor approximations, we estimate the displacement and energy absorbed.

We also assume that the edge does not fail before the top. The is reasonable because an edge has greater structural integrity.

So, assume that we are dealing with edge on which F_{CD} acts. To find the average force, integrate F_{CD} with respect to distance and divide by distance. Denote by x_F the depression at which failure occurs in our original top model. The average force is

$$\overline{F_{\text{CD}}} = EL_{\text{MD}}\left(\frac{x_F^2}{3(l - L_{\text{CD}})}\right).$$

To solve for Δx, observe that if the force is centered at the edge, then

$$\Delta x = \sqrt{\left(\frac{l}{2}\right)^2 + x_{\text{CD-EDGE}}^2} - \frac{l}{2}.$$

Taking a first-order Taylor approximation gives $\Delta x = x^2_{\text{CD-EDGE}}/l$. Using Hooke's law and $\overline{F_{\text{CD}}} = E\Delta x$, we solve for the depression of this spring $x_{\text{CD-EDGE}}$:

$$x_{\text{CD-EDGE}} = \sqrt{L_{\text{MD}}l\left(\frac{x_F^2}{3(l - L_{\text{CD}})}\right)}.$$

The corresponding energy is

$$A_{\text{CD}-EDGE} = \overline{F_{\text{CD}}}\Delta x = EL_{\text{MD}}x^2_{\text{CD-EDGE}}\left(\frac{x_F^2}{3(l - L_{\text{CD}})}\right) + mgx_{\text{CD-EDGE}}.$$

At this point, we assume that even though we have treated the two spring groups (the top and the edge) as separate systems—despite the fact that they move and affect each other dynamically—we can add the depression values x and energy absorption results A. This simplifying assumption is valid because the depressions are small enough that the approximations are the same as in the dynamic case. To obtain $x_{\text{MD-EDGE}}$ and $A_{\text{MD-EDGE}}$, interchange CD and MD.

So, reviewing, we have $x_F = \min(x_{\text{CD}}, x_{\text{MD}}, x_{\text{ML}}, x_{\text{ECT}})$ and total depression $x_{\text{NET}} = x_F + 2x_{\text{CD-EDGE}} + 2x_{\text{MD-EDGE}}$ and $A_{\text{NET}} = A_F + 2A_{\text{CD-EDGE}} + 2A_{\text{MD-EDGE}}$. We calculate

$$\overline{F_{\text{NET}}} = \frac{A_F + 2A_{\text{CD-EDGE}} + 2A_{\text{MD-EDGE}}}{x_{\text{NET}}}.$$

Finally, we take into account the fact that as the mass falls, it gains energy from gravity is countered by the energy gained. This fact leads to the important equation for A_T (the energy change during the top failures):

$$A_T = A_{\text{NET}} - mg(x_{\text{NET}}).$$

Single-Crack Buckling

We deal with energy dissipation for single-crack buckling, which occurs when a single side develops a crack from the top to a side. We model this as two sets of springs (**Figure 3**).

Once the top (side III) and a single side (side I) become weak, all corners but the two adjacent to the crack (C_1, C_2) remain strong. The only nonrigid corners, free to move, are C_1 and C_2. We assume that we are in the elastic range of the cardboard, so we can model this situation with two springs connected to the adjacent corners. We have springs connecting C_4 and C_1, C_5 and C_1, C_3 and C_2, C_6 and C_2. We apply the same methods as used in modeling the top to determine the energy as a function of how much the edges move in. [EDITOR'S NOTE: We do not give all the details.] The total force exerted by the box is

$$F_{\text{NET}} = 2E_{\text{MD}}\frac{l}{10}\left(\sqrt{l^2 + x^2} - l\right) + 2E_{\text{CD}}\frac{l}{10}\left(\sqrt{l^2 + x^2} - l\right)$$

Figure 3. Our model of a box that is buckling.

and the buckling energy is

$$A_B = (E_{\text{MD}} + E_{\text{CD}}) \frac{l}{10} \left(l^2 \ln(\sqrt{l^2 + x^2} + x) + x\sqrt{l^2 + x^2} - 2lx - l^2 \ln l \right)$$
$$+ mgx_{\text{DOWN}}.$$

where x_{DOWN} is the component of x that points downwards from the edge.

Now we use methods similar to those used in modeling the top to determine the maximum x-displacement that can occur before the tensile strength is exceeded.

If the force F_{MD} on the machine direction spring (across the flutes) exceeds $P_{\text{MD}}wl/10$ (the tensile strength), then a crack occurs in the cross-machine direction, with

$$x_{\text{MD}} = \sqrt{\left(\frac{P_{\text{MD}}lw}{E_{\text{MD}}}\right)^2 + \frac{2P_{\text{MD}}wl^2}{E_{\text{MD}}}}.$$

Likewise, if the force F_{CD} on the cross-machine direction spring (along the flutes) exceeds $P_{\text{CD}}wl/10$, then a crack occurs in the machine direction, with

$$x_{\text{CD}} = \sqrt{\left(\frac{P_{\text{CD}}lw}{E_{\text{CD}}}\right)^2 + \frac{2P_{\text{CD}}wl^2}{E_{\text{CD}}}}.$$

The minimum of these x-displacements indicates when failure occurs. After failure, the box has less potential to continue to absorb energy. We also assume that the motorcycle has gone a significant distance, so there is little distance left to compress.

We make one last change, taking into account gravity's contribution. First, we solve for the depression of the tire during buckling, before failure. We have assumed that the buckled edge moves in towards the box's center. The total depression, x_{DOWN}, can be calculated, with a geometric argument, to be $\sqrt{lx - x^2}/\sqrt{2}$. Using this, we get a final value for A_B:

$$A_B = (E_{\text{MD}} + E_{\text{CD}})\frac{l}{10}\left(l^2 \ln(\sqrt{l^2 + x^2} + x) + x\sqrt{l^2 + x^2} - 2lx - l^2 \ln l\right)$$
$$+ \frac{mg\sqrt{lx - x^2}}{\sqrt{2}}$$

and

$$\overline{F_{\text{BNET}}} = \frac{(E_{\text{MD}} + E_{\text{CD}})\frac{l}{10}\left(l^2 \ln\left[\sqrt{l^2 + x^2} + x\right] + x\sqrt{l^2 + x^2} - 2lx - l^2 \ln l\right)}{\frac{\sqrt{lx-x^2}}{\sqrt{2}}} + mg.$$

With the same argument as for the top, we obtain

$$A_B = (E_{\text{MD}} + E_{\text{CD}})\frac{l}{10}\left(l^2 \ln(\sqrt{l^2 + x^2} + x) + x\sqrt{l^2 + x^2} - 2lx - l^2 \ln l\right).$$

Drawbacks of the One-Box Model

- The model does not take torque into account.

- The time-independence of all of our quantities makes it difficult to solve for quantities such as friction.

- The energy absorbed by the top of the box seems lower than desired.

- This model is difficult to extend to interactions between multiple boxes.

Stacking Two Identical Boxes

Consider two identical boxes, one stacked perfectly on the other, and suppose that the tire strikes the top of the higher box. We claim:

- The top box cracks, buckles, and/or punctures first; since it absorbs some of the force that acts on it, force it exerts on the second box is diminished.

- The lower box's top does not crack or puncture, it only buckles. Once the upper box has buckled, we may assume it is reasonably flattened. Then, the effective top of the second is at least two times—or maybe even three (if no punctures have occurred in the top of the first box) times—the thickness of a cardboard top. This effectively doubles or triples the tensile strength of the top, since tensile strength depends on width. Furthermore, the force from the motorcycle tire, now felt through extra cardboard, is spread over a larger area decreasing its ability to depress the top of the box.

The Effects of Friction and Adjacent Boxes

Preliminaries

For large box configurations, we predict that the following occur:

- As the motorcycle propels through boxes, it loses momentum through collisions.

- Each box experiences friction with other boxes and with the ground. Combined, these aid in slowing the motorcycle.

Average Friction Experienced

Suppose that the combined mass of the motorcycle and boxes that have "stuck" to it is m. Furthermore, let m_b be the mass of the box(es) that this system is about to strike horizontally. The frictional force is $\mu \cdot N$, where μ is the coefficient of friction and N is the force. For box-to-box interactions, $\mu \approx 0.4$; and for box-to-ground interactions, $\mu \approx 0.6$.

Let the motorcycle-boxes system have initial mass m and strike a box with initial vertical speed v_{iz} and horizontal y speed v_{iy}. By conservation of momentum, the new vertical speed is $v_y = mv_{iy}/(m + m_b)$. In our one-box model, we developed an expression for the average upwards force acting on a box, namely $\overline{F_{\text{NET}}}$ and $\overline{F_{BNET}}$. These forces are functions of x; for simplicity, we assume that the normal force felt equals the average force exerted upon the motorcycle by the box. We use the precalculated average forces due to buckling, cracking, and/or puncturing.

Thus, the average frictional force experienced is: $f_s = \mu \overline{F}$.

Horizontal Distance Travelled

To calculate the energy (and thus speed) that the motorcycle loses to friction, we determine the horizontal distance that the motorcycle travels while experiencing this frictional force. We make several approximations to estimate the horizontal energy lost during compression. Without loss of generality, suppose that we wish to calculate the horizontal distance travelled in the y-direction.

Since the vertical energy lost is ΔA_z, the final z velocity is

$$v_{fz} = \sqrt{2(A_z - \Delta A_z)/m};$$

and an approximate expression for the average z-velocity during this time is

$$\overline{v}_z \approx \frac{v_{fz} + v_{iz}}{2}.$$

This gives us the approximate time span of this event, $\bar{t} \approx x/\overline{v_z}$. Although the horizontal speed in the y-direction changes due to friction, for the purposes of calculating the horizontal distance d travelled we treat it as constant to obtain

$$d = v_y\bar{t} = \frac{mv_{iy}}{m + m_b} \frac{2x}{\sqrt{2(A_z - \Delta A_z)/m} + v_{iz}}.$$

Thus, the approximate energy lost to friction is

$$\Delta A_y = \mu\overline{F}d = \mu\overline{F} \cdot \frac{mv_{iy}}{m + m_b} \frac{2x}{\sqrt{2(A_z - \Delta A_z)/m} + v_{iz}},$$

and the new horizontal speed after this occurs is

$$v_{fy} = \sqrt{2\left(\frac{1}{2}mv_{iy}^2 - \Delta A_y\right)/(m + m_b)}.$$

Analogous equations are hold for frictional forces acting in the x-direction.

The Dual-Impact Model (DIM)

Since it simplifies computer modeling immensely while maintaining approximate accuracy, our multi-box model consists of a large three-dimensional array of points, where each point represents a 10 cm $\times$ 10 cm $\times$ 10 cm cube. The boxes have side-length 90 cm, 70 cm, or 50 cm and occupy "cubes" of these points in space. This has immediate simplifying consequences:

- Since boxes are modeled within a discrete set, their representations do not have full freedom of movement in the set. Therefore, while calculations involving buckling, cracking, and the like are done for each box, the box is modeled in the set as either existing or being flattened. Furthermore, movement will be rounded to the nearest 10 cm.

- This particular model does not allow boxes to be kept "off-angle," spinning, or modeled as flipping. It is the buckling that slows the motorcycle.

Which Configurations Are Desirable?

We prefer configurations that

- minimize the number of boxes used;

- minimize the magnitude of force acting upon the motorcycle—at most an acceleration of $5g$, if possible; and

- ensure that the motorcycle has no downward component of velocity by the time it reaches the ground (if it ever does) and that the motorcycle goes through as many boxes as possible without hitting the ground.

Preliminary Assumptions

- The front and rear motorcycle wheels have the same velocity.

- The motorcycle has the same angle of inclination when it lands as it did when it took off; that is, the back wheel lands on the cardboard boxes first.

- The motorcycle plus cyclist has sufficient velocity not to fall over.

- The motorcycle moves in the cross-machine direction of the top box.

- The boxes are in layers; boxes in a layer are all the same size.

- The mass of boxes m_b that the motorcycle with mass m strikes are sufficiently small that they can be neglected, i.e., $m + m_b \approx m$.

Step-by-Step Description of the Algorithm

Given a box configuration, the two inputs required by our simulation are the position that the bottom tire strikes the first box at and the velocity vector of the motorcycle.

The first interaction is the stress and failure of the top of the first box struck. Here our simulation uses the One-Box Model extensively. The distance of the tire from the center of the box determines which type of top failure occurs. This failure determines the change in vertical energy; our simulation calculates the energy loss for both horizontal directions.

Once the top fails, we model the buckling of the box, getting the change in vertical velocity and the distance/velocities with which the motorcycle has moved horizontally (taking friction into account).

This entire process is repeated for the front wheel of the motorcycle, as we assume that the front wheel pivots around the rear wheel to a box of its own with similar conditions. We refer to all of these combined interactions, which occur with the back and front wheels on their first box, including top failure and buckling, as the *primary impact*.

The *secondary impact* involves the motorcycle interacting with all boxes after the first. Although many more boxes are involved, the forces tend to be much more well-distributed. The inputs to the simulation are the velocity and position vector of the motorcycle. The only failure that can occur on a box below the first is buckling, when the force exerted exceeds the ECT yield strength. Frictional forces continue to affect the velocity, and some vertical velocity is absorbed in buckling the boxes. The DIM also allows for multiple boxes to buckle at once. In fact, this model automatically allows the box that is covered the most by the current box to buckle, as well as any other boxes whose tops are covered more than 15% by the current box. After this process is evaluated, the motorcycle's horizontal and vertical positions and recorded, and the process continues with the next layer.

Testing the Dual-Impact Model

We use a computer to simulate various patterns and sizes of boxes, including simple stacks of boxes on top of each other in columns, more-random configurations, and pyramidal configurations. For each configuration, we vary the speed at which the motorcycle leaves the ramp. We consider

- the maximum height, to determine whether the jump clears the elephant;

- variations in the speed and angle from which the motorcycle leaves the ramp;

- box-on-box interactions in transferring energy and dissipating heat through friction; and

- whether a configuration would stop the motorcycle's motion in all directions.

We find compelling evidence for using larger boxes in a pyramidal configuration.

The optimal configuration uses three layers of boxes 90 cm on a side stacked so that that every box (except those at the bottom) rest equally on four others. Also, smaller boxes at the bottom is a good strategy for absorbing energy. In fact, when height is an issue, having a large box with smaller boxes beneath it does better than all other smaller alternatives. The second-best configuration is a pyramid with 50 m boxes in the base, 70 cm boxes in the middle layer, and 90 cm boxes on top.

Our tests indicate that buckling is the main source of energy absorption: Buckling takes place over a much great distance than other failures and tends to last much longer.

Decelerations during energy absorption remain reasonable and within our bound of $5g$.

Why are pyramids such effective shapes? When a motorcycle hits a box and eventually interacts with the boxes bordering it below, the more boxes with large areas in contact with the box, the more energy dissipation. Every box buckles, not just the top one, as is the case for a column configuration. Pyramids also have a stability hardly found in standard columns of boxes, which individually collapse quite easily.

Conclusions and Extensions of the Problem

Solving the Problem

A motorcycle clearing a midsized elephant can be stopped effectively by 90 cm boxes but not as effectively by smaller ones, even in greater numbers. In addition, larger boxes have a higher chance of cracking, since the top of a large box has more give than a smaller box; this is useful, since additional energy is absorbed. Finally, one needs fewer large boxes.

Estimating how many boxes to use requires solving for the area in which the motorcycle could land and multiplying it by the number of layers of boxes. The approximate range in the y-direction is

$$
\frac{(v_e + \delta v) \cos \theta}{g} \left[(v_e + \delta v) \sin \theta + \sqrt{(v_e + \delta v)^2 \sin^2 \theta + 2g(h_r - h_b)} \right]
$$
$$
- \frac{(v_e - \delta v) \cos \theta \cos \delta \phi}{g} \left[(v_e - \delta v) \sin \theta + \sqrt{(v_e - \delta v)^2 \sin^2 \theta + 2g(h_r - h_b)} \right],
$$

(3)

where v_e is the expected velocity, δv is the deviation in velocity, $\phi = 0$, and $\delta \phi$ is the offset from the targeted position. The range in the x-direction is

$$
2 \frac{(v_e + \delta v) \cos \theta \sin \delta \phi}{g} \left[(v_e + \delta v) \sin \theta + \sqrt{(v_e + \delta v)^2 \sin^2 \theta + 2g(h_r - h_b)} \right].
$$

(4)

The area to be covered is the product of **(2)** and **(3)**.

Each 90-cm box that buckles absorbs 4 million kg-cm^2/s^2. With the pyramid setup, looking at both wheels, 2 boxes buckle on first impact, 8 on the next level, and 15 on the third (assuming that the first two boxes were separated by one box). Instead of determining the number of boxes that intersect from both the front and back wheels, we assume an upper bound of $N(N + 1)(2N + 1)/6$, where N is the number of levels.

Knowing how much energy the boxes can absorb helps generalize the solution to motorcycles of any mass and jumps of any height.

Strengths of the Model

- All of our assumptions are well-grounded in the literature

- Our time-independent model allows for simple modeling without delving into the realm of differential equations.

- The values we obtain are reasonable.

Weaknesses of Model and Further Study

- Our ability to model certain interactions, such as friction and lateral velocity, is severely limited by the approximations that we are forced to make.

- Our model is discrete and thus cannot incorporate torques, slipping, and other such effects.

References

Abbreviations and definitions. n.d. `http://www.corrugatedprices.com/reference/definitions.html` .

Advantages of corrugated packaging. n.d. `http://www.fcbm.org/technology/advantages.htm` .

Benenson, Walter, et al. (eds.). 2002. *Handbook of Physics*. New York: Springer-Verlag.

ECT vs. # test. n.d. `http://www.papermart.com/packaging/info-ect.htm` .

Formed cardboard, formed hardboard parts. n.d. `http://www.diedrichs.de/uk/pappe_hartf.htm` .

Habitat utilisation in an elephant enclosure. n.d. `http://asio.jde.aca.mmu.ac.uk/new_gis/analysis/elephant.htm` .

Heritage Paper. n.d. `http://www.heritage-paper.net/packaging.html` .

Matcom: The properties of paper and cardboard. n.d. `http://www.enged.com/students/matcom/matcom89.html` .

Motorcycle specs. n.d. `http://home.pacbell.net/will207/motorcycle.htm` .

Motorcycle tire size conversion, speed ratings, load ratings chart. n.d. `http://www.webbikeworld.com/Motorcycle-tires/tire-data.htm` .

MSN learning and research—Elephant. *Encarta*. n.d. `http://encarta.msn.com/encnet/refpages/RefArticle.aspx?refid=761575386` .

Packaging glossary. n.d. `http://www.euro-corrugated-box.com/box_terms.htm` .

Party poopers?: NJ lawmakers limit roller coasters. 2002. WPVI.com Action News (15 September 2002). `http://abclocal.go.com/wpvi/news/09152002_nw_coasters.html` .

Urbanik, Thomas J. 1997. Linear and nonlinear material effects on postbuckling strength of corrugated containers. *Mechanics of Cellulosic Materials* 221: 93–99.

_____ . 1999. Nonlinear finite element modelling of corrugated board. *Mechanics of Cellulosic Materials* 231: 101–106.

Thinking Outside the Box and Over the Elephant

Melissa J. Banister
Matthew Macauley
Micah J. Smukler
Harvey Mudd College
Claremont, CA

Advisor: Jon Jacobsen

Abstract

We present a mathematical model of the collapsing of a box structure, which is to be used to protect a stunt motorcyclist who jumps over an elephant. Reasonable values of the model's parameters cause it to predict that we should construct the structure out of fifty $6\,\text{in} \times 28\,\text{in} \times 28\,\text{in}$ boxes, stacked five high, two wide, and five long. In general, the model predicts that we should use boxes whose height is one-quarter of the harmonic mean of their length and width. We discuss the assumptions, derivation, and limitations of this model.

Introduction

A stunt motorcyclist jumps over an elephant; we use cardboard boxes to cushion the landing. Our goal is to determine how to arrange the boxes to protect the motorcyclist. We determine

- how many boxes to use,

- the size of the boxes.

- the arrangement of the boxes, and

- any modifications to the boxes.

In addition, our model must accommodate motorcyclists jumping from different heights and on motorcycles of different weights. Our goal is to reduce the impulse at landing, thus essentially simulating a much lower jump (of which we assume the rider is capable).
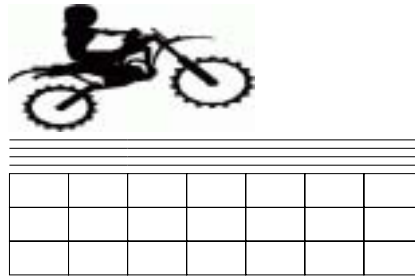
Figure 1. The landing platform (graphic from Just'In Designs [2001]).

As the rider breaks through the top layer of boxes, crashing through cardboard at a high horizontal speed, it will be difficult to maintain balance. It is too dangerous to rely on the cardboard to stop the horizontal motion of the rider, unless we use such a large pile that keeping it from being visible to the camera would be nearly impossible.

We are faced with how to cushion the rider's landing without creating merely a pit of boxes. Imagine jumping from a 10-ft roof. If the jumper lands on a large wooden platform resting on a deep foam pit, the risk for injury is much less; the foam spreads out the jumper's deceleration over a much longer time, simulating a much lower jumping height.

Our goal is to create a landing platform for the motorcyclist that behaves much like the wooden platform on the foam pit. We simulate the foam pit by stacks of boxes. Our "platform" is constructed from boxes unfolded into cardboard flats and placed in a layer on top of the "pit" (**Figure 1**). The idea is that the motorcyclist should never break through this layer of flats but should merely break the boxes underneath it.

Safety Considerations

- Once the motorcycle has landed on the stack of cardboard boxes, its deceleration should to be as uniform as possible as the structure collapses—the more uniform the deceleration, the easier to maintain balance.

- We want the platform to remain as level and rigid as possible. If it is not level, the rider may lose balance; it it is insufficiently rigid, it may bend and collapse into the pile of boxes.

Terminology

- The **flute type** of a gauge of cardboard refers to its corrugated core structure. Three sheets of linerboard compose one sheet of corrugated cardboard;the middle one is shaped into flutes, or waves, by a machine, and then the outer two sheets are glued on either side of it. For example, C-flute corrugated cardboard is the most common form [Mall City Containers n.d.].

- The **edge crush test** (ECT) value of a gauge of cardboard is the force per unit length that must be applied along the edge before the edge breaks. We make extensive use of the concept of such a value; however, the actual numbers given for gauges of cardboard apply to ideal situations that would not be replicated in the cases that we are considering [Boxland Online 1999].

- The **flatwise compression test** (FCT) value of a gauge of cardboard is the pressure that must be applied to collapse it. It does not directly correlate to the stress placed on boxes in practice and therefore is not used as an industry standard [Pflug et al. 2000].

- The **bursting strength** of a gauge of cardboard is the amount of air pressure required to break a sample. Because our model is concerned mainly with the strength of a box edge, but the bursting strength more accurately measures the strength of a face, we do not make use of it [Boxland Online 1999].

- The **stacking weight** of a box is the weight that can be applied uniformly to the top of a box without crushing it. In general, the stacking weight of a box is smaller than the ECT or bursting strength, because it takes into account the structural weaknesses of the particular box. We derive most of our numerical values for box strength from manufacturers' specified stacking weights [Bankers Box 2003].

Assumptions

- *The force exerted on every layer beneath the top platform is horizontally uniform.* The force that the motorcycle exerts on the top platform is concentrated where the wheels touch. Ideally, however, this top platform is perfectly flat and rigid, so it distributes the force evenly to all lower layers. We approach this ideal by adding additional flats to the top platform.

- *The stacking weight of a box is proportional to its perimeter and inversely proportional to its height.* This assumption is physically reasonable, because weight on a box is supported by the edges and because the material in a taller box on average is farther from the box's points of stability than in a shorter box. This claim can be verified from data [Clean Sweep Supply 2002].

- *Nearly all of the work done to crush a box is used to initially damage its structural integrity.* After the structure of a box is damaged, the remaining compression follows much more easily; indeed, we suppose it to be negligible. We denote by d the distance through which this initial work is done and assume for simplicity that the work is done uniformly throughout d. Through rough experiments performed in our workroom, we find that $d \approx 0.03$ m. We assume that this value is constant but also discuss the effect of making it a function of the size of box and of the speed of the crushing object.

Figure 2. Tire before and after landing, acting as a shock absorber.

- *When the motorcycle lands, we ignore the effects of any shock absorbers and assume that the motorcyclist does not shift position to cushion the fall.* This is a worst-case scenario. To calculate how much force the tires experience per unit area, we consider a standard 19-inch tire of height 90 mm and width 120 mm [Kawasaki 2002]. It compresses no less than 50 mm (**Figure 2**). A simple geometry calculation then tells us that the surface area of the tire touching the platform is approximately 3000 mm^2. We assume that the force exerted on the motorcycle on landing is uniformly distributed over this area.

- *The pressure required to compress a stack of cardboard flats completely is the sum of the pressures required to compress each individual flat.*

- *In a uniformly layered stack of boxes, each layer collapses completely before the layer beneath it begins to collapse.* This is probably an oversimplification; however, it is reasonable to suppose that the motorcycle is falling nearly as fast as the force that it is transmitting.

- *The motorcyclist can easily land a jump 0.25 m high.*

The Model

Crushing an Individual Box

For a cardboard box of height h, width w, and length l, by the assumptions made above, the stacking weight S is

$$S(h, l, w) = \frac{k(l + w)}{h},$$

where k is a constant (with units of force).

Once a box is compressed by a small amount, its spine breaks and very little additional force is required to flatten it. Thus, most of the force that the box exerts on the bike is done over the distance $d \ll h$, and we assume that the work is done uniformly over this distance; this work is

$$W = (\text{force})(\text{distance}) = \frac{k(l + w)d}{h}.$$

Crushing a Layer of Boxes

To ensure that a layer of boxes collapses uniformly, we build it out of n identical boxes. The total amount of work required to crush such a layer is

$$W_T = n\,\frac{k(l+w)d}{h}.$$

Once the structure starts to collapse, we want the rider to maintain a roughly constant average deceleration g' over each layer. It follows that the layer should do total work $m(g+g')h$, so

$$W_T = \frac{nkd(l+w)}{h} = m(g+g')h\,. \tag{1}$$

Define $A = nlw$ to be the cross-sectional area of a layer of boxes; rearranging **(1)** produces

$$B \equiv \frac{Adk}{m(g+g')} = \frac{h^2 lw}{l+w}. \tag{2}$$

The constant B gives a necessary relationship among the dimensions of the box if we wish to maintain constant deceleration throughout the collision.

Finally, we would like to minimize the total amount of material, subject to the above constraint. To do so, consider the *efficiency* of a layer with a given composition of boxes to be the ratio of amount of work done to amount of material used. If the motorcyclist peaks at a height h_0, we must do work mgh_0 to stop the motorcycle. We minimize the total material needed by maximizing the efficiency of each layer.

The amount of material in a box is roughly proportional to its surface area, $S = 2(hl + lw + wh)$. Thus the amount of material used by the layer is proportional to $nS = 2n(hl + lw + wh)$. It follows that the efficiency E of a layer composed of boxes of dimensions $h \times l \times w$ is

$$E \propto \frac{W_T}{nS} = \frac{nkd(l+w)}{2nh(hl+lw+wh)} = \frac{kd(l+w)}{2h(hl+lw+hw)}.$$

We maximize E for each layer, subject to the constraint **(2)**. The calculations are easier if we minimize $1/E$. Neglecting constant factors, we minimize

$$f(h,l,w) = \frac{h}{l+w}(hl+hw+lw)$$

subject to the constraint

$$\frac{h^2 lw}{l+w} = B,$$

where B is the constant defined in **(2)**. However, as long as we are obeying this constraint (that each layer does the same total work), we can write

$$f(h,l,w) = h^2 + \frac{hlw}{l+w} = h^2 + \frac{B}{h},$$

and thus f depends only on h. The function f is minimized at

$$h = \sqrt[3]{\frac{B}{2}} = \sqrt[3]{\frac{Adk}{2m(g + g')}}. \tag{3}$$

At this value of h, the constraint reduces to

$$\frac{lw}{l + w} = \frac{B}{h^2} = \sqrt[3]{4B}.$$

This implies that the harmonic mean of l and w should be

$$H \equiv \frac{2lw}{l + w} = 2\sqrt[3]{4B} = 4h.$$

So, in the optimal situation, the box should be roughly four times as long and wide as it is tall. However, there are other considerations.

- For commercially available boxes, we must choose among some discrete set of realizable box dimensions.

- That the number n of boxes in a layer must be an integer affects the possible values of many of the parameters on which h is based (most notably A, the cross-sectional area of the layer). We select the box among the potential candidates which most nearly compensates for this change in parameters.

The Entire Structure

We need to determine the gross parameters of the entire structure. We determine the cross-sectional area of the structure by considering how much space the motorcyclist needs to land safely. The motorcycle has length about 1 m; we should leave at least this much space perpendicular to the direction of travel. We need substantially more in the direction of travel, to ensure that the motorcyclist can land safely with a reasonable margin of error. So we let the structure be 1 m wide and 3 m long, for a cross-sectional area of 3 m^2.

How many corrugated cardboard flats should we use? We do not want them all to crease under the weight of the motorcycle and rider, for then the motorcyclist could be thrown off balance. So we must determine how much we can expect the flats to bend as a result of the force exerted by the motorcycle.

To calculate the number of flats required, we use the flatwise compression test (FCT) data in Pflug et al. [2000] for C-flute cardboard. Though our goal is to prevent substantial creasing of the entire layer of flats, we note that if we have a reasonable number of flats, creasing the bottom flat requires completely crushing a substantial area along most of the remaining layers. Less than 20% of this pressure is required to dimple a sheet of cardboard to the point where it may be creased. Since we assume that the pressure required to crush the flats scales linearly with the number of flats, we find the maximum pressure that

the motorcycle will ever exert on the flats and divide it by the FCT value for a single C-flute cardboard flat order to obtain the total number of sheets needed.

A brief examination of a piece of cardboard demonstrates that bending it in the direction parallel to the flutes is much easier than bending it in the direction perpendicular to the flutes. Hence, it would be risky to orient all flats in the same direction; if force is applied along a strip of the surface, all of the flats may easily give way and bend in succession. So, it would be wise to alternate the orientation of the flats in the stack. To make sure that we have the full strength in any direction, we use *twice* the number of flats calculated, alternating the direction of the flutes of each flat as we build the stack. Then, no matter how the motorcycle is oriented when it lands on the stack, at least the required strength exists in every direction.

Finally, we determine the overall height h_1 of the structure as follows. The motorcycle accelerates downward at a rate of g from the peak of its flight to the top of the structure; this distance is $h_0 - h_1$. It then decelerates constantly at a rate of g' until it reaches the ground, over a distance h_1. Since the motorcycle is at rest both at the apex of its flight and when it reaches the ground, the relation

$$(h_0 - h_1)g = h_1 g'$$

must hold. It follows, then, that

$$h_1 = \frac{h_0 g}{g + g'}. \tag{4}$$

Finding the Desired Deceleration

To determine g', we need the height H of the jump. We discuss how to build the platform so that the rider does not experience a deceleration greater than for a 0.25-m jump.

We assume that most of the cushion of the landing is in the compression of the tires, which compress $\Delta x = 5$ cm. The vertical velocity of the rider on impact is $\sqrt{2gH}$. We also make the approximation that the motorcycle experiences constant deceleration after its tires hit the ground. So the rider travels at an initial speed of $\sqrt{2gH}$ and stops after 0.05 m. We determine the acceleration:

$$v_0^2 + v_f^2 = 2ax,$$
$$\left(\sqrt{2gH}\right)^2 + 0 = 2a(0.05).$$

Solving yields $a = 20gH$. That is, if the motorcyclist jumps to a height of 4 m, on landing the ground exerts a force on the motorcycle that feels like 80 times the force of gravity; if the jump were from 0.25 m, this force would be only $5mg$. To simulate a 0.25-m fall, we should have the motorcyclist decelerate at a rate of $5g$.

Numerical Results

We now return to the question of determining the number of flats needed for the top layer. By Pflug et al. [2000], the flatwise compression test (FCT) result for C-flute board is 1.5×10^5 Pa. We expect the motorcyclist to experience an acceleration of approximately $5g$ upon landing, distributed over a surface area of 3000 mm^2 = 0.003 m^2. We assume that the motorcycle has mass 100 kg [Kawasaki 2002] and the rider has mass 60 kg. The pressure exerted on the cardboard is

$$P = \frac{(160\,\text{kg})(5)(9.8\,\text{m/s}^2)}{0.003\,\text{m}^2} = 2.61 \times 10^6\,\text{Pa}.$$

For the cardboard at the bottom of the stack of flats to be bent significantly, enough pressure must be applied to crush most of the cardboard above it. Thus a lower bound on the number of flats is $\lceil (2.61 \times 10^6\,\text{Pa})/(1.50 \times 10^5\,\text{Pa}) \rceil = \lceil 17.4 \rceil = 18$ flats. To be perfectly safe, we double this figure and cross-hatch the flats; that is, we want 36 flats in the top platform, the flutes of which alternate in direction.

Next, we calculate the total mass of cardboard for these flats. We assume that the flats are 1 m × 3 m. From Gilchrist et al. [1999], we know that the density of C-flute corrugated cardboard is 537 g/m^2; we obtain a mass of 1.611 kg per flat, or about 60 kg for 36 flats, which is comparable to the weight of a second person. The thickness of a C-flute flat is 4.4 mm [Mall City Containers n.d.]; with 36 flats, the height of the stack is 158.4 mm.

We now plug some reasonable values into **(3)** and get a good approximation of the desired height of the boxes. Let the stacking weight constant $k = 800$ N; this is roughly the mean value found in Clean Sweep Supply [2002]. These values, along with $g' = 5g$, give an optimal h of roughly

$$h = \sqrt[3]{\frac{(3\ \text{m}^2)(0.05\ \text{m})(800\ \text{N})}{2(220\ \text{kg})\bigl[9.8 + 5(9.8)\ \text{m/s}^2\bigr]}} \approx 0.17\ \text{m}.$$

So the harmonic mean of l and w must be on the order of $4h = 0.67$ m.

Converting these values into inches gives $h = 6.5$ in and a value of roughly 26.5 in for the harmonic mean of l and w. The two commercially available box sizes that most closely approximate these values are 6 in × 26 in × 26 in and 6 in × 28 in × 28 in [Uline Shipping Supplies 2002]. Note that we must increase the cross-sectional area beyond what was calculated in order to keep the number of boxes per layer an integer. Doing so increases the total value of $B = Akd/m(g + g')$; thus, we ideally want a somewhat larger box than calculated. Since we cannot increase h (any commercially available box of this rough shape and size has a height of 6 in), we increase l and w. This choice increases the amount by which the cross-sectional area is larger than previously calculated. Since optimum values of l and w only change as $A^{1/3}$, however, the larger box is the closer to the optimum.

To have a landing pad of size at least $1\,\text{m} \times 3\,\text{m}$, we need two of these boxes lengthwise and five widthwise, for a total of 10 boxes per layer. We determine the total height h_1 of the pile as follows The average height of an adult male African elephant is $3.2\,\text{m}$ [Theroux 2002]; the motorcyclist could easily clear such an elephant with a jump of $h_0 \approx 4\,\text{m}$. From this value, and **(4)**, we obtain

$$h_1 = \frac{h_0 g}{g + g'} = \frac{h_0}{6} \; ;$$

thus, we want $h_1 \approx 0.67\,\text{m} = 26.2\,\text{in}$. To exceed this number with 6-inch layers, we need 5 layers.

To summarize: We use $6\,\text{in} \times 28\,\text{in} \times 28\,\text{in}$ boxes. There are 10 boxes in each layer of the stack, in a 2×5 grid, and the stack consists of 5 layers of boxes with 36 layers of cross-hatched cardboard flats piled on top.

Changing the Parameters

Because the dimensions of the boxes used vary as the cube root of B, which is either linear or inversely linear in most of our parameters, our results are fairly resistant to change in any parameter. For example, changing one of them by a factor of 2 changes the optimal box dimensions by only 25%; even increasing a parameter by an order of magnitude only doubles the dimensions.

The one exception is the jumping height. Since B is independent of that, so are the optimum box dimensions, except insofar as the height affects the amount of area. However, the jumping height does affect the height of the box pile; we want that to increase linearly with the jumping height, in a ratio given by the desired deceleration g'. Additionally, a very high or very low jumping height will cause our model to break down completely.

For C-flute cardboard in the flats, the total amount of cardboard needed essentially depends only on the weight of the motorcycle and rider and on the net deceleration. This may at first glance appear counterintuitive: Should we not expect the jumping height to affect the stress put on the flats? In fact, the height is irrelevant as long as the assumptions of the model are justified. Since the boxes below the flats are calculated to break upon experiencing a force mg', the force transmitted through the flats by the motorcyclist is never larger than this. The only exception is the initial force that the flats experience on first being hit by the motorcycle. If the jumping height is sufficiently large, the assumption—that this initial force is dominated by the normal force exerted by the boxes underneath—will break down, and we may need to increase the thickness beyond the value calculated. However, for jumping heights this large, it is probable that other parts of our model will break down.

Certain predictions of our model are independent of its parameters, so long as our assumptions are justified. Most notable is the observation that to best conserve material for a given result, the height of a box should be one-quarter

the harmonic mean of its other two dimensions, the ratio of which can be specified arbitrarily.

Finally, for very large jumps, we may need to revise our calculation of g'. While a rider may be comfortable with a deceleration of $5g$ for a small fraction of a second, it is less reasonable to assume the same comfort level if the deceleration is to last several seconds. However, we shouldn't be too concerned about this, since for jumps that are high enough for it to be an issue, our model is likely to break down in other ways.

Weaknesses of the Model

The primary weakness of our model is its dependence on the adjustable parameter d, the distance through which the work of crushing the box is done. We assume that over the box sizes that we are concerned with, d is roughly independent of the dimensions of the box; verifying the truth of this assertion would require experimentation. However, so long as d varies at most linearly with h (which is reasonable, since for any box we must have $d < h$), our method still works; we can still find a uniform optimal box size for the pile. If d depends substantially on the amount of force applied (or the velocity of the motorcycle), this will no longer be the case: the optimal box size will vary with position in the stack of boxes. However, we think this hypothesis is unlikely.

Our assumption that each layer collapses in a reasonably uniform manner is also a weakness in the model, at least for some parameter values. If the motorcycle hits the structure with too much velocity, or the desired cross-sectional area of the structure is too large, it may not be possible to layer enough flats on top of the structure to ensure uniform collapse, especially if restricted to commercially available cardboard sizes.

Finally, it is unlikely that we could find easily a supply of boxes whose faces are as large as $1\,\mathrm{m} \times 3\,\mathrm{m}$, to create the flats we want. While we could custom-order such flats, this would likely drive the price of construction up substantially. The other alternatives are to use several smaller flats in the place of each large one, or to unfold large cardboard boxes to make the flats. Doing this could weaken the structure, but this problem could likely be circumvented by varying the positions of the weak spots in each layer of flats (and possibly by slightly increasing the safety factor in the number of flats used).

Conclusion

We have designed a landing platform out of cardboard boxes for a stunt motorcyclist who will jump over an elephant. Our model of this platform predicts that we can minimize the material used by using boxes with dimensions $6\,\mathrm{in} \times 28\,\mathrm{in} \times 28\,\mathrm{in}$.

The size of the boxes used depends neither on the mass of the motorcyclist and jumper nor the height of the jump. To accommodate a higher jump, just use more layers of boxes. The calculations are based on simulating the landing of a 0.25-m jump. To simulate a lower jump, we would use slightly taller boxes.

An advantage to our model is the small size of the cardboard stack—less than 3 m^3—and specifically its short height. It should be easy to hide such a structure from the camera.

References

Bankers Box. 2003. Bankers Box frequently asked questions. `www.bankersbox.com/service/index.cfm`.

Baum, G.A., D.C. Brennan, and C.C. Habeger. 1981. Orthotropic elastic constants of paper. *Tappi Journal* 64 (2): 97–101.

Boxland Online. 1999. Flutes. `www.boxland.com/flutes.html`.

Clarke, J.W., and J.A. Marcondes. 1998. What pallet manufacturers should know about corrugated boxes. Tech. rept. 2. Blacksburg, VA: Center for Unit Load Design, Virginia Polytechnic Institute. `www.unitload.vt.edu/technote/980918/980918.htm`.

Clean Sweep Supply, Inc. 2002. Recycled Liberty Plus storage boxes. `http://www.cleansweepsupply.com/pages/skugroup13316.html`.

Gilchrist, A.C., J.C. Suhling, J. C., and T.J. Urbanik. 1999. Nonlinear finite-element modeling of corrugated board. *Mechanics of Cellulose Materials* 85: 101–106.

Just'In Designs. 2001. Free goldwig clipart. `www.just-in.net/clipart/dirt/index.htm`.

Kawasaki,Inc. 2002. Kawasaki motorcross off-road series. `www.fremontmotorsports.com/HTML/Kawasaki/kawasaki-MX-1.htm`.

Korchak, R. 2002. Motorcycle tire sizes. `www.webbikeworld.com/Motorcycle-tires/sizes.htm`.

Mall City Containers. n.d. Packaging basics. `www.mallcitycontainers.com/Packaging.htm`.

Pflug, J., I. Verpoest, and D. Vandepitte. 2000. Folded honeycomb cardboard and core material for structural applications. In *Proceedings of the 5th International Conference on Sandwich Construction*, 361–372.

Theroux, S. 2002. Animal records: Size. `www.swishweb.com/Animal_Kingdom/animal06.htm`.

Uline Shipping Supplies. 2002. Uline: Shipping supply specialists. `www.uline.com/Boxes_Search.asp`.

You Too Can Be James Bond

Deng Xiaowei
Xu Wei
Zhang Zhenyu
Southeast University
Nanjing, China

Advisor: Chen Enshui

Abstract

We divide the jump into three phases: flying through the air, punching through the stack, and landing on the ground. We construct four models to minimize the number and the cost of boxes.

In the Ideal Mechanical model, we consider the boxes' force on the motorcycle and stunt person as constant. In the Realistic Mechanical model, we focus on how the boxes support the motorcycle and stunt person, which includes three phases: elastic deformation, plastic deformation, and and crush-down deformation. However, in the Ideal Air Box model, the internal air pressure of each box can't be ignored. As a matter of fact, the boxes are unsealed, so we amend the Ideal Air Box model to develop a Realistic Air Box model. We discuss the strengths and weaknesses of each model.

We define a metric U, which is a function of the cost and the number of boxes. By mathematical programming, we calculate the size and the number of the boxes. In normal conditions, we that assume the safe speed is 5.42 m/s. For a total weight of stunt person and motorcycle of 187 kg, we need 196 boxes of size 0.7 m $\times$ 0.7 m $\times$ 0.5 m. We analyze the accuracy and sensitivity of the result to such factors as the total weight, the contact area, and the velocity. We also offer some important suggestions on how to pile up the boxes and how to change the shape of the boxes.

Assumptions and Analysis

About Boxes and the Pile of Boxes

- All the boxes are the same size. The ratio of length to width has little effect on the compression strength of a cardboard box; so to simplify the problem, we assume a square cross section.

Table 1.

Variables, parameters, and physical constants.

Notation		Description	Units
Box	h	height of box	m
	r	length of side of box	m
	Z	perimeter around top of box	m
	A_0	total surface area of box	m^2
	P	pressure in box (cylinder)	Pa
	P_t	pressure in box at time t when it collapses	Pa
	k	pressure in box at time t, in atmospheres	atm
	σ	rate of air leaking from box	m^3/s
	σ_i	rate of air leaking from box in time interval i	m^3/s
	V	volume of box (cylinder)	m^3
	V_i	volume of box in time interval i	m^3
Pile	L_{pile}	length of the pile	m
	W_{pile}	width of the pile	m
	H_{pile}	height of the pile	m
	L	number of layers of boxes in the pile	
	Num	total number of boxes	
	Cost	cost of boxes	
	S	upper surface area of pile	m^2
Jump	H_{elephant}	average height of the elephant	m
	H_{max}	maximum height of the jump	4 m
	ν	fraction of H_{max} that a person can reach	
	H_0	height of the ramp	m
	θ	angle of the ramp	
	v_0	launch speed	m/s
	v_{safe}	safe speed at which to hit the ground	m/s
	M	mass of motor plus stunt person	kg
Kellicut formula	P	compressive strength of the box	
	P_x	comprehensive annular compressive strength of the paper	
	dx_2	corrugation constant	
	Z	circumference of the top surface of the box	m
	J	box shape coefficient	
	F_0	maximum supporting force from the box	N
	F	buffering force of the box	N
	b	constant concerning the properties of paper	
Other	x, z	distance that the cylinder is compressed	m
	x_t	cylinder displacement when box collapses	m
	z_m	compression distance at which box collapses	m
	dt	interval of time	s
	W	work done	J
	D_s, k_1, k_2	quantities related to cost	
	λ_h, λ_c	weight factors	
	T, U	functions to be optimized	
Constants	g	acceleration due to gravity, at Earth's surface	m/s^2
	P_0	standard atmospheric pressure at Earth's surface	Pa

- After the box has been crushed down to some extent, we ignore the supporting force that it can still supply.

- Considering the practical production and transport limitations, the size of the box should not be too large.

- The boxes are piled together in the shape of a rectangular solid.

- When the motorcycle impacts one layer, it has little effect on the next layer. The layer below is considered to be rigid flat (its displacement is ignored).

- We ignore the weight of the boxes; they are much lighter than the person plus motorcycle.

About the Stunt Person and the Motorcycle

- We ignore the resistance of the air to the horizontal velocity of the person and motorcycle. The friction is so little that it is negligible.

- The stunt person has received professional training, is skilled, and is equipped with anything allowable for protection.

- The average weight of a stunt person is 70 kg.

- We choose a certain type of motorcycle (e.g., Yamaha 2003 TT-R225), which weighs 259 lb [Yamaha Motor Corp. 2003].

About the Elephant

- The elephant keeps calm during the jump.

- We adopt the classic value of 3.5 m for the height of the elephant [PBS Online n.d.].

About the Weather

The weather is fine for filming and jumping, including appropriate temperature and humidity. On a gusty day, the wind might make the person lose balance in the air.

About the Camera

The most attractive moment is when the person is over the elephant and at maximum height H_{max}. We have to make sure that the boxes do not appear on camera, namely, we need $H_{\mathrm{pile}} \leq \nu H_{\mathrm{max}}$, where the coefficient ν is best determined empirically. In our model, we set $\nu = 0.625$.

About the Ramp for Jumping

The ramp for jumping is a slope at angle θ of length L_{slope}, as determined by the jump height or horizontal distance for landing.

The Development of Models

When the stunt person begins to contact the cardboard boxes or the ground, he or she may suffer great shock. To absorb the momentum, the contact time must be extended.

We divide the whole process into three independent phases, that is:

1. flying through the air,

2. punching through the stack, and

3. landing on the ground.

We find out the maximum height in phase 1, the greatest speed of hitting the ground in phase 3, and how the person plus motorcycle interact with the boxes is based on the results of phases 1 and 3. Phases 1 and 3 are simple and we solve them first.

Flying through the Air

The stunt person leaves the ramp with initial speed v_0 at angle θ to the horizontal at height H_0 (**Figure 1**).
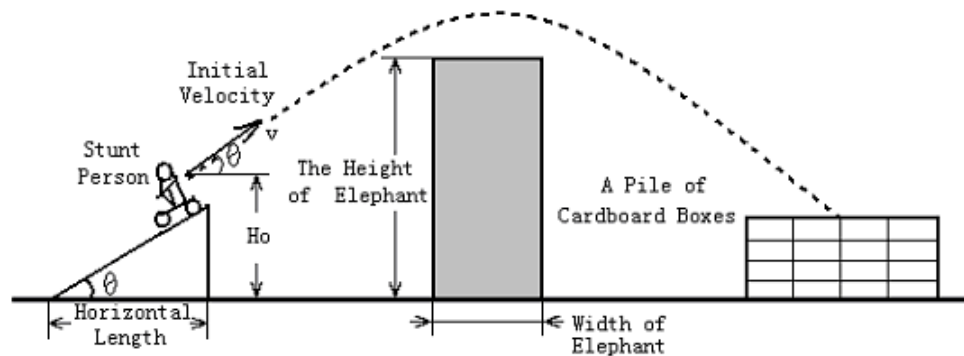
Figure 1. The jump.

In the air, the stunt person on the motorcycle is affected only by the constant acceleration of gravity. Based on Newton's Second Law, we have

$$x(t) = (v_0 \cos \theta)t,$$
$$y(t) = (v_0 \sin \theta)t - \tfrac{1}{2}gt^2,$$

where $x(t)$ and $y(t)$ are the horizontal and vertical displacements from the launch point after t seconds. The launch speed v_0 and the maximum height $H_{\max}$ are related by

$$v_0 \sin \theta = \sqrt{2g(H_{\max} - H_0)}.$$

For an elephant of height 3.5 m, we take $H_{\max} = 4$ m. For $H_0 = 0.5$ m and $\theta = 30°$, we get $v_0 = \sqrt{2 \cdot 9.8 \cdot 3.5}/0.5 = 16.6$ m/s. With a 2 m-high box-pile, the stunt person hits the pile with vertical speed 6.3 m/s and horizontal speed 14.3 m/s; the distance between the landing point and elephant is $D = 9.2$ m.

Would the Landing Be Safe?

To simplify the problem, we ignore the complex process when the person begins to touch the ground. We consider that there is a critical *safe speed* v_{safe}. If the speed hitting the ground is less than or equal to that speed, the person would not be injured. The safe speed is related to the ground surface (hard, grassplot, mud, etc.) and materials used (paper, rubber etc.). Our simulation uses a typical value, $v_{\text{safe}} = 5.42$ m/s.

Is the Pile Area Large Enough?

The height H_{pile} of the pile of boxes is related to the maximum height $H_{\max}$ that the stunt person reaches and also to the vertical speed of hitting the boxes. The greater $H_{\max}$, the greater H_{pile} is required, with $H_{\text{pile}} = Lh$, where L is the number of the layers of boxes and h is the height of a single box.

Would L_{pile} equal to the length of the person be enough? The answer is no. When accelerating on the ramp, the stunt person can't make the initial jump speed exactly what we calculate. We think that 3–5 times the length of the person is needed.

The stunt person does not leave the ramp aligned exactly alomg the central axis and does not keep the motorcycle exactly along that axis after hitting the boxes. That there may be some horizontal movement means that W_{pile} should be 2–4 times the length of the person.

In our simulation, we let $L_{\text{pile}} = 6$ m, $W_{\text{pile}} = 4$ m.

Boxes: How to Cushion the Person

Ideal Mechanical Model

Based on our general assumptions, we suppose that while the stunt person is destroying the boxes of the current layer, boxes in lower layers are seldom affected and keep still.

To illustrate the process of collision with just one layer separately, we suppose that the mutual effect of the stunt person and the box-pile is motion with a constant acceleration. During that, the stunt person plus motorcycle is supported by a constant vertical force F— that is, we treat F as the average force during the whole process.

It can be proved that although the stunt person strikes the boxes of different layers at different initial velocities, the work consumed to fall through each box is the same (**Appendix A**). The number of layers L of the box-pile is determined by the formula

$$\text{Work} \times L - mgh \geq \tfrac{1}{2}mv_0^2 - \tfrac{1}{2}mv_{\text{safe}}^2,$$

where L is the smallest integer that satisfies this inequality.

Strength and Weaknesses

This model is simple and efficient. However, we have ignored the detailed process and substituted constant work, though in fact the force changes with time.

Realistic Mechanical Model

First we study the empirical deformed load curve of the cushion system, showing the boxes' deformation under a static load (**Figure 2**) [Yan and Yuan 2000].
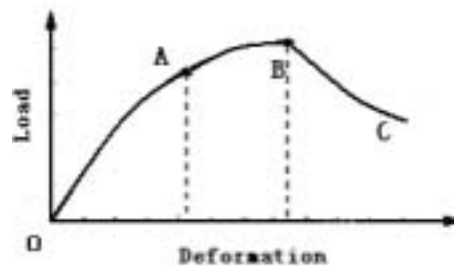
Figure 2. Deformation curve.

The compression process is divided into three phases, as shown in the figure:

- OA phase: Elastic deformation, according to Hooke Law.

- AB phase: Plastic deformation. The compression grows more slowly and reaches the maximum.

- BC phase: Crush-down deformation: After compression reaches the maximum, the rate of deformation starts to fall. The unrecoverable deformation goes on increasing.

According to the *Kellicut formula* [Yan and Yuan 2000; Zhao et al.], the compressive strength of a box is

$$P = P_x \left(\frac{dx_2}{Z/4} \right)^{1/3} ZJ,$$

where

P is the compressive strength of the box,

P_x is the comprehensive annular compressive strength of the paper,

dx_2 is the corrugation constant,

Z is the circumference of the top surface, and

J is the box shape coefficient.

For the stunt person plus motorcycle, the maximum supporting force from the box is nearly

$$F_0 = P \frac{s}{(Z/4)^2} = P_x \left(\frac{dx_2}{Z/4} \right)^{2/3} ZJ \frac{s}{(Z/4)^2} = bZ^{-5/3}s,$$

where b is a constant concerning the properties of paper.

We assimilate the static loading process to the dynamical process of getting impacted and obtain the following buffering force and its deformation graph (**Figure 3**).

$$F = \begin{cases} \dfrac{F_0}{a} x, & x \geq a; \\ F_0, & a \leq x \leq b; \\ F_0 \exp\left(\dfrac{-a(x-b)}{h} \right), & x \geq b. \end{cases}$$

The model describes the mechanical capability of the box and offers an appropriate curve of the relationship between buffering power and deformation. We can measure the energy consumed by the crushing of boxes. One limitation is the Kellicut formula, which applies only to certain kinds of cardboard boxes. Error may also occur in replacing the dynamical process with a static process.

Ideal Air Box Model

We consider the depleting energy consumed by the resistance of air in the process of compression. We divide the process into two phases:

Phase 1: Assume that the cardboard is closed (gas can't escape). The pressure in the box rises from standard atmospheric pressure P_0 to $P_t = kP_0$ (k atmospheres) at time t when the box ruptures. We consider that the impact is so
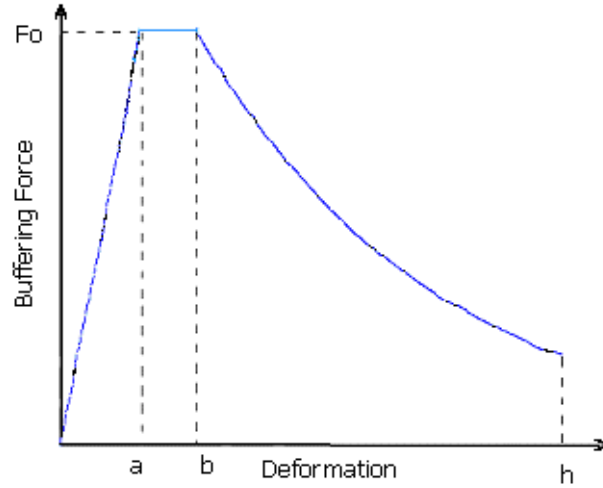
Figure 3. Force-deformation figure.

quick that the gas in the cardboard doesn't exchange energy with environ-
ment. So we can just deem it an adiabatic compression process. Using the
First Law of Thermodynamics, we get

$$PV^{1.4} = \text{constant}. \tag{1}$$

The proof is in **Appendix B**.

Phase 2: Under the effect of the impact and internal air pressure, cracks appear
in the wall of the cardboard box. The internal air mixes with the air outside,
quickly falling to standard atmospheric pressure P_0. We assume that the
cardboard box is a rigid cylinder and the compressive face (top surface) of
the box is a piston (**Figure 4**).

We calculate the internal pressure when the piston shifts downward a dis-
tance x from height h. Let s be the area of the top of the cylinder. According
to **(1)**, we have

$$P_0 \cdot [hs]^{1.4} = P \cdot [(h - x)s]^{1.4},$$

$$P = P_0 \left(\frac{h}{h - x} \right)^{1.4}. \tag{2}$$

The graph of P is shown in **Figure 5**.
Consider Phase 1. According to **(2)**, we have

$$P_t = kP_0 = P_0 \left(\frac{h}{h - x} \right)^{1.4}.$$

We solve for the displacement at time t:

$$x_t = h \left(1 - k^{-5/7} \right).$$
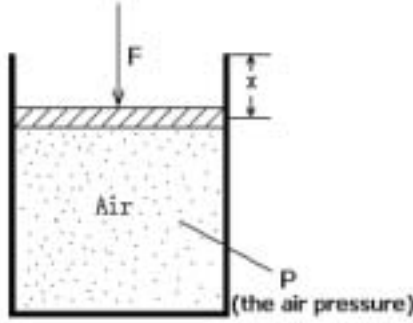
Figure 4. The cylinder model.
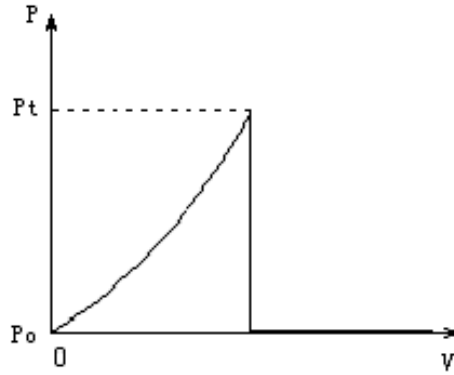
Figure 5. Internal pressure as a function of the volume of compressed air.

The compression work done in Phase 1 is

$$W_1 = \int_0^{x_t} P\, dV = s \int_0^{h\left(1-k^{-5/7}\right)} P_0 \left[\left(\frac{h}{h-x} \right)^{1.4} - 1 \right] dx$$

$$= P_0 s h \left(\frac{5}{2} k^{2/7} - \frac{7}{2} + k^{-5/7} \right). \tag{3}$$

Consider Phase 2. The compression work of Phase 2 is

$$W_2 = \int (P_0 - P_0)\, dV = 0,$$

so the total work done is given by **(3)**.

In this model, first we get the curve of internal pressure and deformation. Based on the graph, we calculate the energy consumed by the resistance of gas. However, considering the box as a rigid cylinder may be inaccurate. Another weakness is the airtightness of the box; actually, the internal gas leaks during the whole process of compression.

Realistic Air Box Model

The height of the box is less than 1 m, so the speed of the motorcycle and stunt person changes little when passing through one box height's distance; hence, we think of it as constant during compression of a single box. The effect of the air in the crushing process is just like the air in a cylinder with a hole to leak air. In **Figure 6**, we have

s is the area of the top of the box (top of the cylinder),

h is the height of the box (cylinder),

σ is the air-leaking rate,

z is the crushing distance from the top of the box (cylinder), and

v is the speed of the motorcycle and stunt person.
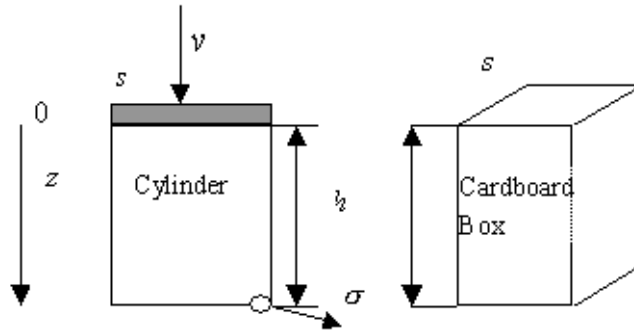
Figure 6. The unsealed cylinder model.

In the crushing process, the cardboard box's deformation becomes larger and larger. As a result, the air leaks more quickly. Generally, when a cardboard box is pressed to about half of its original height, the effect of air-leaking is so prominent that we cannot ignore it.

We assume that the air-leaking rate changes with the crushing distance z via

$$\sigma(z) = 2e^{4z/h}s,$$

for $z \in (0, h)$. Let $x = z/h$ for $x \in (0, 1)$.

The goal is to calculate the total work that the air does to the motorcycle and stunt person. It is necessary to calculate the pressure of the air in a box while the crushing is occurring. We divide the crushing process into N time periods; in each time period, the pressure of the air can be calculated according to the universal gas law $PV = nRT$. We assume that temperature is constant, so PV is constant.

In the first time period, we have

$$P_0V_0 = P_0\sigma_0\,dt + (V_0 - sv\,dt)P_1,$$

$$P_1 = \frac{P_0(V_0 - \sigma_0\,dt)}{V_0 - sv\,dt}.$$

In general, we get

$$P_i = \frac{P_{i-1}(V_{i-1} - \sigma_{i-1}\,dt)}{V_{i-1} - sv\,dt},$$
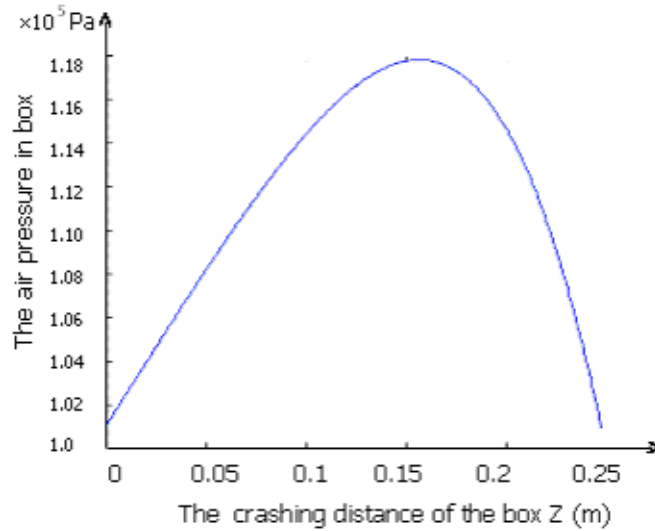
where

$$dt = \frac{h}{vN},$$

σ_i is the air-leaking rate in time period i, and

V_i is the volume of the box in time period i.

So in every time period, the pressure of air in the cylinder can be calculated recursively:

$$P_i = \frac{(V_{i-1} - \sigma_{i-1}\,dt)}{V_{i-1} - sv\,dt} \cdot \frac{(V_{i-2} - \sigma_{i-2}\,dt)}{V_{i-2} - sv\,dt} \cdots \frac{(V_0 - \sigma_0\,dt)}{V_0 - sv\,dt}.$$

Let $h = 0.5$ m and $N = 1000$. The air pressure in the box increases from P_0 (standard atmospheric pressure) to a maximum of $1.66P_0$ at about one-third of the box's height and drops steeply to P_0 at about half the box's height (**Figure 7**).

Figure 7. Air pressure in the box as a function of distance crushed.

The energy that the air in box does to the motorcycle and stunt person is

$$W = -\int f\,dz = -\int_0^{z_m} P(z)s\,dz,$$

where z_m is the distance at which the air pressure equals P_0 and s is the area of the top of the box. Let $s = 0.5$ m^2; then the energy that the air in box does to motorcycle and stunt person is $W = -1322$ J.

The consideration of the box's air-leaking effect makes this model more realistic, particularly since an exponential function is used to describe the air-leaking effect. With numerical methods, this model is to solve. However,

there are some parameters to identify, and the assumption of constant speed for motorcycle plus stunt person is not correct.
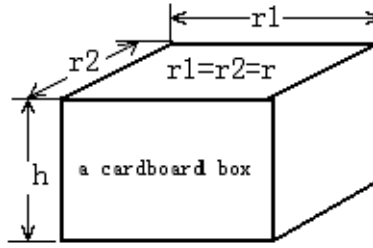
Use the Model

We need to keep the height of the box-pile lower than the elephant so that the action can be filmed without the box-pile being seen. The height of the pile is the number of layers L times the height h of a single box:

$$H_{\text{pile}} = Lh.$$

The total number of boxes used is

$$\text{Num} = \frac{LS}{r^2},$$

where r is the width of a box (**Figure 8**) and S is the upper surface area of the box-pile.

Figure 8. Dimensions of a box.

The cost is

$$\text{Cost} = \text{Num} D_s,$$

where D_s is the unit price, which depends on the materials, transportation cost and other factors. We set $D_s = k_1 A + k_2$, where

k_1 is the fabrication cost per square meter.

k_2 includes the average cost for transportation and some other factors, and

A_0 is the total surface area of a single box: $A_0 = 4rh + 2r^2$.

Then the cost is

$$\text{Cost} = \text{Num} D_s = k_2 \text{Num} + k_1 A_0 \text{Num} = k_2 \text{Num} + k_1 A,$$

where A is the total surface area of all of the Num boxes.

A metric T that takes into account both minimizing cost and the total box-pile height is

$$T = \lambda_h H_{\text{pile}} + \lambda_c \text{Cost},$$

where the λs are weight factors. So we must solve the following optimization problem:

$$\text{minimize} \quad T(r, h, L) = \lambda h\, H_{\text{pile}} + \lambda_c \, \text{Cost}$$

$$\text{subject to} \quad \sum_{i=1}^{L} W_i - Lmgh \geq \tfrac{1}{2}mv_0^2 - \tfrac{1}{2}v_{\text{safe}}^2, \tag{4}$$

$$v_0^2 = 2g(H_{\text{max}} - Lh), \tag{5}$$

where W_i is the energy that the motorcycle and stunt person lose passing through layer i. The inequality **(4)** makes the piles hard and numerous enough to slow the falling stunt person to the safe speed, while equation **(5)** defines initial speed in terms of the maximum height of the jump and the height of the pile.

Results and Analysis

Although the Ideal Mechanical model is practical and easy to calculate, it requires that many parameters be determined by experiments. The Realistic Mechanical model gives mechanical support to the Air Box models. The Realistic Air Box model develops from the Ideal Air Box model by considering air-leaking; its results may be more credible, so we give results for the Realistic Air Box Model instead of for the others.

Results of the Unsealed Air Box Model

Case A

To give some typical results and analyze stability, we assume that the maximum height of the box-pile is $H_{\text{pile}} = 2.5$ m and the safe speed is $v_{\text{safe}} = 5.42$ m/s. Considering that the height must be lower than the given maximum height, we ignore its effect in T. Let $k = k_2/k_1$; then the utility function can be written as

$$U = \frac{\text{Cost}}{k_1} = k\, \text{Num} + A.$$

We use enumeration to find the best solution that minimizes U (that is, minimizes total cost). The step size for r and h in our enumeration is 0.1 m. Different weights of stunt person plus motorcycle give different solutions; details are in **Table 2**. The solution of r, h, and L changes little with k.

Case B

To find out how contact area influences the solution, we fix $M = 187$ kg and $v_{\text{safe}} = 5.42$ m/s and vary the area s of the top of a box. The solution does not change with k, so we let k equal 0 (**Table 3**).

Table 2.

Results for Case A.

M (kg)	k	Solution r (m)	h (m)	L	A (m^2)	U
150	0	0.4	0.8	1	240	240
	5	"	"	"	"	990
	∞	"	"	3	437	∞
187	0	0.7	0.5	4	466	466
	5	"	"	"	"	1447
	∞	"	"	"	"	∞
200	0	0.5	0.6	3	490	490
	5	0.6	0.5	4	515	1855
	∞	"	"	"	"	∞
230	0	0.4	0.8	3	720	720
	5	"	"	"	"	29700
	∞	"	"	""""	720	∞
250	any	No solution				

Table 3.

Results for Case B, with $M = 187$ kg and $v_{\text{safe}} = 5.42$ m/s.

s (m)	r (m)	h (m)	L	A (m^2)	U
1.0	0.8	0.6	1	122	122
0.8	"	0.8	"	146	146
0.6	0.7	0.7	2	288	288
0.5	"	0.5	4	466	466
0.4	0.4	0.7	"	864	864
0.2	No solution				

Case C

To find out how the safe speed influences the solution, we fix $s = 0.5$ m^2 and $M = 187$ kg. Details can be seen in **Table 4**.

Analysis of the Results

The parameter k influences the solution only slightly; that is, our model is stable, since we can easily get an optimum solution without paying attention to having an accurate value of k, whose value in fact is hard to obtain.

Lightening the weight remarkably decreases the value of U (Table 2). So the stunt coordinator should try to reduce the total weight.

Increasing the contact area to some extent reduces cost (Table 3). So the stunt

Table 4.

Results for Case C, with $M = 187$ kg and $s = 0.5$ m^2.

| v_{safe} (m/s)	r (m)	h (m)	L	A (m^2)	U
4.64	No solution				
4.85	0.4	0.6	3	576	576
5.05	"	"	"	"	"
5.24	"	0.7	2	432	432
5.42	0.7	0.5	4	466	466

person should try to touch the boxes with both wheels, to enlarger the contact area. The size of wheels also influences the contact area.

The safe speed has a significant effect on the cost (Table 4). To decrease cost, increase the safe speed by selecting a soft landing surface (e.g., grass or sand) instead of cement.

Further Discussion

How to Pile the Cardboard Boxes

The farther the flight in the air, the longer the box-pile needs to be. So the best shape of the underside of the stack may be like a sector, whose further side would be a little wider than the nearer one (**Figure 9**). Another idea is to pile the boxes like a hill whose central part is higher than the other parts, since the contact area between the stunt person plus motorcycle and the box is much smaller than the area of the pile. The cushioning effect is from the contacting area, so we are more interested in the height of the boxes of the contact part of the pile. If we can determine accurately where the landing will be, we can save lots of boxes **(Figure 10)**.
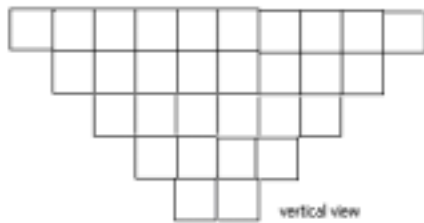

Figure 9. Vertical view of the box-pile.
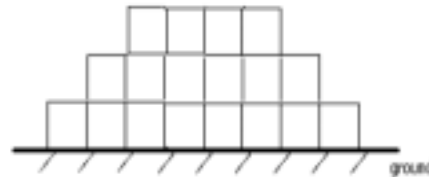
Figure 10. Lateral view of the box-pile.

Tying together boxes in the same layer may be helpful, because doing so supplies a larger horizontal effect and make the layer effect obvious. Another advantage is to prevent the stunt person from falling into a gap between boxes.

Change the Shape of the Boxes

To simplify the problem, we assumed that the cross section is square. Yan and Yuan [2000] give the relationship between the compression strength of the box and the ratio of length to width (**Figure 11**). We could change that ratio for best effect.
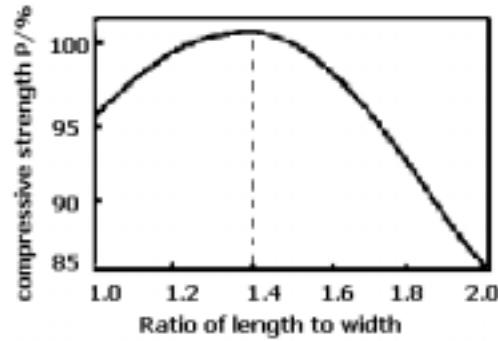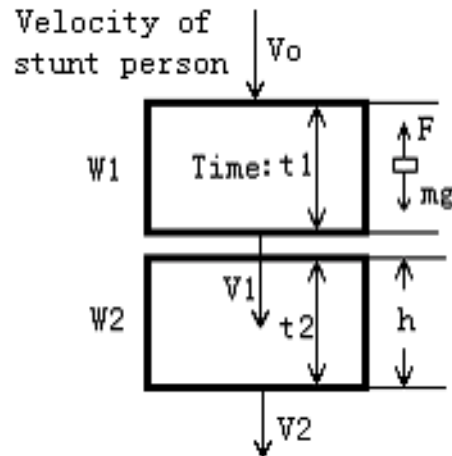

Figure 11. Compression strength as a function of ratio of length to width of the box.

Appendix A: Same Work for Each Box

We analyze the process between boxes of two adjacent layers (**Figure A1**)and show that two boxes do the same amount of work: $W_1 = W_2$, where

$$W_1 = \tfrac{1}{2}mV_1^2 - \tfrac{1}{2}mV_0^2 + mgh,$$
$$W_2 = \tfrac{1}{2}mV_2^2 - \tfrac{1}{2}mV_1^2 + mgh.$$

Figure A1. Diagram of two boxes.

Using the average velocity, and since both boxes have the same height h, we have

$$h = \tfrac{1}{2}(V_0 + V_1)t_1 = \tfrac{1}{2}(V_1 + V_2)t_2,$$

so

$$\frac{t_1}{t_2} = \frac{V_1 + V_2}{V_0 + V_1}.$$

Use the Newton's Second Law, we have that $F/m = a_1 = a_2$ and

$$V_1 = V_0 + a_1 t_1, \qquad V_2 = V_1 + a_2 t_2,$$

so that

$$\frac{t_1}{t_2} = \frac{V_1 - V_2}{V_0 - V_1}.$$

Setting the two expressions for t_1/t_2 equal and cross-multiplying gives

$$V_1^2 - V_0^2 = V_2^2 - V_1^2.$$

Appendix B: $PV^{1.4}$ Is Constant

We assume that the impact is so quick that the gas in the cardboard doesn't exchange energy with environment, so we have an adiabatic compression process. According to First Law of Thermodynamics, we get

$$\Delta E + W_Q = 0,$$

where ΔE is the increment of the gas's internal energy and W_Q is the work done by the adiabatic gas. We also then have

$$dE + P\,dV = 0,$$

where P is the pressure of the gas and V is the volume. We put them into the Ideal Gas Internal Energy Formula:

$$E = \frac{M}{\mu} \cdot \frac{i}{2} RT \qquad \text{and} \qquad C_\nu = \frac{i}{2} R,$$

where

M is the mass of the gas,

i is the number of degrees of freedom of the gas molecule,

μ is the molar mass of the gas.

R is the molar gas constant,

T is the temperature of the gas, and

C_ν is the constant volume molar heat capacity.

Then we have:

$$\frac{M}{\mu} C_\nu \, dT + P \, dV = 0.$$

We differentiate the ideal-gas state equation

$$PV = \frac{MR}{\mu} T$$

getting

$$P \, dV + V \, dP = \frac{MR \, dT}{\mu}.$$

We eliminate dT from the last two equations to get

$$\frac{dP}{P} + \frac{C_\nu + R}{C_\nu} \cdot \frac{dV}{V} = 0.$$

Integrating, we get $PV^r = $ constant, where

$$r = \frac{C_\nu + R}{C_\nu} = \frac{2 + i}{i}.$$

The main composition of the air is nitrogen and oxygen, so $i = 5$ and $r = 1.4$, so $PV^{1.4} = $ constant.

References

Johansen P.M., and G. Vik. 1982. Prediction of air leakages from air cushion chamber. *Pressure Tunnels: Tunneling Machines/Underground Storage* 2 (1): 935–938.

Martin, David. 1982. Rockbursts imperil construction of Norway's largest underground power station. *Tunnels and Tunnelling* 14 (10): 23–25.

Mildin, R.D. 1945. Dynamics of package cushioning. *Bell System Technical Journal* 24: 353–461.

Mokhtari, Mohand, and Michel Marie. 2000. *Engineering Applications of MAT-LAB5.3 and SIMULINK 3*. New York: Springer-Verlag.

PBS Online. n.d. Wild Indonesia: Classroom resources. Why do elephants have big feet? `http://www.pbs.org/wildindonesia/resources/bigfeet.html` .

Yamaha Motor Corp. 2003. `http://www.yamaha-motor.com/products/unitinfo.asp?lid=2&lc=mcy&cid=28&mid=35` .

Yan, Lamei, and Youwei Yuan. 2000. Calculation of the compression strength of corrugated paper boxes and computer-aided design. *Journal of Zhuzhou Institute of Technology* 14 (1).

Zhao, Maiqun, Digong Wang, and Xingxiang Xu. 2000. Modification to Kellicut formula. *Journal of Xi'an University of Technology* 16 (1).

Cardboard Comfortable When It Comes to Crashing

Jeffrey Giansiracusa
Ernie Esser
Simon Pai
University of Washington
Seattle, WA

Advisor: James Allen Morrow

Abstract

A scene in an upcoming action movie requires a stunt person on a motorcycle to jump over an elephant; cardboard boxes will be used to cushion the landing.

We formulate a model for the energy required to crush a box based on size, shape, and material. We also summarize the most readily available boxes on the market. We choose a maximum safe deceleration rate of $5g$, based on comparison with airbag rigs used professionally for high-fall stunts.

To ensure that the stunt person lands on the box rig, we analyze the uncertainty in trajectory and extract the landing point uncertainty.

We construct a numerical simulation of the impact and motion through the boxes based on our earlier energy calculations. After analyzing the sensitivity and stability of this simulation, we use it to examine the effectiveness of various configurations for the box stack (including different box sizes, types of boxes, and stacking patterns). We find that 200 kg is the most desirable combined mass of the motorcycle and stunt person, and a launch ramp angle of $20°$ is optimal when considering safety, camera angle, and clearance over the elephant.

A stack of $(30 \text{ in})^3$ boxes with vertical mattress walls spaced periodically is optimal in terms of construction time, cost, and cushioning capacity. We recommend that this stack be 4 m high, 4 m wide, and 24 m long. It will consist of approximately 1,100 boxes and cost \$4,300 in materials. The stunt person's wages are uncertain but fortunately the elephant works for peanuts.

Introduction

Airbag rigs are commonly used for high-fall stunts [M&M Stunts 2003], but they are designed only to catch humans. The alternative is a cardboard-box rig—a stack of boxes that crush and absorb impact.

Our objectives are:

- to catch the stunt person and motorcycle safely, and

- to minimize the cost and size of the box rig.

Our approach is:

- We investigate the relationship between the size/shape/material of a box and the work (*crush energy*) required to crush it.

- We review the available cardboard boxes.

- By comparison with an airbag rig, we estimate the maximum acceptable deceleration that the stunt person can experience during landing.

- We analyze the trajectory of the motorcycle and the uncertainty in its landing location. This determines the proper placement of the box rig and how large an area it must cover.

- Using the crush energy formula, we estimate the number of boxes needed.

- We formulate a numerical simulation of the motorcycle as it enters the box rig. Using this model, we analyze the effectiveness of various types of boxes and stacking arrangements for low, medium, and high jumps.

- As an alternative to catching the stunt person while sitting on the motorcycle, we analyze the possibility of having the stunt person bail out in mid-air and land separately from the motorcycle.

- We make recommendations regarding placement, size, construction, and stacking type of the box rig.

Energy Absorbed by Crushing Cardboard

We estimate the energy required to crush a box, based on physical considerations and experimentation. We assume that the primary source of energy absorption is the breakdown of the box walls due to edge compressive forces.

Commercial cardboard is rated by the edge crush test (ECT), which measures edge compressive force parallel to the flute (the wavy layer between the two wall layers) that the cardboard can withstand before breaking. This can be interpreted as the force against the edge per unit length of crease created [Pflug et al. 1999; McCoy Corporation n.d.]. Once a crease has formed, very little work is required to bend the cardboard further.

To understand how the formation of wall creases relates to the process of crushing a box, we conducted several experiments (**Figure 1**). We found:

- The first wall-creases typically form in the first 15% of the stroke distance.

- These creases extend across two faces of the box; a schematic of one such crease is illustrated in **Figure 2**.
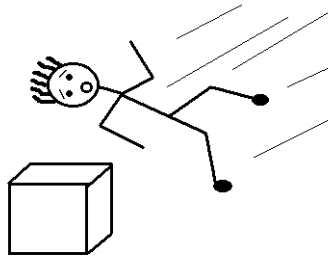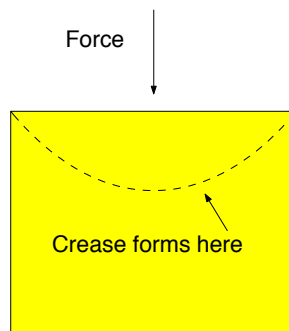
Figure 1. Experimental apparatus for crushing boxes: We dropped a *crush-test dummy* (i.e., team member) onto several boxes and observed how the structure (the box, not the dummy) broke down.

Figure 1a. Crush-test dummy in action. (Left: Jeff Giansiracusa; right: Simon Pai.)

Figure 1b. Crushed box with creases. (Photos courtesy of Richard Neal.)

Figure 2. The first crease forms in a curve across the side faces as the box is compressed.

- Once these have formed, the box deforms further with comparatively little resistance, because additional creases are created by torque forces rather than edge compressive forces.

- The primary creases each have length approximately equal to the diagonal length of the face.

The work done in crushing the box is given by the average force applied times the distance through which it is applied. This and our experimental qualitative results lead us to write the following equation for energy absorbed by a box of dimension $l_x \times l_y \times l_z$ crushed in the z-direction:

$$E = \text{ECT} \times 2\sqrt{l_x^2 + l_y^2} \times l_z \times 0.15 \tag{1}$$

As a reality check, we compute the crush energy for a standard 8.5 in $\times$ 17 in $\times$ 11 in box with ECT = 20 lbs/in and a C-flute (the type commonly used to store paper). With these numerical values, **(1)** gives an energy of 187 J. This corresponds roughly to a 140-lb person sitting on the box and nearly flattening it. Crush-test dummy results confirm this estimate.

Energy can also be absorbed in the process of flattening the flute within the cardboard walls. However, the pressure required to do this is approximately 150 kPa [Pflug et al. 1999] and the surface area involved is more than 1 m^2, so a quick calculation shows that the stunt person would decelerate too quickly if the kinetic energy were transferred into flattening boxes. We therefore ignore this additional flattening effect.

So, any successful box rig configuration must dissipate all of the kinetic energy of the stunt person and motorcycle through box-crushing alone.

Common Box Types

Minimizing cost is important. The cardboard box rig will consist of perhaps hundreds of boxes, and wholesale box prices can range up to $10 or $20 per unit; so we restrict our attention to commonly available box types (**Table 1**).

Table 1.

Commonly available box types [Paper Mart n.d.; VeriPack.com n.d.]

Type	Size (in)	ECT rating (lbs/in)	Price
A	$10 \times 10 \times 10$	32	$0.40
B	$20 \times 20 \times 20$	32	$1.50
C	$20 \times 20 \times 20$	48	$3.50
D	$30 \times 30 \times 30$	32	$5.00
E	$44 \times 12 \times 12$	32	$1.75
F	$80 \times 60 \times 7$	32	$10.00

Some Quick Estimates

Maximum Safe Acceleration

To determine acceptable forces and accelerations for the stunt person, we compare the box rig with other cushioning devices. In the stunt rigging business, it is common practice to use an air bag for high falls of up to 30 m; such airbags are approximately 4 m deep.

Assume that a stunt person falls from 30 m above the airbag. Gravity accelerates the performer from rest to speed v when the performer strikes the airbag and is decelerated completely, so we have

$$\sqrt{2gd_{\text{fall}}} = \sqrt{2a_{\text{bag}}h_{\text{bag}}},$$

where d_{fall} is the fall distance, a_{bag} is the deceleration rate the stunt person experiences in the airbag, h_{bag} is the height of the airbag, and g is the acceleration due to gravity. Thus,

$$a_{\text{bag}} = \frac{d_{\text{fall}}}{h_{\text{bag}}} g = \frac{30 \text{ m}}{4 \text{ m}} g = 7.5g.$$

We therefore conclude:

- When using an airbag, the stunt person experiences an average acceleration of at most $7.5g$. This provides an upper bound on the maximum acceleration that a person can safely withstand.

- With the airbag, the stunt person is able to land in a position that distributes forces evenly across the body. In our stunt, however, the stunt person lands in the box rig while still on the motorcycle, with greater chance for injury under high deceleration.

- We choose $5g$ as our maximum safe deceleration.

Displacement and Energy Estimates

If the deceleration is constant through the boxes, then we can estimate the distance required to bring them to rest. Since any deviation from constant acceleration increases either the stopping distance or the peak deceleration, this will give us a lower bound on the stopping distance and hence on the required dimensions of the box rig.

Suppose that the stunt person enters the rig at time $t = 0$ with speed v_0 and experiences a constant deceleration a until brought to rest at time $t = t_f$. The person's speed is $v(t) = v_0 - at$. Since the stunt person is at rest at time t_f, we have

$$t_f = v_0/a.$$

Let $x(t)$ be the displacement from the point of entry as a function of time. Since $x(0) = 0$, we have

$$x(t) = v_0 t - \tfrac{1}{2} a t^2$$

and so the total distance traveled through the boxes is

$$\Delta x = x(t_f) = \frac{v_0^2}{a} - \frac{1}{2}\, a \left(\frac{v_0}{a}\right)^2 = \frac{v_0^2}{2a}.$$

Therefore, we arrive at:

- Given an impact velocity $v_0 \approx 20$ m/s and deceleration bounded by $5g$, the stunt person requires *at least* 4 m to come to rest.

The energy that must be dissipated in the boxes is roughly equal to the kinetic energy that the motorcycle and stunt person enter with. (Since the box rig should be only 3–4 m high, the potential energy is a much smaller fraction of the total energy.) Thus, for $v_0 = 20$ m/s and a mass of 200 kg, the change in energy is 40,000 J. From **(1)**, we calculate that the crush energy of a standard $(30 \text{ inch})^3$ box is 633 J, so we need. $40,000/633 \approx 60$ boxes.

Trajectory Analysis and Cushion Location

Cardboard boxes won't dissipate any energy unless the stunt person lands on them. It is therefore important to consider the trajectory, so we know where to place the box rig and what the uncertainty is in the landing location.

We calculate trajectories by solving the following differential equation, where v is the speed, k is the drag coefficient, and $\vec{x}$ is the position:

$$(\vec{x})'' = -g\hat{z} - \frac{k}{m}|v|^2\hat{v}$$

We used Matlab's ODE45 function to solve an equivalent system of first-order equations. We use an air drag coefficient of $k = 1.0$ [Filippone 2003]. We see from **Figure 5** that it would be unwise to ignore air resistance, since it alters the landing position by up to several meters.

It is unreasonable to expect the stunt person to leave the ramp with exactly the same initial velocity and angle every jump. We therefore need to allow for some uncertainty in the resulting trajectory and ensure that the cardboard cushion is large enough to support a wide range of possible landing locations. The ramp angle ϕ is constant, but the motorcycle might move slightly to one side as it leaves the ramp. Let θ be the azimuthal angle between the ramp axis and the motorcycle's velocity vector. Ideally θ should be zero, but small variations may occur. The other uncertain initial condition is the initial velocity v_0.

In modeling possible trajectories, we assume the following uncertainties:

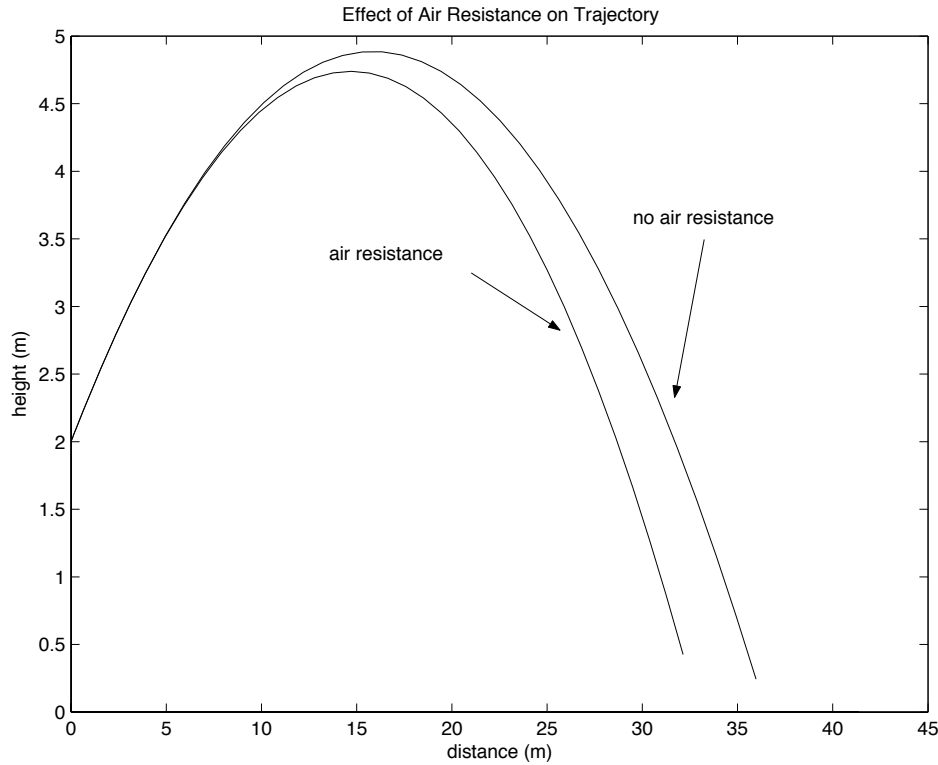- Initial velocity: $v_0 = v_{\text{intended}} \pm 1$ m/s

Effect of Air Resistance on Trajectory

Figure 3. Air resistance significantly changes the trajectory.

- Azimuthal angle: $\theta = 0° \pm 2°$

We use this to identify the range of possible landing locations by plotting the trajectories that result from the worst possible launches (**Figure 6**).

If the intended initial velocity is 22 m/s, the ramp angle is $20°$, and the mass of the rider plus motorcycle is 200 kg, then the distance variation is $\pm$ 2.5 m and the lateral variation is $\pm$ 1.5 m.

Impact simulation

To evaluate the effectiveness of various box rig configurations, we construct a numerical simulation of the motion of the stunt person and motorcycle through the box rig.

Assumptions

The full physics of the box rig is far too complex to model accurately. We make the following assumptions to approximate and simplify the problem.

- *The problem is two dimensional.* We restrict out attention to the plane of motion of the stunt person.
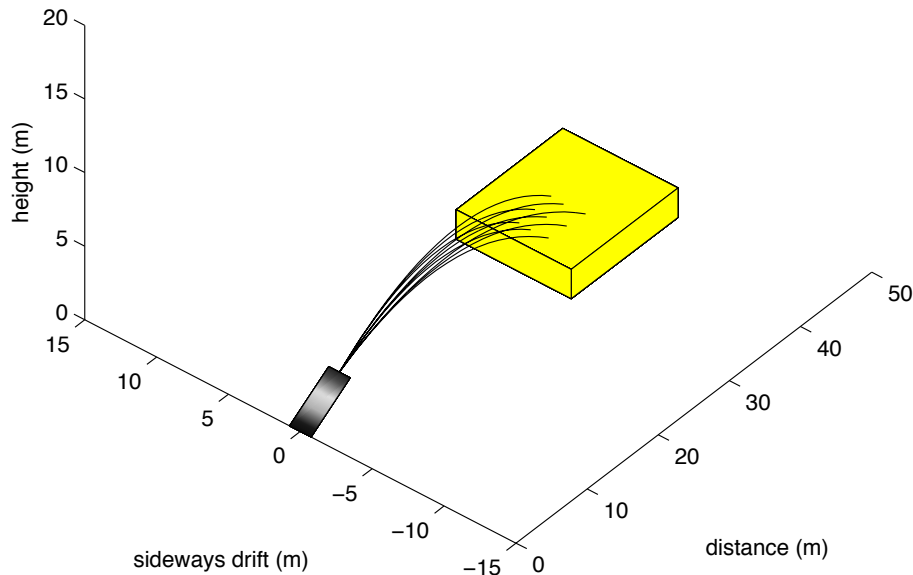
Figure 4. Trajectory uncertainty due to launch uncertainties (box rig is not to scale).

- *As the motorcycle plows through the boxes, a thick layer of crushed boxes accumulates against its front and lower surfaces.* These layers increase the effective size of the motorcycle and cause it to strike a larger number of boxes as it moves. This assumption captures the effects of internal friction and viscosity within the boxes.

- *In striking a large number of boxes, the velocity magnitude is reduced but the direction is unchanged.*

- *Boxes are crushed rather than pushed out of the way.* In practice, this can be ensured by placing a strong netting around the three sides of the box rig that face away from the incoming stunt person.

- *Boxes are crushed to a uniform level.* Some boxes may be crushed only slightly while others are completely flattened, but these effects disappear when we average over a large number of collisions.

Formulation

We formulate the simulation as follows:

- The motorcycle with stunt person is represented by a bounding rectangle that is initially 1.2 meters long, 1.2 m high and 0.7 m wide.

- The box rig is represented by a two-dimensional stack of boxes.

- We numerically integrate the motion in discrete time steps of 0.05 s. The only object in motion throughout the simulation is the stunt person plus motorcycle—all boxes are stationary.

- When the bounding rectangle intersects a box, the box is considered crushed. We modify the stunt person's velocity according to the kinematics described later and ignore further interactions with the crushed box.

- For each box crushed, we add a layer of additional thickness to either the front or the bottom of the motorcycle bounding rectangle. We assume that boxes are crushed to 20% of their length or height. We allow the front layer to extend above and below the original bounding rectangle (and likewise for the bottom layer), so that the force of the motorcycle striking a tall box is effectively distributed along the length of the box. These debris layers increase the effective size of the motorcycle and therefore cause it to strike a larger number of boxes as it moves. We use this process to account for the effects of friction.

- The vertical component of the velocity is set to zero when the bounding rectangle strikes the ground.

Kinetics

As the stunt person with motorcycle falls into the rig, each box collided with collapses and absorbs a small amount ΔE of kinetic energy, thereby slowing the descent. The crushed box is then pinned against the forward moving face of the stunt person and motorcycle and must move with them, contributing an additional mass of m_{box}.

We calculate the change in this velocity using conservation of energy and assuming that the velocity direction remains unchanged (this is a good approximation in the average of a large number of collisions):

$$\tfrac{1}{2}(m_0 + m_{\text{box}})v_{\text{new}}^2 = \max\left(\tfrac{1}{2}m_0 v_0^2 - \Delta E, 0\right).$$

We take the maximum to avoid imparting more energy to the box than the motorcycle has. Solving for v_{new} yields

$$v_{new} = \sqrt{\max\left(\frac{m_0 v_0^2 - 2\Delta E}{m_0 + m_{\text{box}}}, 0\right)} \tag{2}$$

We use this equation to calculate the new velocity after each collision.

Stability and Sensitivity Analysis

Given the crude nature of our collision detection, there is the danger of finding results that depend sensitively on the initial location of the motorcycle relative to the phase of the box-rig periodicity (typically less than 1.5 m). To show that these phase alignment effects are negligible we vary the initial location of the motorcycle by 0.4 m (37% of the rig periodicity) in either direction. Deceleration rates and stopping distance vary by less than 5%. The simulation

is therefore insensitive to where the motorcycle lands relative to the period of the box rig.

As a second check, we vary the time step size from 0.025 s to 0.1 s (our standard value is 0.05 s). There are no distinguishable changes in results; the simulation is highly insensitive to the size of the time step.

Configurations Considered

We consider the following configurations for the stunt:

- *Seven different stacking arrangements.* Details are shown in **Table 2** and **Figure 7**.

Table 2.

The seven box rig configurations. Refer to **Table 1** for data on the lettered box types.

Stack type	Cost/m^2	Description
1	$40	Standard rig, box type B (20-in cube).
2	$94	Standard rig, heavy-duty box type C (20-in cube, ECT 48).
3	$43	Standard rig, box type D (30-in cube).
4	$47	Like type 3, but type-A boxes (10-in cube) inside the D boxes.
5	$46	Modification of type 3: additional vertical walls of type F mattress boxes.
6	$41	Like type 5, but horizontal mattress box walls.
7	$46	Mattress boxes (type F) stacked horizontally, with periodic vertical walls

- *Three values for the total mass of the motorcycle and stunt person:* 200 kg, 300 kg, and 400 kg.

- *Three flight trajectories for the motorcycle and stunt person: low, medium, and high.* These provide three different entry angles and velocities for the simulation. Each trajectory is designed to clear an elephant that is roughly 3 m tall [Woodland Park Zoo n.d.]. Details of these trajectories are given in **Table 3** and are shown to scale in **Figure 8**.

Table 3.

The three test trajectories.

Jump type	Initial speed (m/s)	Ramp angle angle	Jump distance (m)
Low	29	10°	30.0
Medium	22	20°	28.5
High	20	30°	30.4
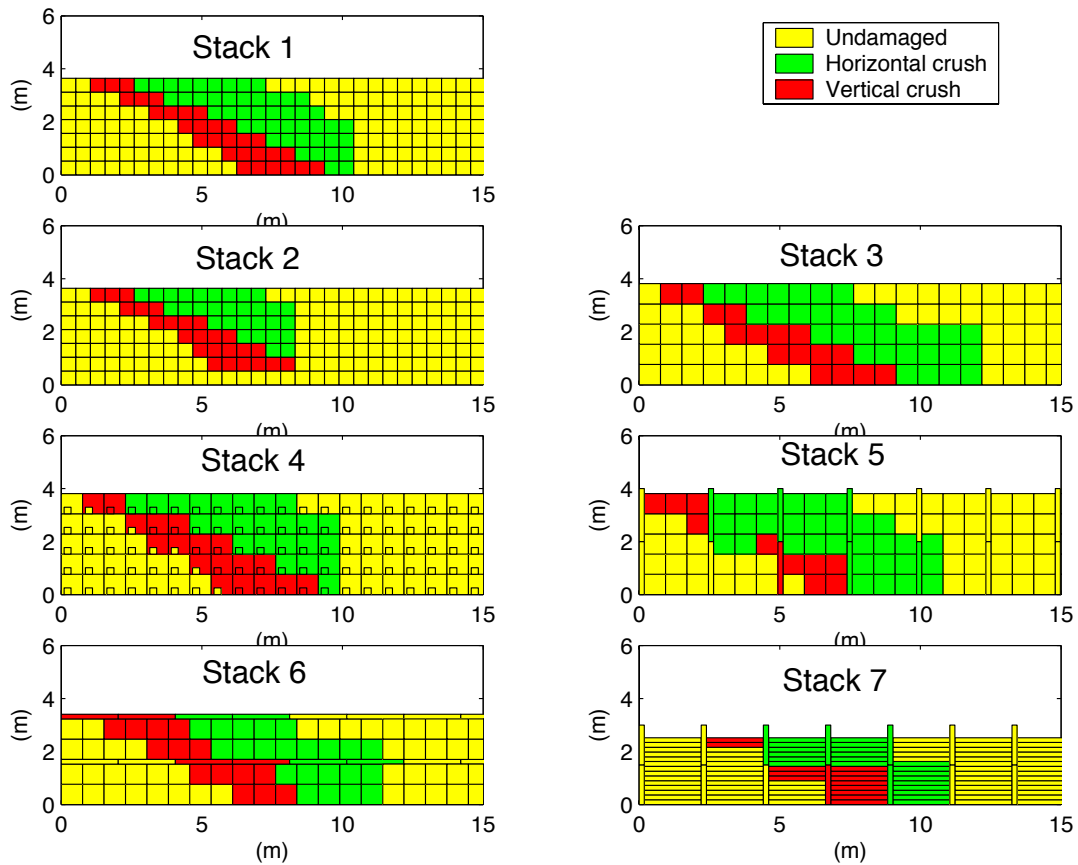
Figure 5. Box stacking configurations. Crush patterns are the result of simulated impacts of a 200-kg mass in the low trajectory.

Data Analysis

The simulation provides us the velocity as a function of time. The plots appear jagged and step-like because of the discrete way in which our simulation handles collisions. We obtain the acceleration by fitting a straight line to the velocity vs. time plot and measuring the slope (**Figure 9**).

In examining the plots for the runs, we look at:

1. deceleration experience by the stunt person, averaged over the entire time from impact to rest;

2. maximum of deceleration averaged over 0.1 s intervals; and

3. whether or not the boxes completely arrest vertical motion before the stunt person hit the ground.

If either (1) or (2) ever exceeds the maximum safe deceleration threshold of $5g$, or (3) fails, we consider the configuration unsafe.
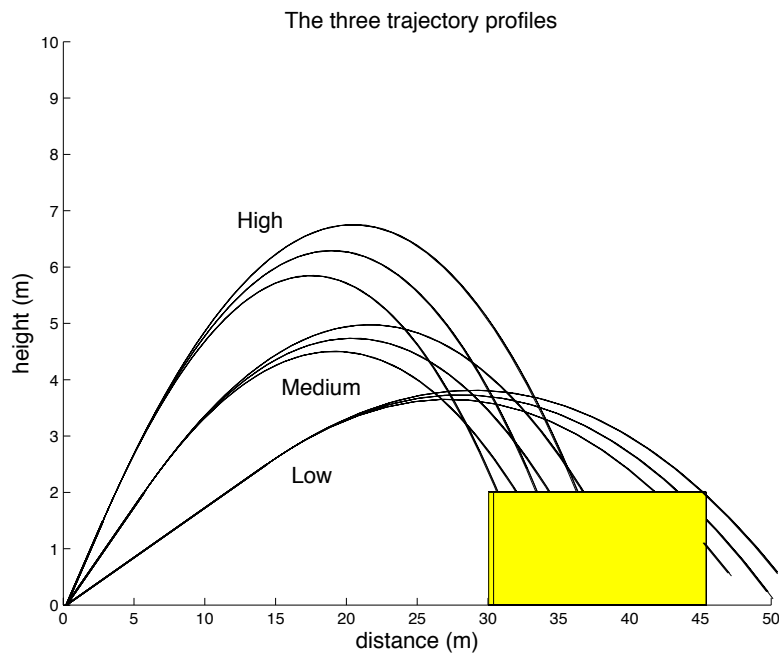
Figure 6. The three trajectories tested.
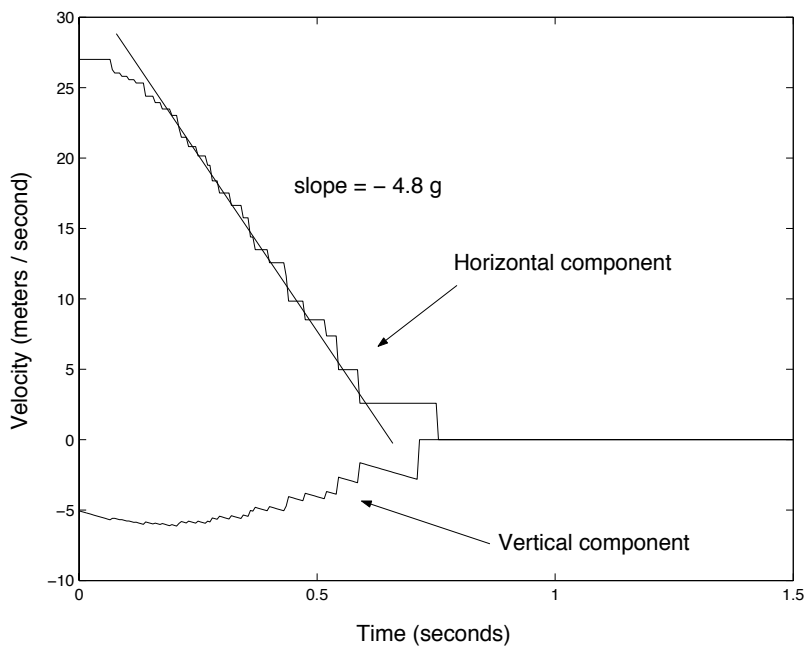
Figure 8. Velocity vs. time for a 200-kg low trajectory impact on a box stack of 20 in cubes stacked in standard style.

Results

Mass

For a mass of 400 kg, the boxes give way beneath the incoming motorcycle too easily; such a mass would require a stack of boxes nearly 6 m high. A mass of 300 kg is marginal, and 200 kg is optimal.

Stacking Types

We measure stopping distance from the point of impact to the furthest box damaged and report the stopping distance for the medium trajectory. (The motorcycle actually comes to rest in a significantly shorter distance, but it pushes a wall of debris several meters ahead of it.) The results for the stack types in **Figure 6** are:

1. Made from the cheapest and most common boxes, this stack resulted in $4.8g$ deceleration; it stopped the motorcycle in 11 m.

2. Rejected—deceleration of over $6g$ but brings the motorcycle to rest in only 7 m.

3. Very soft deceleration of $3.6g$ to $4.1g$. But this stack did not completely stop the vertical motion and took 13 m to bring the motorcycle to rest.

4. Marginally safe deceleration from $4.8g$ to $5.1g$, but this stack is the best at arresting the vertical motion; stopping distance of 9 m.

5. Behavior is similar to type (3), but stopping distance is reduced to 11 m.

6. The extra horizontal mattress boxes make very little difference. Deceleration is $4.1g$, and vertical motion is not slowed enough to prevent hitting the ground hard.

7. Rejected because deceleration ($5.2g$ to $5.7g$) is unsafe.

The difficulty of slowing the vertical motion enough might be overcome by stacking the box rig on top of a landing ramp.

Conclusion: Type (1) stacking is optimal without a ramp. However, with a landing ramp under the boxes, type (3) or type (5) stacking gives a much softer deceleration.

We tried additional variations on the type (5) stack. We conclude that

30-in boxes (type D) with mattress box walls spaced every 4 boxes is optimal.

An Alternative: Bailing Out

It may be desirable for the stunt person and motorcycle to separate before impacting the box rig, since doing so would reduce the chance of injury resulting from the stunt person being pinned against the motorcycle.

We assume that they separate after clearing the elephant and allowing for a clear camera shot, corresponding to a distance of about 25 m. We run the same simulation as before but alter the vertical velocity at the point of separation and then follow separately the two trajectories. An estimate of the change of momentum is necessary to figure out the corresponding changes in velocity. If the stunt person jumps vertically away from the motorcycle, it makes sense to consider the analogy of a person jumping on the ground. A decent jump corresponds to about 0.5 m. Since the initial velocity is $v_0 = \sqrt{2gd}$ where d is the height, we find that v_0 is roughly 3 m/s. Accordingly, we increase the stunt person's vertical velocity by 3 m/s. Then the corresponding change in velocity for the motorcycle is given by conservation of momentum. The resulting trajectories are plotted in **Figure 10**.
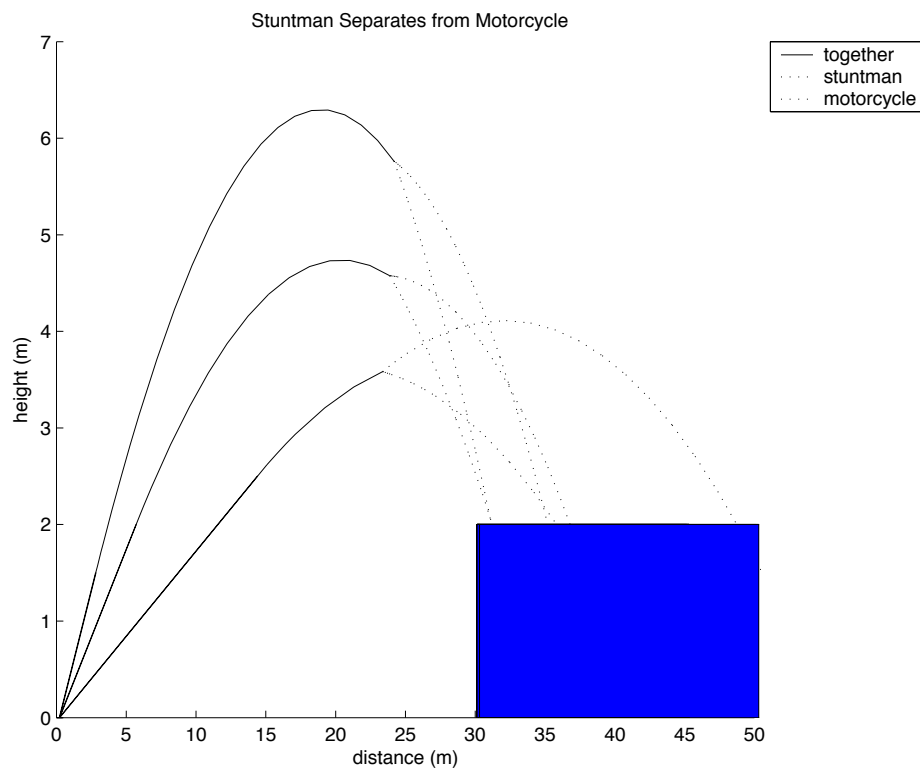

Figure 9. Stunt person separating from motorcycle in three possible trajectories.

When the trajectory is medium or high, stunt person and motorcycle are separated by only about 6 m at the landing point. When the trajectory is low, however, this separation increases to around 15 m. This presents a problem if we want to protect both the motorcycle and the stunt person. Naturally, the safety of the person is the most important, and it is simple to extend the box

rig to the projected landing location of the stunt person.

Unfortunately, simulations show that a box configuration designed to decelerate the combined mass of motorcycle and stunt person smoothly doesn't work as well when there is just the mass of the person to contend with. In fact, it's possible that the stunt person will decelerate so quickly that our g-force tolerance is exceeded. Our simulations show that this is in fact the case for *all* of the box stacks that we considered. For the heights and speeds considered, a box rig is unsafe. However, if the boxes are stacked loosely enough with some spacing between the boxes as in **Figure 11**, then it is possible to decelerate the stunt person at a reasonable rate. Therefore, the best solution is to redesign the box rig, using a softer material and/or looser stacking.
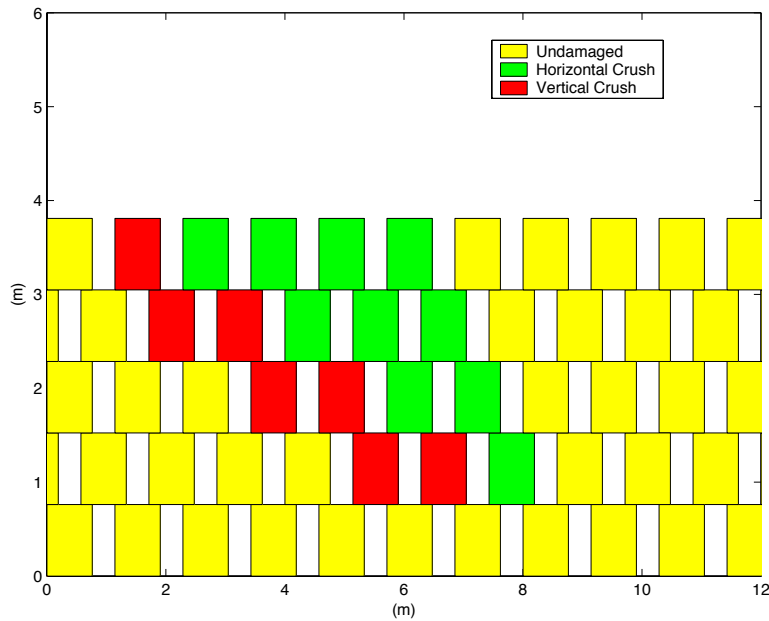
Figure 10. Box stacking arrangement suitable for catching a stunt person who has separated from the motorcycle.

Recommendations

- **Which mass is best?** A 400 kg mass is simply too much to be slowed adequately by a box stack less than 4 m high. The motorcycle invariably falls through the rig and hits the ground beneath at greater than 5 m/s; the motorcycle could easily tumble over in the boxes and crush the stunt person. A 300 kg mass is marginal, but the safest is 200 kg.

- **Which trajectory is best?** The low trajectory (10°) provides the least risk but allows only minimal clearance over the elephant (only 1 m for a tall elephant) and requires the highest speed (which increases the risk).

- **Which type of boxes and stacking is best?** The type (1) stack, made of $(20 \text{ in})^3$ boxes, is best for landing without a ramp. With a ramp under the rig, type (3), made from $(30 \text{ in})^3$ boxes, and type (5), which is type (3) with added vertical mattress box walls, are optimal. The added walls of type (5) decrease the landing distance by 2 m, so fewer boxes are required and construction cost is reduced.

- **What size must the rig be?** With the 200 kg mass, our simulation shows that 3 m height is usually enough for the low trajectory, but 4 m is necessary for the high trajectory. This can be reduced to as little as 2 m if the rig is stacked on top of a landing ramp. Stopping distance is between 10 and 13 m (measured from point of entry to the front of the debris wall) depending on stack type, and we estimate that the landing location uncertainty is 1 m laterally and 3 m forwards or backwards. We consider an additional 50% beyond these uncertainties to be necessary. Therefore our recommendations are:

    - Height: 4 m without landing ramp, 2 m with ramp.
    - Width: 4 m.
    - Length: 24 m for type (1) or (5) stacking, and 29 m for type (3) stacking.

- **How much does it cost?** The cost is between $4,300 for type (1) and $5,300, depending on the precise configuration; this is approximately the cost of renting an airbag rig for a day [M&M Film Stunt 2003].

- **How many boxes?** Type (1) stack requires 2,000 $(20 \text{ in})^3$ boxes and type (3) requires 1,100 $(30 \text{ in})^3$ boxes. Type (5) uses the same number as (3) and a few additional mattress boxes.

Final Recommendation

The overall best type of box rig uses $(30 \text{ in})^3$ boxes stacked as usual, with vertical mattress box walls every couple of meters to distribute the forces over a larger number of boxes. This configuration gives the softest deceleration and requires the fewest boxes.

References

Filippone, A. 2003. Aerodynamics database. `http://aerodyn.org/Drag/tables.html/#man`. Accessed 8 February 2003.

M&M Film Stunts Ltd. 2003. Stunt equipment rentals. `http://www.mmstunts.com`. Accessed 7 February 2003.

McCoy Corporation. n.d. `http://www.4corrugated.com`. Accessed 8 February 2003.

Paper Mart. n.d. `http://www.papermart.com`. Accessed 7 February 2003.

Pflug, Jochen, Ignaas Verpoest, and Dirk Vandepitte. 1999. Folded honeycomb cardboard and core material for structural applications. `http://www.mtm.kuleuven.ac.be/Research/C2/poly/downloads/SC5_TorHex_Paper.pdf`. Accessed 7 February 2003.

VeriPack.com. n.d. `http://www.veripack.com`. Accessed 7 February 2003.

Woodland Park Zoo. n.d. African elephant. `http://www.zoo.org/chai/site/learn/african.htm`. Accessed 8 February 2003.

Editor's Note

The authors' model emphasizes the important role that creases play in the breakdown of a box, based on their own experimental results with "crash dummies."

The authors' conclusions about this are confirmed in Peterson [2003], which summarizes some of the research on crumpling, and from which we quote and summarize:

> [T]he energy that goes into bending and stretching a material as it is crumpled is concentrated in the network of narrow ridges . . . [C]rumpled sheets can be described in terms of the pattern of ridges and peaks that cover the surface. By adding together the deformation energies associated with individual ridges, scientists can estimate the total energy stored in a given crumpled sheet. . . .
>
> The researchers also discovered that increasing a sheet's size has an unexpectedly small effect on the total amount of energy required to crumple it. For instance, it takes only twice as much energy to crumple a sheet whose sides are eight times [as long] . . .

A team of students from Fairview High School in Boulder, Colorado—Andrew Leifer, David Pothier, and Raymond To—won an award at this year's Intel International Science and Engineering Fair for their study of crumpling. They found that ridges in crumpled sheets show a fractal pattern, with a power law describing the lengths of ridges produced from buckling a single ridge and with a Weibull probability distribution describing the frequency distribution of ridge lengths.

> Their result supported the notion that paper crumpling can be viewed as a repetitive process of buckling multiple ridges and their daughter products.

Peterson gives extensive references to literature on crushing, crumpling, and buckling of thin sheets.

References

Peterson, Ivars. 2003. Ivars Peterson's Math Trek: Deciphering the wrinkles of crumpled sheets. `http://www.maa.org/mathland/mathtrek_05_26_03.html` .

Fly With Confidence

Hu Yuxiao
Hua Zheng
Zhou Enlu
Zhejiang University
Hangzhou, China

Advisor: Tan Zhiyi

Abstract

We develop a model to design a pile of cardboard boxes to cushion the fall of a stunt motorcycle; the kinetic energy of the motorcycle is consumed through breaking down the boxes.

We ignore the scattering effect of the boxes and begin by analyzing a single box. The energy to break it down has three components: the upper surfaces, the side surfaces, and the vertical edges. When big boxes are used, the upper surface provides the main supporting force; when small ones are used, the vertical edges play a great role.

We extend our analysis to the pile of boxes. Taking into account the maximum impulse that a person can bear, along with the camera effect and cost concerns, we determine the size of a box.

We conceive several stacking strategies and analyze their feasibility. We incorporate their strengths into our final strategy. We also examine several modifications to the box to improve its cushioning effect.

To validate our model, we apply it to different cases and get some encouraging results.

Assumptions

- *The stunt person and the motorcycle are taken as a system,* which we refer to as the motorcycle system or for brevity as the motorcycle. We ignore relative movement and interaction between them.

- *The motorcycle system is a uniform-density block.* We consider only the movement of its mass center, so we consider the motorcycle system as a mass particle.

- *The cardboard boxes are all made of the same material*, single wall S-1 cardboard 4.5 mm thick [Corrugated fiberboard . . . n.d.]

- *The cardboard box is cubic and isotropic.*

- *Cost is proportional to the total surface area of cardboard.*

Symbols and Terms

<div align="center">

Table 1.

Symbols.

</div>

Motorcycle parameters

$\bar{a}$	mean acceleration during the landing
b	drag coefficient for the motorcycle plus rider
E	kinetic energy of the motorcycle when it hits the pile of boxes
H	height of the stage from which the motorcycle leaves
m	total mass of the motorcycle system
S	cross-sectional area of the motorcycle system, which we assume is 1.5 m^2
σ_m	standard deviation of v_0
σ_d	standard deviation of the direction of v_0
θ	angle between motorcycle direction and the horizontal
v_0	initial projection speed of the motorcycle
v	speed of the motorcycle when it lands on the pile

Box parameters

E_{box}	energy that a single box can absorb during its breakdown
ℓ	edge length of the box
p_{pole}	pressure needed to break down the pole of a box
p_{side}	pressure needed to break down the side of a box
τ	coefficient for transfer of pressure from side to pole
ρ	density of energy absorption (DEA) of a box
V_{box}	original volume of a single box

Pile parameters

h	height of the pile
S_{total}	total combined surface area of all boxes in the pile
V_{pile}	combined volume of all boxes in the pile

Cardboard parameters

b_s	bursting strength of the cardboard
e_s	edgewise crush resistance of the cardboard

Rider parameter

a_{max}	the maximum acceleration that a person can bear.

Pole: the vertical edge of the box

Edge: the horizontal edge of the box

Corner: the intersection of poles and edges

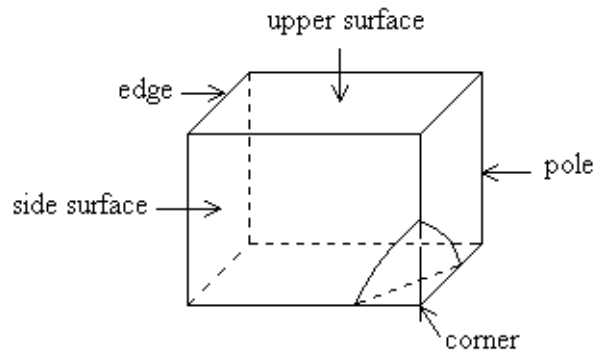**Bursting strength:** the maximum pressure on the cardboard before it bursts

Figure 1. Illustration of terminology.

Edgewise crush resistance: the maximum force on unit length of the edge before the side surface crushes

Piercing Strength: the energy of an awl piercing the cardboard

Problem Analysis

Our primary goal is to protect the stunt person. Having ensured this, we should minimize the height of the pile (to get a good film effect) and minimize the total superficial area of boxes (to lower the cost).

From the analysis of the jump, we get the pile area and kinetic energy of the motorcycle system. Then we consider the cushion process. Since the maximal impulse a person can bear is 12 kN [UIAA Safety Regulations n.d.], the problem is to ensure that the force exerted on the person stays within the range during the cushioning.

Consider the motorcycle landing in a pile of cardboard boxes. The boxes provide a supporting force to decelerate it. We examine the cushioning effect of both big boxes and small boxes. In our modeling, we focus on energy and reduce the problem to analyzing the energy to break down the boxes. We search for the relation between this energy and the size and number of the boxes. We then improve the cushioning by changing stacking approaches and modifying the box.

Model Design

The Jump

Local Assumptions

- The speed v and direction of the motorcycle are random variables that are normally distributed.

- The standard deviation (σ_m) of the magnitude of v_0 is $0.05v_0$.

- The standard deviation (σ_d) of the direction of v_0 is $5°$.

- The stunt is considered safe if the probability of landing on top of the box pile is more than 99.7%.

Local Variables

- v_0: initial speed,

- θ: angle between velocity and horizontal direction,

- H: height of stage,

- m: mass of motorcycle system.

We first examine the path that the motorcycle follows. Taking the air resistance into account, we get two differential equations

$$\frac{dv_x}{dt} = -\frac{bv_x}{m}, \qquad \frac{dv_y}{dt} = \frac{bv_y}{m} - g, \tag{1}$$

where

$$v_x = v_0 \cos\theta, \qquad v_y = v_0 \sin\theta, \qquad \text{and} \qquad \frac{dx}{dt} = v_x, \qquad \frac{dh}{dt} = v_y. \tag{2}$$

The drag coefficient b can be obtained by computing the mass and terminal speed of a skydiver [Halliday et al. 2001]. For $v = 60$ m/s and $m = 200$ kg, we have $b \approx 30$ N/(m/s).

A typical elephant is 3 m high and 5 m long, with a trunk 2 m long [Estes 1999]. To jump it over safely, we assume that the stage is higher than the elephant's trunk reach, which is 5 m.

Solving equations **(1)–(2)** with Matlab, we get a quasiparabola. Air resistance makes a difference of no more than 5%, so we neglect it. With height difference H and initial speed v_0, neglecting air resistance, the landing point is $v_0\sqrt{2H/g}$ from the projecting point.

Determine the Area of the Pile

The area of the box pile must be large enough for the actor to land on, that is, the upper face of the pile must capture more that 99.7% of falls. (Very few may crush into the side face, which is still quite safe.) To meet this criterion, the surface must extend to cover six standard deviations (three on each side of the mean) of both the projection speed v_0 and its direction [Sheng et al. 2001].

We calculate the landing point in the combinations of $v_0 \pm 3\sigma_m$ for the speed and $\pm 3\sigma_d$ for deviation from straight. The resulting length is 3.03 m and the

width is 5.23 m. Taking the size of the motorcycle into account, the length needs to be approximately 4.5 m and the width 6 m. Since the motorcycle has a high horizontal speed, the box pile must in fact be longer to cushion the horizontal motion.

The Cushioning Process

Definitions

Big box: The cross-sectional area is much larger than that of the motorcycle, so the motorcycle interacts with only one box when hitting the cushion. We ignore the deformation and resistance of edges and poles. Thus, we need to consider only the interaction between motorcycle and the upper surface of that box.

Small box: The cross-sectional area is smaller than or comparable to that of motorcycle, so the motorcycle interacts with a number of them simultaneously. In this situation, the edges and poles play a great role in cushioning.

Since big and small boxes have different interactions, we analyze the two situations separately and compare their cushioning effect to determine the box size.

Analysis of Big Box

The motorcycle has considerable velocity when it hits the upper surface of the box, exerting a force on the upper surface. Because the corrugated cardboard is to some extent elastic, it first stretches a little. After some elongation, it goes into the plastic region and finally ruptures. This process is too complicated for us to calculate the total energy that results in the final rupture, so we reduce it to the following extreme situation.

The area of the upper surface of the cardboard is infinitely large and the motorcycle can be taken as a point compared with the cardboard. The piercing strength of the corrugated paper is 4.9 J [Corrugated fiberboard ... n.d.]. The total energy of the motorcycle is $E = mv^2/2$; since the order of magnitude of v is 10 m/s, the energy is approximately 10^4 J. Thus, the kinetic energy of the motorcycle is about 10^3 times the energy needed to pierce the cardboard. So the cardboard is easily pierced and provides little cushioning.

Although we examine the extreme situation, we can safely reach the following conclusion: The bigger the box, the easier for the motorcycle to penetrate the upper surface. In fact, as the cardboard becomes smaller, the motorcycle cannot be taken as a point again, so the force distributes over the surface, making it more difficult to penetrate the upper surface.

When the box becomes even smaller, the edges and poles of the box provide great support. But the cost increases at the same time.
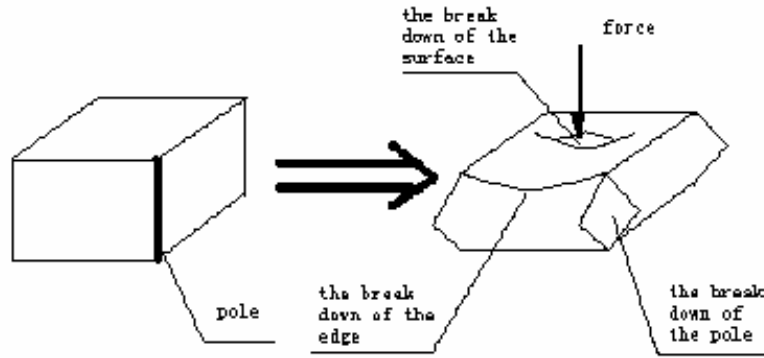
Small Box Model

Figure 2. Energy to break down a box.

Energy to break down a box. The breakdown of a box consists of three processes:

- breakdown of the upper surface,

- breakdown of the side surfaces, and

- breakdown of the poles.

After all three components break down, the box is completely damaged and cannot provide any cushioning. The the total energy required to break down a box is

$$E_{\text{box}} = E_{\text{upper}} + E_{\text{side}} + E_{\text{pole}}.$$

After some analysis (see **Appendix**), we find that E_{upper} and E_{side} are rather small compared with E_{pole}, so

$$E_{\text{box}} \approx E_{\text{pole}}. \tag{3}$$

We cannot find any data for calculating E_{pole}, so we make a rough estimate. Our analogy is to steel, for which we have data. We obtain the relationship between the maximum pressure to break the pole and the side:

$$p_{\text{pole}} = \tau p_{\text{side}},$$

where p_{pole} is the breakdown pressure for the pole, p_{side} is the breakdown pressure for a side surface, and τ is the transfer coefficient.

The breakdown pressure for a side surface is inversely proportional to the length ℓ of a side, so with edgewise crush resistance of the cardboard e_s we have

$$p_{\text{side}} = \frac{e_s}{\ell}. \tag{4}$$

Height of the pile. The motorcycle lands in a pile with an initial velocity and ultimately decelerates to zero, trapped in this pile. During that process, the force exerted on the motorcycle must be smaller than the maximum force that a person can bear; otherwise, the stunt person would be injured. Since 12 kN is the threshold, we consider 6 kN the safety bound. Thus, a 60 kg person can bear a maximum acceleration of $a_{\max} = 6000/60 = 100$ m/s². We want the mean acceleration to be smaller than this: $\bar{a} \leq a_{\max}$; we use mean acceleration because the cushion process has approximately constant deceleration. Thus, using kinematics, we obtain

$$\bar{a} = \frac{v^2}{2h} \leq a_{\max}, \qquad \text{or} \qquad h \geq \frac{v^2}{2a_{\max}}.$$

Thus, we let the pile height h be $v^2/2a_{\max}$, so that the motorcycle just touches the ground when it stops. In terms of the kinetic energy $E = mv^2/2$ of the motorcycle, we have

$$h = \frac{E}{ma_{\max}}. \tag{5}$$

Size of Boxes

To see how a box cushions the motion of the motorcycle, we define the *density of energy absorption* (DEA) of a box as

$$\rho = \frac{E_{\text{box}}}{V_{\text{box}}},$$

where E_{box} is the energy that the box can absorb during its breakdown and V_{box} is the original volume of the box. This density reflects the average cushioning ability of the box, and ρ can be thought of as the proportion of energy that is absorbed.

In a homogenous pile, all the boxes have the same DEA. The total energy that the pile absorbs is ρV_{pile} for the collapsed boxes. The height of the stack of boxes is h and the cross-sectional area of ones collapsed by the motorcycle is S, so

$$E = \rho V_{\text{pile}} = \rho Sh = \rho S \cdot \frac{E}{ma_{\max}} \tag{6}$$

from **(5)**. Cancelling the Es, we get

$$\rho = \frac{ma_{\max}}{S}.$$

We assume that the work done in breaking down a single box is proportional to p_{pole}, with proportionality coefficient k. In breaking down the pile of boxes,

this pressure is exerted across an area S and through a distance h, for total work $kp_{\text{pole}}Sh$. Equating this work to absorbed energy $E = \rho Sh$, we have

$$\rho Sh = E = kp_{\text{pole}}Sh,$$

so

$$\rho = \frac{ma_{\max}}{S} = kp_{\text{pole}};$$

and substituting $p_{\text{pole}} = \tau e_s/\ell$, we get

$$\ell = \frac{k\tau e_s}{ma_{\max}} S, \qquad \text{together with the previous} \qquad h = \frac{v^2}{2a_{\max}}. \qquad \textbf{(7)}$$

Substituting

$$m = 200 \text{ kg}, \quad a_{\max} = 100 \text{ m/s}, \quad v = 13 \text{ m/s},$$
$$k = 0.5, \quad e_s = 4 \times 10^3 \text{ N/m}, \quad S = 1.5 \text{ m}^2, \quad \text{and} \quad \tau = 1.5,$$

we get

$$\ell = 0.225 \text{ m}, \qquad h = 0.845 \text{ m}.$$

Number of Boxes

The landing area, 4.5 m by 6 m, needs to be extended to take the horizontal motion into account. The maximum length h that the motorcycle system can penetrate is sufficient for cushioning horizontal motion, so the pile should be $(4.5 + h) \times 6 \times h$ (meters) in dimension. From this fact, we can calculate the number of boxes needed in the pile.

From **(7)**, we have

$$h = \frac{mv^2}{2k\tau e_s S} \ell.$$

Thus, we know the dimensions of the pile:

$$N_h = \left\lceil \frac{h}{a} \right\rceil = \left\lceil \frac{mv^2}{2k\tau e_s S} \right\rceil = 4, \qquad N_w = \left\lceil \frac{6}{\ell} \right\rceil, \qquad N_l = \left\lceil \frac{4.5 + h}{\ell} \right\rceil. \qquad \textbf{(8)}$$

Numerically, we get

$$N_h = 4, \qquad N_w = 27, \qquad N_l = 24;$$

and the total number of boxes needed is $N = 4 \times 27 \times 24 = 2592$, with total surface area

$$S_{\text{total}} = 6a^2 N = 6 \times 0.225^2 \times 2592 \approx 780 \text{ m}^2.$$

Next, we analyze the change in cost if we alter the edge length of the boxes. As an approximation, we use

$$N = \frac{V_{\text{pile}}}{V_{\text{box}}} = N_h \cdot \frac{6 \times (4.5 + h)}{\ell^2} = \frac{108 + 24h}{\ell^2} = \frac{108 + \frac{12m\ell v^2}{k\tau e_s S}}{\ell^2}.$$

We have calculated for minimum h and ℓ. If we increase ℓ, that is, use bigger boxes, we need fewer boxes but the total cost increases, since

$$S_{\text{total}} = 6a^2 N = 6 \cdot \left(108 + \frac{12m\ell v^2}{k\tau e_s S}\right) \approx 648 + 540\ell.$$

The number of layers is 4 regardless of edge length; but for increased ℓ, the pile is lengthened to ensure that the motorcycle will not burst out of the pile due to the reduction of DEA.

In conclusion, smaller boxes lower the pile and are cost efficient; from computation, we should choose the minimum size 22.5 cm on a side, and need 2592 boxes.

Stacking Strategy

In the above discussion, we assume that we stack the boxes regularly stacked (no overlapping). We examine several other stacking strategies.

Pyramid Stack

Pyramid stacking stacks fewer boxes on top and more boxes at the bottom. When a stress is exerted on the pile, it is divided into the normal stress and shearing force along the slopes so that the downward stress diverge [Johnson 1985]. Furthermore, a pyramidal stack is more stable than a regular stack.

Mixed Stack

Mixed stacking is to stack boxes of different sizes in the pile; a common practice is to lay big boxes on the top and small boxes at the bottom.

For a regular stack, we considered the cushioning a motion with constant acceleration because we assumed that the supporting force provided by boxes is constant. However, this is not the case; generally speaking, the force is larger in the first few seconds, so decreasing the supporting force in the beginning is good for cushioning.

We have shown that big boxes provide less support than small boxes. So the mixed stack can be characterized as softer on the top and stiffer at the bottom. In fact, this kind of pile is similar to a sponge cushion, which is often used in stunt filming, high jump, pole vault, etc. In addition, cardboard is superior to a sponge cushion in this situation; a sponge cushion is too soft, so the motorcycle may lose balance.

Sparse Stack

Sparse stacking reserves a space c between adjacent boxes. Because each box absorbs a constant amount of energy, the spaces decrease the density of energy absorption ρ. Thus, given the initial kinetic energy, the height of the pile must increase to compensate for the decrease in ρ. Since $\rho S h = E$ from **(6)**, we have

$$\frac{h_{\text{new}}}{h_{\text{old}}} = \frac{\rho_{\text{old}}}{\rho_{\text{new}}} = \frac{1/\ell^2}{1/(\ell + c)^2} = \left(1 + \frac{c}{\ell}\right)^2.$$

So, the cushioning distance h is proportional to the square of $(1 + c/\ell)$. The sparse stack saves some material at the cross section but increase the cushioning distance. With no change in base area, for rectangular stacking the surface area is constant, while in a pyramid stacking it decreases.
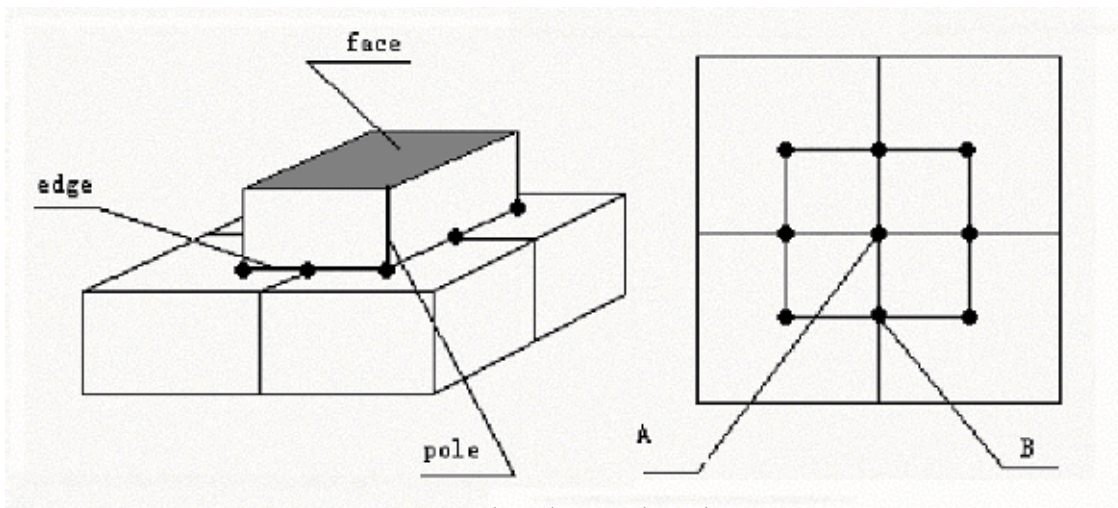
Crossed Stack

Figure 3. Crossed stacking: side and top views.

Crossed stacking is to lay the upper boxes on the intersection of the lower boxes, as shown in **Figure 3**. There are two kinds of interactions on the surface:

- vertex-to-face: the interaction between pole of the upper box and the surface of the lower box. Because the pole is much stronger than the edge and surface, the pole will not deform but the upper surface may break down.

- edge-to-edge: the interaction between edge of the upper box and the perpendicular edge of the lower box. The two edges both bend over. **Figure 4** shows the deformation of the boxes.

To determine whether crossed stacking is better than regular stacking, we compare the pile height of the two approaches.
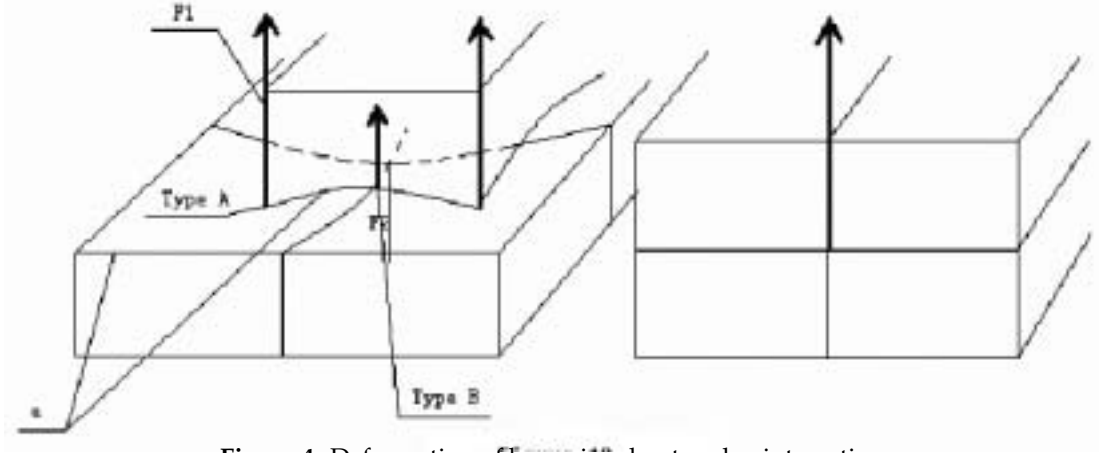
Figure 4. Deformation of boxes in edge-to-edge interaction.

The force provided by vertex-to-face structure is $F_1 = b_s a^2$; the force provided by edge-to-edge structure is $F_2 = e_s a$. Thus, introducing the same analysis as above, the pile height of the crossed stack is

$$h = \frac{mv^2 \ell^2}{8kS(F_1 + F_2)} = \frac{mv^2 \ell^2}{8kS(e_s \ell + b_s \ell^2)} = \frac{1}{8(e_s + b_s \ell)} \cdot \frac{\ell mv^2}{kS},$$

compared to the pile height of the regular stack,

$$h' = \frac{m\ell}{2k\tau e_s S} \cdot v^2 = \frac{1}{2\tau e_s} \cdot \frac{\ell mv^2}{kS},$$

For all edge lengths, we have $h < h'$: Crossed stacking needs a smaller pile height than regular stacking.

The Final Stacking Strategy

Synthesizing the analyses of several stacking approaches, we present our final stack approach (**Figure 5**). The far end of the pile is a quasislope, and big boxes are on the top while small boxes are cross-stacked at the bottom. The slope is in the same direction as the initial velocity of the motorcycle. Therefore, the stress that the motorcycle exerts on the pile dissipates along this direction.

Modifications to the Box

In search for a better solution, we may make some modifications to the boxes to make the pile more comfortable, as well as lower and cheaper.

Changing Edge Ratio

We have assumed the box to be cubic; we now investigate the energy absorbing properties of a box that is not cubic.
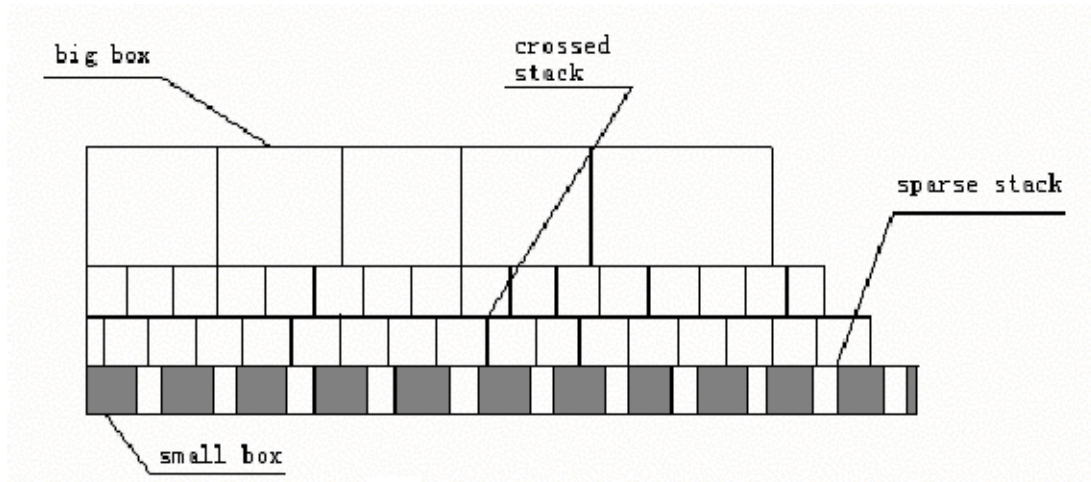
Figure 5. The final stacking strategy (cross-sectional view).

According to Wolf's empirical formula [Sun 1995, 4] we have

$$P = \frac{1.1772 P_m \sqrt{tz}(0.3228 R_L - 0.127 R_L^2 + 1)}{100 H_0^{0.041}}, \tag{9}$$

where

- P is the stiffness of the box,

- P_m is the edgewise crash resistance of cardboard,

- t is the thickness of cardboard,

- z is the perimeter of the box,

- R_L is the ratio of the length and width of the box, and

- H_0 is the height of the box.

Because the exponent of H_0 is 0.041, the height makes little difference to the stiffness of the box. Thus, we should choose a small value for H_0, since a lower height means lower center of gravity and thus better stability for the pile.

Stuffing the Box

After the collapse process, the box no longer provides any supporting force. To lengthen the effective time, we may add elastic material in the box, such as foam and corrugated paper. They must be soft and loose enough, or else they may prevent the box from collapsing or occupy too much space when the box breaks down, defeating one of the reasons why a box pile is preferable to foam or a spring cushion.

Adding Supporting Structures

Apart from stuffing the box, we may also add supporting structures, such as vertical struts. They strengthen the box by preventing tangential displacement and supporting the upper surface of the box. There are different ways, such as triangular or square buttresses in the corners. These supporting structures bring considerable improvement to the mechanics while the total cost increases insignificantly. Because these structure significantly strengthen the box, the size of the box should be increased.

Other Considerations

To make the landing comfortable, the upper layers should be more elastic while the lower layers stiff. To accomplish this, we can put taller boxes with stuffing in the upper layers and shorter ones with supporting structures in the bottom layers.

Generalizing the Result

The General Process

We assumed that a 60 kg stunt person riding a 120 kg motorcycle jumps horizontally from a 5 m stage at 10 m/s. Now we offer a more general statement.

Let the masses of the rider and the motorcycle be m_r and m_m; the new a and m are $6kN/m_r$ and $(m_r + m_m)$. We also calculate the values of final speed v and kinetic energy E, using the initial speed v_0 and stage height H:

$$E = mgH + \tfrac{1}{2}mv_0^2, \qquad v = \sqrt{\frac{2E}{m}}.$$

We can then apply **(7)** to calculate the edge of box and the height of the pile, and we get the dimensions of the pile from **(8)**.

We can also make small adjustments by changing the structure of boxes and the pile, according to the approaches introduced in the section on stacking strategy.

Quick Reference Card for the Stunt Coordinator

To see how our model works with different circumstances, we suppose that a stunt team has an actor (65 kg) and an actress (50 kg) and four motorcycles, namely, Toyota CBX250S, Jialing JH125, Yamaha DX100, and Yamaha RX125 [Zhaohu n.d.].

We summarize the results in **Figure 6** for the stunt coordinators' quick reference in practical filming work. Note that the team needs only two types of boxes. Sensitivity analysis—varying v_0, H_0, m_r, and m_m by 10%—shows that h and ℓ are not sensitive to small changes in these variables.

The box size

Mass of Actor (kg)	Mass of Motorcycle (kg)	Basal Area (m²)	Box size (cm)	Alternative Box Size (cm)	Adjustment
50	129	1.342	18.7	22.5	Sparse Placement
50	105	1.500	24.2	22.5	Buttress
50	97	1.372	23.3	22.5	Stuffing
50	83.5	1.408	26.4	28.0	Sparse Placement
65	129	1.342	22.5	22.5	
65	105	1.500	28.7	28.0	Stuffing
65	97	1.372	27.5	28.0	Crossed Placement
65	83.5	1.408	30.8	28.0	Buttress

The pile height

Actor's Mass (kg)	Stage Height (m)	Initial Velocity (m/s)	Pile Height (m)	Actor's Mass (kg)	Stage Height (m)	Initial Velocity (m/s)	Pile Height (m)
65	15	15	2.81	50	15	15	2.16
65	15	5	1.73	50	15	5	1.33
65	5	15	1.75	50	5	15	1.35
65	5	5	0.67	50	5	5	0.51

Figure 6. Quick reference card for the stunt coordinator.

Model Validation

Validation of Homogeneity Assumption

Our main model is based on the assumption that when the boxes are small, we consider the box pile as a homogenous substance. Now we use Wolf's empirical formula **(9)** to validate our assumption.

Because we consider all the boxes as cubes and because the exponent of H_0, 0.041, is so small, the denominator can be considered as a constant 100. We simplify the expression to

$$P = \frac{1.1772 \cdot 5880 \cdot \sqrt{0.0045 \cdot 2\ell \cdot 100}(0.3228 - 0.127 + 1)}{100},$$

so that

$$p = \frac{P}{(100\ell)^2} = 7.85(100\ell)^{-\frac{3}{2}};$$

the derivative of p is $dp/d\ell = -11.78 \times 10^{-3} a^{-\frac{5}{2}}$. We graph the derivative in **Figure 7**. For $\ell > 5$ cm, we have $dp/d\ell \approx 0$, so p is independent of ℓ when $\ell > 5$ cm. So we have proved our assumption of homogeneity.
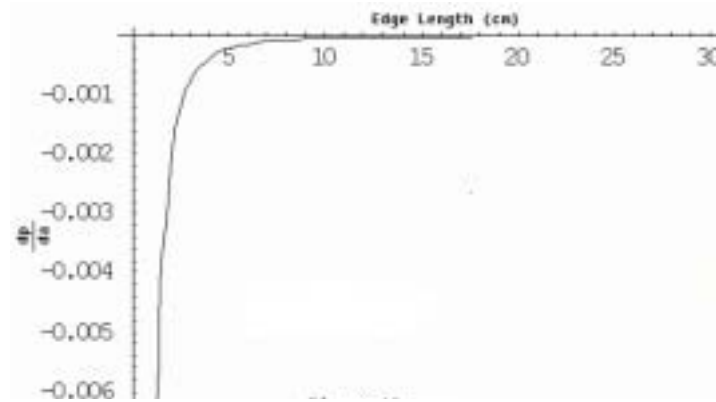
Figure 7. Derivative of p as a function of edge length ℓ.

Validation of Small Box Model

Consider a single box with generalized dimensions $\ell \times w \times h$. We assume that the stiffness is proportional to the average force that the box is subjected to when it is collapsed, with proportionality coefficient k. Thus the work it does, or the energy that it absorbs from the colliding object, is $W = kPh$. Equating W with E, we have $kPh = \rho Sh =$
$rho\ell wh$, or $kP = \rho\ell w$. We use Wolf's formula **(9)** for P and minimize the surface area of the box subject to the resulting constraint on ℓ, w, and h:

$$\text{minimize} \qquad S = 2(\ell w + wh + \ell h)$$

$$\text{subject to} \qquad k \cdot \left(\frac{1.772 P_m \sqrt{t(\ell + w)}(0.3228 R_L - 0.1217 R_L^2 + 1)}{100 h^{0.041}} \right) = \rho\ell w.$$

This optimization model is nonlinear, so we cannot easily get an analytical solution. However, adding our assumption that the box is a cube significantly simplifies the constraint equation. We wrote a program to search for the optimum value and found that the minimum surface area is 2.1×10^3 cm^2 when the edge length is 19.1 cm.

This result is consistent with our earlier one, $S = 3.0 \times 10^3$ cm^2 and $a = 22.5$ cm, confirming the correctness of our model.

Strengths and Weaknesses

Strengths

- We carefully built our model on the limited information that we could find; some of the data crucial to our solution are from cardboard company advertisements. Although there are not enough data available for us to justify our model fully, we compared our result with available data. We also visited such Websites as `http://www.stuntrev.com`, and examined stunt videos.

We found that most of their cushioning facilities agree well with our model. So, we believe our result has practical value.

- We abstract the pile of boxes into a simple homogenous model, which proves reasonable.

- We apply careful mechanical analysis in our model design. Given reasonably accurate data, the model can provide a good result.

- The model examines various stacking approaches and modifications to the boxes. It helps to find the best way to design a pile of box for cushioning.

- We generalize the model to different situations and get good results.

Weaknesses

- We ignore the scattering of boxes when they are crushed, which may contribute to cushioning.

- The model is only as accurate as the data used, but some data are dubious. We are forced to obtain a crucial data by analogy with a material (steel) of similar structure for which data are available.

- The number of boxes is very large (more than 2,000); this may be caused by our choice of the thinnest corrugated cardboard.

- We ignore air resistance; the error introduced is about 5%.

Appendix

Corner Structure

According to structure mechanics, the corner structure is a stable structure. That is why the "T shape L shape and I shape structure" are used widely in buildings and bridges [Punmia and Jain 1994].

We study the extension of the side surface when the crush happens. We consider a small bending of the pole after the outer force acts on the upper surface (see **Figures 8–9**)

The force F_p is composed of two equal forces F_{p1} and F_{p2} produced by the extension of the side surface, so $F_p = \sqrt{2}F_{p1} = \sqrt{2}F_{p2}$. The flexibility of the cardboard is described by Young's modulus. We have

$$E \cdot \frac{\Delta L}{a} = \frac{F_{p1}}{A},$$

where ΔL is the small extension of the side surface and A is the cross-sectional area (thickness plus side length) of the cardboard.
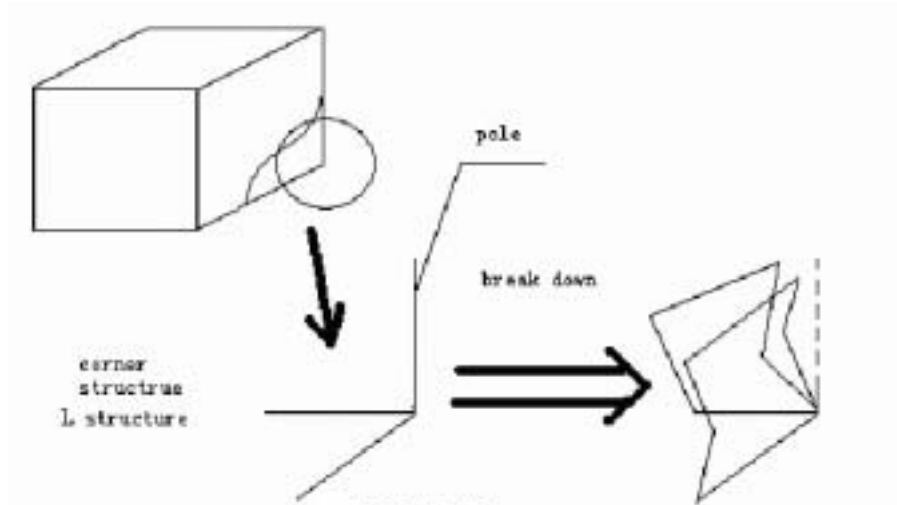
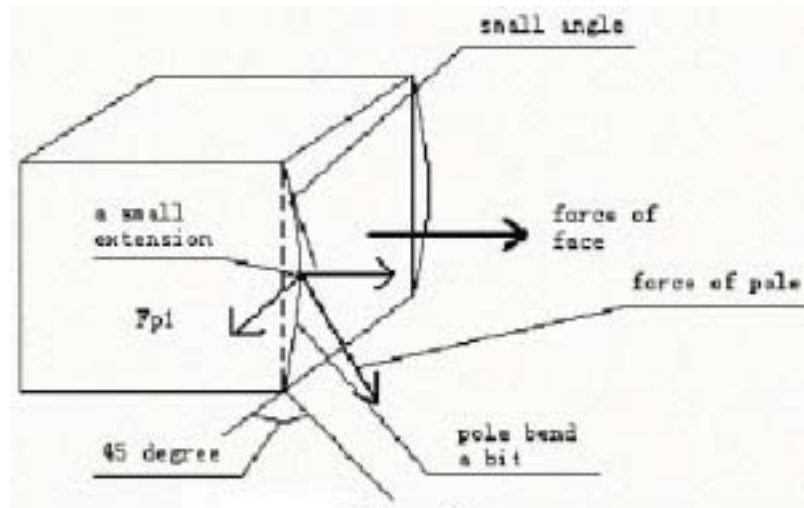**Figure 8.** Breakdown of a corner structure.

Figure 9. Bulging of a side under pressure on the top surface.

We do not find Young's modulus for corrugated cardboard on the handbook; but from the values for similar materials, we suppose that is is about 0.5 MPa. Building the force balance equation, we assume $F_p = F_f$; then

$$\Delta L = \frac{F_f a}{AE}; \qquad \max F_f = e_s a^2; \qquad \Delta L = \frac{e_s a^3}{AE}$$

For $a = 10$ cm, $A = 2.5$ cm^2, and $e_s = 4 \times 10^3$ Pa, we get $\Delta L = 3.2$ mm.

This result means that the maximum force F_f that can make the side surface deform can bring only a tiny (3.2-mm) extension to the pole. This is a strong support for our supposition that $F_p \gg F_f$, which supports **(3)**, $E_{\text{box}} \approx E_{\text{pole}}$.

The Determination of τ

To compute the p_{pole} value of is an enormous difficulty because of the lack of data. As in the iron industry, we set $p_{\text{pole}} = \tau p_{\text{side}}$, where τ is a constant depending on the material.

We determine τ by analogy to the method in the iron industry, for which there is theory about the axial compression of column with cross-sectional shapes that are rectangular or L-shaped. The former has strength parameter 0.77 to 0.93 while the latter has strength parameter 0.56 to 0.61; the ratio τ of the two is between 1.26 and 1.66. The average value 1.46; for simplicity, we let $\tau = 1.5$. [Huang et al. 2002].

References

Ai, Zhaohu. 1999. *Imported and Domestic Motorcycles*. People's Posts and Telecommunications Publishing House.

Corrugated fibre board for export products GB 5034-85. 2001. `http://main.pack.net.cn/wlz/wlz_article/fl2.htm`.

Estes, Richard D., and Kathryn S. Fuller. 1999. Elephant, *Loxodonta africana*. `http://www.nature-wildlife.com/eletxt.htm`. In *The Safari Companion: A Guide to Watching African Mammals, Including Hoofed Mammals, Carnivores, and Primates*, by Richard D. Estes, Daniel Otte, and Kathryn S. Fuller. White River Junction, VT: Chelsea Green Publishing Company.

Halliday, David, Robert Resnick, and Kenneth S. Krane. 2001. *Physics*. 5th ed. Vol. 1. New York: Wiley.

Huang, Chengkui, Dan Wang, and Bo Cui. 2002. Study of ultimate axial compression of the special-shaped columns. *Journal of Dalian University Technology* 42 (2): 213–217.

Johnson, K.L. 1985. *Contact Mechanics*. New York: Cambridge University Press.

Leavitt, Steven. n.d. The Art of Stunts. `http://www.stuntrev.com`.

Punmia, B.C., and A.K. Jain. 1994. *Strength of Materials and Mechanics of Structure*. New Delhi: Lakshmi Publications.

Sheng, Zhou, Shiqian Xie, and Chenyi Pan. 2001. *Probability and Statistics*. Higher Education Press.

Sun, Cheng. 1995, *Package Structure Design*. China Light Industry Press.

UIAA Safety Regulations. n.d. International Mountaineering and Climbing Federation. `http://www.cc.nctu.edu.tw/~mclub/meichu/teach/equip/equipment2_1.html`.

Judge's Commentary:
The Outstanding Stunt
Person Papers

William P. Fox
Dept. of Mathematics
Francis Marion University
Florence, SC 29501
`bfox@fmarion.edu`

Introduction

Once again, Problem A proved to be a nice challenge for both the students and the judges. The students did not have a wealth of information for the overall model from the Web or from other resources. Students could find basic information for helping model the jumping of the elephant from many sources. This problem turned out to be a "true" modeling problem; the students' assumptions led to the development of their model. The judges had to read and evaluate many diverse (yet sometimes similar) approaches in order to find the "best" papers. Judges found mistakes even in these "best" papers, so it is important to note that "best" does not mean perfect. Many of these papers contain errors in modeling, assumptions, mathematics, and/or analysis. The judges must read and apply their own subjective analyses to evaluate critically both the technical and expository solutions presented by the teams.

No paper analyzed every element nor applied critical validation and sensitivity analysis to all aspects of their model.

Advice to Students and Advisors

At the conclusion of the judging, the judges offered the following comments:

- Follow the instructions

  - Clearly answer all parts.
  - List all assumptions that affect the model and justify your use of them.

– Make sure that your conclusions and results are clearly stated. Any mission directives or additional questions need to be addressed.

– Restate the problem in your words.

– At the end, ask yourselves the question, "Does our answer make intuitive and/or common sense?"

- "Executive" Summary (Abstract) of Results

  The summary is the first piece of information read by a judge. It should be well written and contain the bottom-line answer or result. It should motivate the judge to read your paper to see how you obtained your results. The judges place considerable weight on the summary, and winning papers are sometimes distinguished from other papers based on the quality of the summary. To write a good summary, imagine that a reader may choose whether or not to read the body of the paper based on your summary. Thus, a summary should clearly describe your approach to the problem and, most prominently, your most important conclusions. Summaries that are mere restatements of the contest problem or are cut-and-pasted boilerplate from the Introduction are generally considered weak.

  – Put the "bottom line results and managerial recommendations" in the summary.

  – Be succinct; do not include a discussion of methods used, and do not just list a description or historical narrative of what you did.

- Clarity and Style

  – Use a clear style and do not ramble.

  – Do not list every possible model or method that could be used in a problem.

  – A table of contents is very helpful to the judges.

  – Pictures, tables, and graphs are helpful; but you must explain them clearly.

  – Do not include a picture, table, or graph that is extraneous to your model or analysis.

  – Do not be overly verbose, since judges have only 10–30 min to read and evaluate your paper.

  – Include a graphic flowchart or an algorithmic flow chart for computer programs used/developed.

- The Model

  – Develop your model—do not just provide a laundry list of possible models even if explained.

- Start with a simple model, follow it to completion, and then refine it. Many teams built a model without air resistance and—before determining the number of boxes needed—they refined only that part of the model to include air resistance.

- Computer Programs

  - If computer programs are included, clearly define all parameters.
  - Always include an algorithm in the body of the paper for any code used.
  - If running a Monte Carlo simulation, be sure to run it enough times to have a statistically significant output.

- Validation

  - Check your model against some known baseline, if possible, or explain how you would do this.
  - Check sensitivity of parameters to your results.
  - Check to see if your recommendations/conclusions make common sense.
  - Use real data.
  - The model should represent human behavior and be plausible.

- Resources

  - All work needs to be original or else references must be cited—with specific page numbers—in the text of the paper; a reference list at the end is not sufficient. (This particular problem lent itself to a good literature search.)
  - Teams may use only inanimate resources. This does not include people.
  - Surf the Web, but document sites where you obtained information that you used.

Judging

The judging is accomplished in two phases.

- Phase I is "triage judging." These are generally only 10-min reads with a subjective scoring from 1 (worst) to 7 (best). Approximately the top 40% of papers are sent on to the final judging.

- Phase II, at a different site, is done with different judges and consists of a calibration round followed by another subjection round based on the 1–7 scoring system. Then the judges collaborate to develop an unique 100-point scale that will enable them to "bubble up" the better papers. Four or more longer rounds are accomplished using this scale, followed by a lengthy discussion of the last final group of papers.

Reflections of the Triage Judges

- Lots of good papers made it to the final judging

- The summary made a significant difference. A majority of the summaries were poor and did not tell the reader the results obtained. A large number of teams simply copied and pasted their introductory paragraphs, which have the different purpose of establishing the background for the problem.

- The biggest thing that caught the judges' eye was whether or not the team paid attention to the questions asked in the problem. A number of teams addressed what they knew but didn't consider the real question—they got cut quickly.

- The next deciding factor was whether a team actually did some modeling or simply looked up a few equations and tried to shoehorn those into the problem. We looked for evidence that modeling had taken place; experiments were good to see.

- A final concern was the quality of writing—some was so poor that the judge couldn't follow or make any sense out of the report.

    Triage and final judges' pet peeves include:

- Acronyms that are not immediately understood and tables with columns headed by Greek letters.

- Definition and variable lists that are embedded in a paragraph.

- Equations used without explaining terms and what the equation accomplished.

- Copying derivations from other sources—a better approach is to cite the reference and explain briefly.

Approaches by the Outstanding Papers

    Six papers were selected as Outstanding submissions because they:

- developed a workable, realistic model from their assumptions and used it to answer all elements of the stunt person scenario;

- made clear recommendations as to the number of boxes used, their size, and how they should be stacked, and offered a generalization to other stunt persons;

- wrote a clear and understandable paper describing the problem, their model, and results; and

- handled all the elements.

  The required elements, as viewed by the judges, were in two distinct phases.

- Models needed to consider the mission of the stunt person. A model had to be developed that ensured that the stunt person could jump over the elephant. The better teams then worked to minimize the speed with which to accomplish this jump. Teams that used a high-speed jump were usually discarded by the judges quickly.

- In Phase II, the model had to consider the landing; this included speed, energy, force, and momentum of the jumper, so that the boxes could be used safely to cushion the fall.

Most of the better papers did an extensive literature and Web search for information about cardboard. However, many teams spent way too much energy researching cardboard; their time would have been better spent in modeling.

The poorest section in all papers, including many of the Outstanding papers, was the summary.

Another flaw found by the judges was the misuse of ECT (Edge Compression Testing) in a proportionality model. It is true that a proportionality exists, as shown in **Figure 1**; but that proportionality is not the one used by the teams.
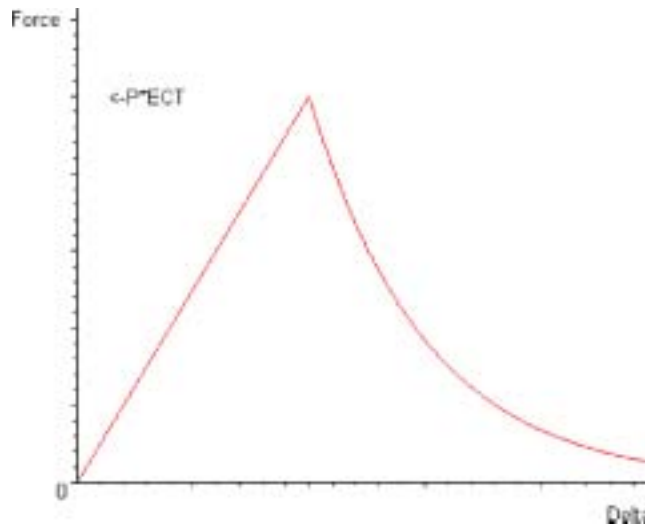
Figure 1. Force as a function of delta in ECT.

Many started with

$$BCS = 5.87 \times \text{ECT} \times \sqrt{Pt},$$

where P is the perimeter of the box and t is its thickness. Many went on to develop an energy model, where energy is the area under the curve, namely $\frac{1}{2} \times P \times \text{ECT} \times h(\text{magic number})$. However, this proportionality is flawed. The potential energy is an area but it is $\frac{1}{2} \times P \times \text{ECT} \times \delta$, which is not an equivalent statement (see **Figure 1**).

The better papers used a variety of methods to model the safe landing. These included kinematics, work, and energy absorption. The discussion of the boxes and how they were to be secured was also an important feature. One team laid many large mattress boxes flat on top of the stacked boxes to give a smooth landing area. The judges enjoyed the creativity of the teams in this area.

About the Author

Dr. William P. Fox is Professor and the Chair of the Department of Mathematics at Francis Marion University. He received his M.S. in operations research from the Naval Postgraduate School and his Ph.D. in operations research and industrial engineering from Clemson University. Prior to coming to Francis Marion, he was a professor in the Department of Mathematical Sciences at the United States Military Academy. He has co-authored several mathematical modeling textbooks and makes numerous conference presentations on mathematical modeling, as well as being a SIAM lecturer. He is currently the director of the High School Mathematical Contest in Modeling (HiMCM). He was a co-author of last year's Airline Overbooking Problem.

The Genetic Algorithm-Based Optimization Approach for Gamma Unit Treatment

Sun Fei
Yang Lin
Wang Hong
Donghua University
Shanghai, China

Advisor: Ding Yongsheng

Abstract

The gamma knife is used to treat brain tumors with radiation. The treatment planning process determines where to center the shots, how long to expose them, and what size focusing helmets should be used, to cover the target with sufficient dosage without overdosing normal tissue or surrounding sensitive structures.

We formulate the optimal treatment planning for a gamma-knife unit as a sphere-packing problem and propose a new genetic algorithm (GA)-based optimization approach for it. Considering the physical limitations and biological uncertainties involved, we outline a reasonable, efficient and robust solution.

First, we design a geometry-based heuristic to produce quickly a reasonable configuration of shot sizes, locations, and number. We first generate the skeleton using a 3D-skeleton algorithm. Then, along the skeleton, we use the GA-based shot placement algorithm to find a best location to place a shot. By continuously iterating the algorithm, we obtain the number, sizes, and the locations of all shots. After that, we develop a dose-based optimization method.

Then we implement simulations of our models in Matlab. We did numerous computer simulations, using different shape or size targets, to examine the effectiveness of our model. From the simulation results, we know that the geometry-based heuristic with the GA optimization approach is a useful tool for in the selection of the appropriate number of shots and helmet sizes. Generally, all of the optimized plans for various targets provide full-target coverage with 90% of the prescription isodose.

Moreover, we do sensitivity analysis to our model in the following aspects:

- the sensitive structures;

- at the 30%, 40%, 60%, or 70% isodose level;

- the issue of global versus local optimality;

- conformality; and

- the robustness. We also discuss the strengths and limitations of our model.

The results indicate that our approach is sufficiently robust and effective to be used in practice. In future work, we would fit ellipsoids instead of spheres, since some researchers note that the dose is skewed in certain directions.

Introduction

The gamma knife unit delivers ionizing radiation from 201 cobalt-60 sources through a heavy helmet. All beams simultaneously intersect at the *isocenter*, resulting in an approximately spherical dose distribution at the effective dose levels. Delivering dose is termed a *shot*, and a shot can be represented as a spheres. Four interchangeable outer collimator helmets with beam channel diameters of 4, 8, 14, and 18 mm are available. For a target volume larger than one shot, multiple shots can be used.

Gamma knife treatment plans are conventionally produced using a manual iterative approach. In each iteration, the planner attempts to determine

- the number of shots,

- the shot sizes,

- the shot locations, and

- the shot exposure times (weights) that would adequately cover the target and spare critical structures.

For large or irregularly shaped treatment volumes, this process is tedious and time-consuming, and the quality of the plan produced often depends on both the patience and the experience of the user. Consequently, a number of researchers have studied techniques for automating the gamma knife treatment planning process [Wu and Bourland 2000a; Shu et al. 1998]. The algorithms that have been tested include simulated annealing [Leichtman et al. 2000; Zhang et al. 2001], mixed integer programming, and nonlinear programming [Ferris et al. 2002; 2003; Shepard et al. 2000; Ferris and Shepard 2000].

The objective is to deliver a homogeneous (uniform) dose of radiation to the tumor (the target) area while avoiding unnecessary damage to the surrounding tissue and organs. Approximating each shot as a sphere [Cho et al. 1998] reduces the problem to one of geometric coverage. Kike [Liu and Tang 1997], we formulate optimal treatment planning as a sphere-packing problem and we propose an algorithm to determine shot locations and sizes.

Assumptions

To account for all physical limitations and biological uncertainties involved in the gamma knife therapy process, we make several assumptions as follows:

A1: The shape of the target is not too irregular, and the target volume is a bounded. As a rule of thumb, the target to be treated should be less than 35 mm in all dimensions. Its three-dimensional (3D) digital image, usually consisting of millions of points, can be obtained from a CT or MRI.

A2: We consider the target volume as a 3D grid of points and divide this grid into two subsets, the subset of points in and out of the target, denoted by T and N, respectively.

A3: Four interchangeable outer collimator helmets with beam channel diameters $w = \{4, 8, 14, 18\}$ mm are available for irradiating different size volumes. We use (x_s, y_s, z_s) to denote the coordinates of the center location of the shot and $t_{s,w}$ to denote the time (weight) that each shot is exposed. The total dose delivered is a linear function of $t_{s,w}$. For a target volume larger than one shot, multiple shots can be used to cover the entire target. There is a bound n on the number of shots, with typically $n \leq 15$.

A4: Neurosurgeons commonly use isodose curves as a means of judging the quality of a treatment plan; they may require that the entire target is surrounded by an isodose line of $x\%$, e.g., 30–70%. We use an isodose line of 50%, which means that the 50% line must surround the target.

A5: The dose cloud is approximated as a spherically symmetric distribution by averaging the profiles along x, y, and z axes. Other effects are ignored.

A6 The total dose deposited in the target and critical organ should be more than a fraction P of the total dose delivered; typically, $25\% \leq P \leq 40\%$.

Optimization Models

Analysis of the Problem

The goal of radiosurgery is to deplete tumor cells while preserving normal structures. An optimal treatment plan is designed to:

R1: match specified isodose contours to the target volumes;

R2: match specified dose-volume constraints of the target and critical organ;

R3: constrain dose to specified normal tissue points below tolerance doses;

R4: minimize the integral dose to the entire volume of normal tissues or organs;

R5: minimize the dose gradient across the target volume; and

R6: minimize the maximum dose to critical volumes.

It also is constrained to

C1: prohibit shots from protruding outside the target,

C2: prohibit shots from overlapping (to avoid hot spots),

C3: cover the target volume with effective dosage as much as possible (at least 90% of the target volume must be covered by shots), and

C4: use as few shots as possible.

We design the optimal treatment plan in two steps.

- We use a geometry-based heuristic to produce a reasonable configuration of shot number, sizes and locations.

- We use a dose-based optimization to produce the final treatment plan.

Geometry-Based Heuristic for Sphere-Packing

We model each shot as a sphere, and we use the medial axis transform (known as the *skeleton*) of the target volume to guide placement of the shots. The skeleton is frequently used in shape analysis and other related areas [Wu et al. 1996; Wu and Bourland 2000b; Zhou et al. 1998]. We use the skeleton just to find good locations of the shots quickly. The heuristic is in three stages:

- We generate the skeleton using a 3D skeleton algorithm.

- We place shots and choose their sizes along the skeleton to maximize a measure of our objective; this process is done by a genetic algorithm (GA)-based shot placement approach.

- After the number of focusing helmets to be included in the treatment plan is decided, the planning produces a list of the possible helmet combinations and a suggested number of shots to use.

Skeleton Generation

We adopt a 3D skeleton algorithm that follows similar procedures to Ferris et al. [2002]. We use a morphologic thinning approach [Wu 2000] to create the skeleton, as opposed to the Euclidean-distance technique. The first step in the skeleton generation is to compute the contour map containing distance information from the point to a nearest target boundary. Then, based on the contour map, several known skeleton extraction methods [Ferris et al. 2002; Wu et al. 1996; Wu and Bourland 2000b; Zhou et al. 1998; Wu 2000] can be used. Since the method in Ferris et al. [2002] is simple and fast, we use it.

Genetic Algorithm-Based Shot Placement

We restrict our attention to points on the skeleton. We start from a special type of skeleton point, an *endpoint* (**Figure 1**): A point in the skeleton is an endpoint if it has only one neighbor in the skeleton.

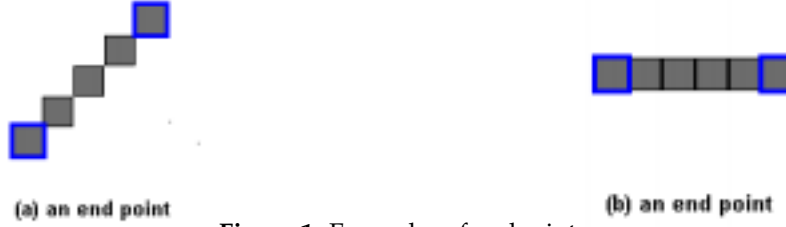(a) an end point   (b) an end point

Figure 1. Examples of endpoints.

Starting from an endpoint, we look for the best point to place a shot and determine the shot size by using GA [Goldberg 1989; Mann et al. 1997]. In the GA-based shot placement algorithm, we must solve the following problems:

The encoding method. In general, bit-string (0s and 1s)) encoding is the most common method adopted by GA researchers because of its simplicity and tractability. However, in this case, if we directly encode the point coordinates (x_s, y_s, z_s) into a bitstring, crossover and mutation generate some points that are not in the skeleton. To solve this problem, we build a table of correspondence between the point coordinates and the point number (1 to M); instead of encoding the point, we encode the point number. We select m points from all points of the skeleton to form a population; a single point is a *chromosome*.

Performance evaluation. The key to the GA-based approach is the fitness function. Ideally, we would like to place shots that cover the entire region without overdosing within (or outside) of the target. Overdosing occurs outside the target if we choose a shot size that is too large for the current location, and hence the shot protrudes from the target. Overdosing occurs within the target if we place two shots too close together for their chosen sizes.

Before defining a fitness function, we give some definitions:

- *Fraction*: A target part that is not large enough to be destroyed by the smallest shot without any harm to the surrounding normal tissue.
- *Span*: The minimum distance between the current location and the endpoint at which we started.
- *Radius*: The approximate Euclidean distance to the target boundary.

We would like to ensure that the span, the radius, and the shot size w are as close as possible. Therefore, we choose a fitness function that is the sum of the squared differences between these three quantities. The fitness function can ensure that the generating fraction is the smallest after every shot is placed on the target [Ferris et al. 2002]:

$$\text{Fit} = \phi_{s,r}(x, y, z) + \phi_{s,w}(x, y, z) + \phi_{r,w}(x, y, z),$$

where

$$\phi_{s,r}(x,y,z) = \big[\text{span}(x,y,z) - \text{radius}(x,y,z)\big]^2, \tag{1}$$

$$\phi_{s,w}(x,y,z) = \big[\text{span}(x,y,z) - w\big]^2, \tag{2}$$

$$\phi_{r,w}(x,y,z) = \big[\text{radius}(x,y,z) - w\big]^2. \tag{3}$$

- Equation **(1)** ensures that we pack the target volume as well as possible, that is, the current span between shots should be close to the distance to the closest target boundary.

- Equation **(2)** is used to choose a helmet size that fits the skeleton best for the current location.

- Equation **(3)** favors a location that is the appropriate distance from the target boundary for the current shot size.

Genetic operators. Based on the encoding method, we develop the genetic operators in the GA: crossover and mutation.

- Crossover/recombination is a process of exchanging genetic information. We adopt one-point crossover operation; the crossover points are randomly set.

- Mutation operation. Any change in a gene is called a *mutation*; we use point mutation.

We propose the following GA-based shot placement algorithm:

1. Find a skeleton and all its endpoints. Take one of the endpoints as a starting point.

2. Randomly search all the points in the skeleton using the GA to find the location and size of the best shots as follows:

   (a) Generate randomly m (= 100) points from all the points (e.g., $M = 1000$) in the skeleton. The m points are the chromosomes. Set the crossover rate $p_c = .95$, the mutation rate $p_m = .05$, the desired Fit function, and the number n_g of generations.

   (b) Calculate the Fit of all the m points in the skeleton.

   (c) If the algorithm has run n_g steps, or if one of the m points satisfies the desired Fit, the GA stops (at this time, the best shot is chosen); else encode m points into the bit strings.

   (d) To do crossover and mutation operation to the m bitstrings, go to 2b.

3. Considering the rest of the target in whole as a new target, repeat Steps 1–2 until the rest of the target are fractions (at this time, all best shots are found).

Dose-Based Optimization

After we obtain the number, sizes and the locations of shots, we develop a dose-based optimization method.

We determine a functional form for the dose delivered at a point (i, j, k) from the shot centered at (x_s, y_s, z_s). The complete dose distribution can be calculated as a sum of contributions from all of the individual shots of radiation:

$$D(i, j, k) = \sum_{(s,w) \in S \times W} t_{s,w} D_{s,w}(x_s, y_s, z_s, i, j, k),$$

where $D_{s,w}(x_s, y_s, z_s, i, j, k)$ is the dose delivered to (i, j, k) by the shot of size w centered at (x_s, y_s, z_s) with a delivery duration of $t_{s,w}$. Since $D_{s,w}$ is a complicated (nonconvex) function, we approximate it by

$$D_{s,w}(x_s, y_s, z_s, i, j, k) = \sum_{i=1}^{2} \lambda_i \left(1 - \int_{-\infty}^{x} \frac{1}{\sqrt{\pi}} e^{-x^2} \, dx \right), \qquad \textbf{(4)}$$

where $x = (t - r_i)/\sigma_i$ and λ_i, γ_i, and σ_i are coefficients [Ferris and Shepard 2000].

To meet the requirement of matching specified isodose contours to target volume at the 50% isodose line, the optimization formulation should impose a constraint on the 50% isodose line that must surround the target. We impose strict lower and upper bounds on the dose allowed in the target, namely, for all $(i, j, k) \in T$, the dose $D(i, j, k)$ satisfies

$$0.5 \leq D(i, j, k) \leq 2. \qquad \textbf{(5)}$$

To meet the requirement (R2) to match specified dose-volume constraints of the target and critical organ, based on assumption (A3) (which sets out the size of the beam channel diameters), no more than n shots are to be used; so in each *card* (any section of the target) we have

$$\text{card}\big[\{(s, w) \in S \times W \mid t_{s,w} > 0\}\big] \leq n. \qquad \textbf{(6)}$$

The value of tolerance doses of the normal tissue points is q, $D(i, j, k) < q$ for all (i, j, k). The number of shots n is no more than 15, so the tolerance doses of a specified normal tissue point should be $q = 15/201 = 7.46\%$, or

$$0 \leq D(i, j, k) < q = 7.46\%, \qquad \textbf{(7)}$$

for all $(i, j, k) \in N$.

To meet requirement (R3) (keep the does at normal tissue below a certain level), based on assumption (A6) (which sets the does levels), the tolerance dose radio of the total dose deposited in the target and critical organ to the total dose delivered by a plan is

$$\frac{\sum_{(i,j,k) \in T} D(i, j, k)}{\sum_{(i,j,k) \in T \cup N} D(i, j, k)} \geq P, \qquad P \in [.25, .40]. \qquad \textbf{(8)}$$

We wish to satisfy constraint (C3) (at least 90% of the target volume must be covered). We set

V = the total volume of target;

V_s = the total effective dosage volume of the target whose dose value at the point is more than 0.5; and

f = the effective dosage rate, which satisfies the inequality

$$90\% \le f = \frac{V_s}{V} \le 100\%. \tag{9}$$

The exposure time of each shot $t_{s,w}$ should be nonnegative:

$$t_{s,w} \ge 0. \tag{10}$$

We introduce a binary variable $\delta_{s,w}$ that indicates whether shot s uses width w or not, i.e.,

$$\delta_{s,w} = \begin{cases} 1, & \text{if shot } s \text{ uses width } w; \\ 0, & \text{otherwise.} \end{cases}$$

Moreover, we have the constraints (C1) (no shots protrude outside the target), (C2) (shots do not overlap), and (C4) (as few shots as necessary).

Given all these constraints **(5)–(10)**, and based on the requirement (R4) (minimize dose to normal tissue), the goal is to minimize the dose outside of the target.

Also, to meet the requirement (R5) (minimize the dose gradient across the target volume), the treatment plan needs to be both conformal and homogeneous. It is easy to specify homogeneity in the models simply by imposing lower and upper bounds on the dose delivered to points in the target T. Typically, however, the imposition of rigid bounds leads to plans that are overly homogeneous and not conformal enough—that is, they provide too much dose outside the target. To overcome this problem, the notion of *underdose* (UD) is suggested in Ferris and Shepard [2000]. UD measures how much the delivered dose is below the prescribed dose on the target points. In our models, we either constrain UD to be less than a prespecified value or attempt to minimize the total UD.

In practical application, rather than calculating the dose at every point, it is easy to estimate accurately the total dose delivered by a plan based solely on the $t_{s,w}$ variables and other precalculated constants. An upper bound is also placed on the dose to the target. Given these constraints, the optimizer seeks to minimize the total underdosage in the target. A point is considered to be underdosed if it receives less than the prescribed isodose θ, which for the example formulation is assumed to be 1. We actually use the optimization process to model UD, which is constrained to be

$$\text{UD}(i,j,k)m = \max\left[0, 1 - D(i,j,k)\right]$$

at every point in the target. We can implement this construct using linear constraints

$$\theta \leq \mathrm{UD}(i,j,k) + D(i,j,k), \tag{11}$$
$$0 \leq \mathrm{UD}(i,j,k) \tag{12}$$

for all $(i,j,k) \in T$.

Our second minimization problem is

$$\text{Objective: } \min \sum_{(i,j,k)\in N} \mathrm{UD}(i,j,k)$$

subject to the same constraints **(5)–(10)** as earlier plus **(11)–(12)**.

To meet the requirement (R6) (minimize maximum dose to critical volumes), we have the additional optimization problem

$$\text{Objective: } \min \sum_{(i,j,k)\in N} D(i,j,k) \text{ for all } (i,j,k) \in T \text{ for which } \delta_{s,w} = 0$$

subject to the same constraints **(5)–(10)** as earlier.

All of the formulations are based on the assumption that the neurosurgeon can determine a priori a realistic upper bound n on the number of shots needed. Several issues need to be resolved to create models that are practical, implementable, and solvable (in a reasonable time frame). Two main approaches are proposed in the literature [Ferris et al. 2002; 2003; Shepard et al. 2000; Ferris and Shepard 2000], namely mixed integer programming and nonlinear programming, to optimize simultaneously all of the variables.

Simulation Results and Model Testing

We developed an optimization package to implement the algorithms of our models in Matlab and perform numerous computer simulations using targets of different shapes and sizes.

To examine its correctness, we plot a dose-volume histogram for the four different helmets using **(4)**, as shown in **Figure 2**. The histogram depicts the fraction of the volume that receives a particular dose for the target volume. The fit is best for the small shots and decreases slightly in accuracy for the larger ones. The lines show the fraction of the target and critical organ that receives a particular dosage.

Generally speaking, the shape of the target is not too irregular, so we choose five typical shapes of the targets in different sizes. In **Figure 3a**, we illustrate the maximum section of a typical bean-shaped target, whose maximum dimension is 35 mm. Using the skeleton generation algorithm, we get the corresponding skeleton shown in **Figure 3b**. Then, we apply the GA-based shot placement algorithm, resulting in three shots for the target: one 14 mm helmet and two
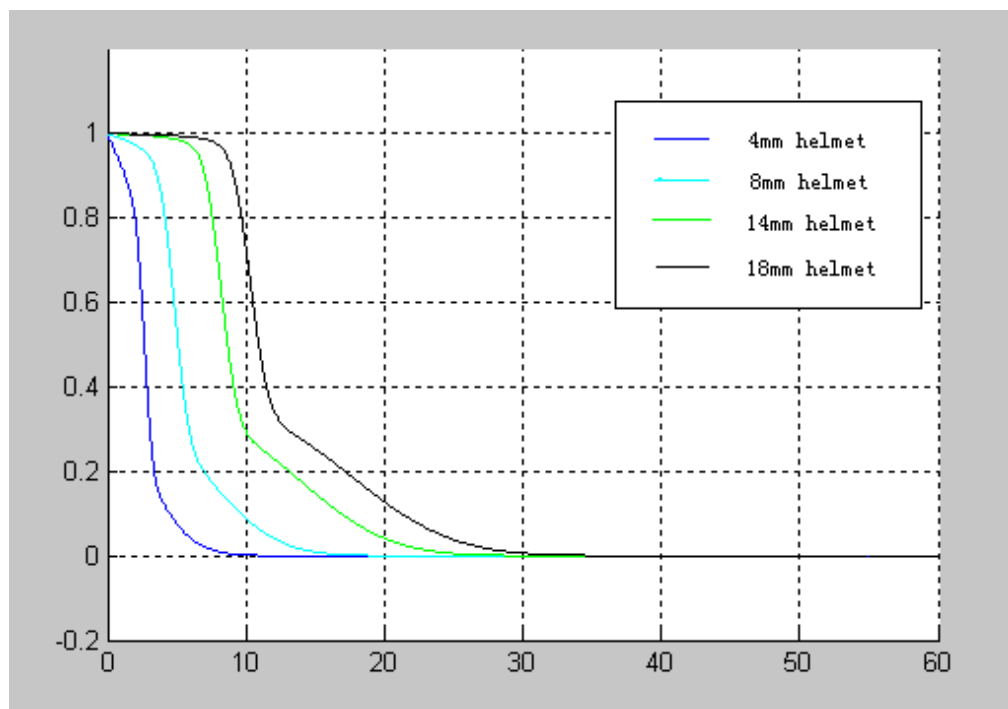
Figure 2. Dose–volume histograms for four different helmets.

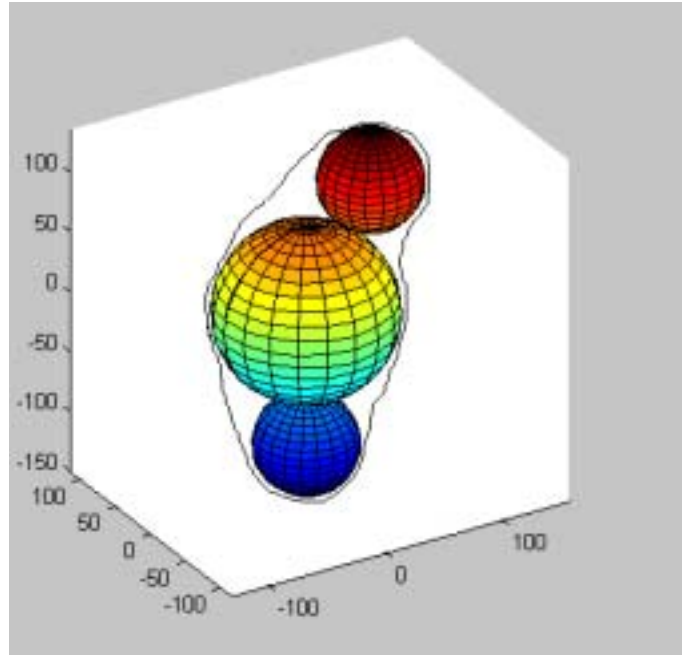**Figure 3a.** The maximum section of the target.

Figure 3b. The skeleton.

Figure 3c. The locations and sizes of the helmets, in 2D.

Figure 4. The 3D shot placements in the target.

8 mm helmets. The locations and sizes of the helmets in 2D are indicated in **Figure 3c**, while 3D shot placements are shown in **Figure 4**.

For this target, we also plot six different isodose lines: 30%, 40%, 50%, 60%, 70%, and 100% (**Figure 5**). The thick (red) line is the target outline, and the thin (black) line is the isodose line. In **Figure 5c**, the 50% isodose line covers all the points of the target, while in **Figure 5f** for the 100% isodose line, no point of the shots exceeds the boundary of the target. We also present the 3D shot placements for four other target shapes in **Figure 6**.

The optimized plans for all of the five shapes of the targets are shown in **Table 1**, together with the minimum target doses and the percentage coverages.

From all of the results, we know that the geometry-based heuristic with the GA optimization approach is a useful tool for assisting in the selection of the appropriate number of shots and helmet sizes. Also, they indicate that our model exceeds the predefined quality of the treatment planning.

Sensitivity Analysis

- *Can the model be applied to sensitive structures?* Yes, by applying more dose constraints, such as an upper bound on either the mean dose or the maximum dose to the sensitive structures

- *Can we treat the tumor at an isodose level other than 50%?* In **Figure 5**, with a lower isodose line, the dose outside of the target volume decreases rapidly, resulting in a reduction in the integral dose to normal tissue. With a higher
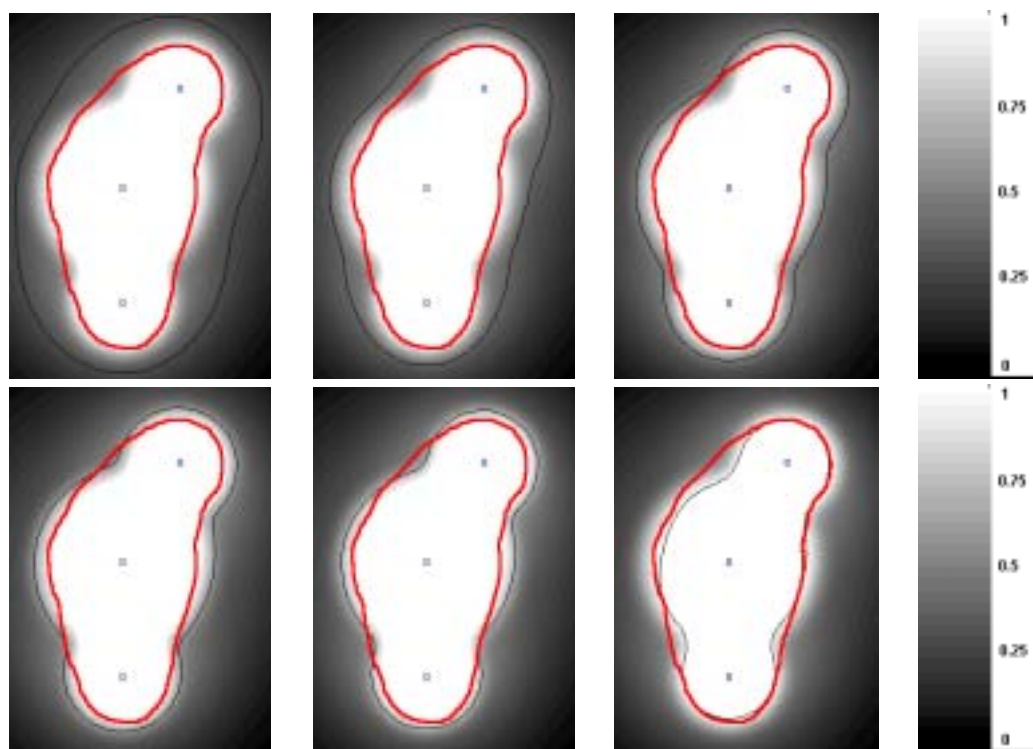
Figure 5. The specified isodose lines of different values: 30%, 40% 50%; 60%, 70%, 100%.

Table 1.

Optimized plans for five targets.

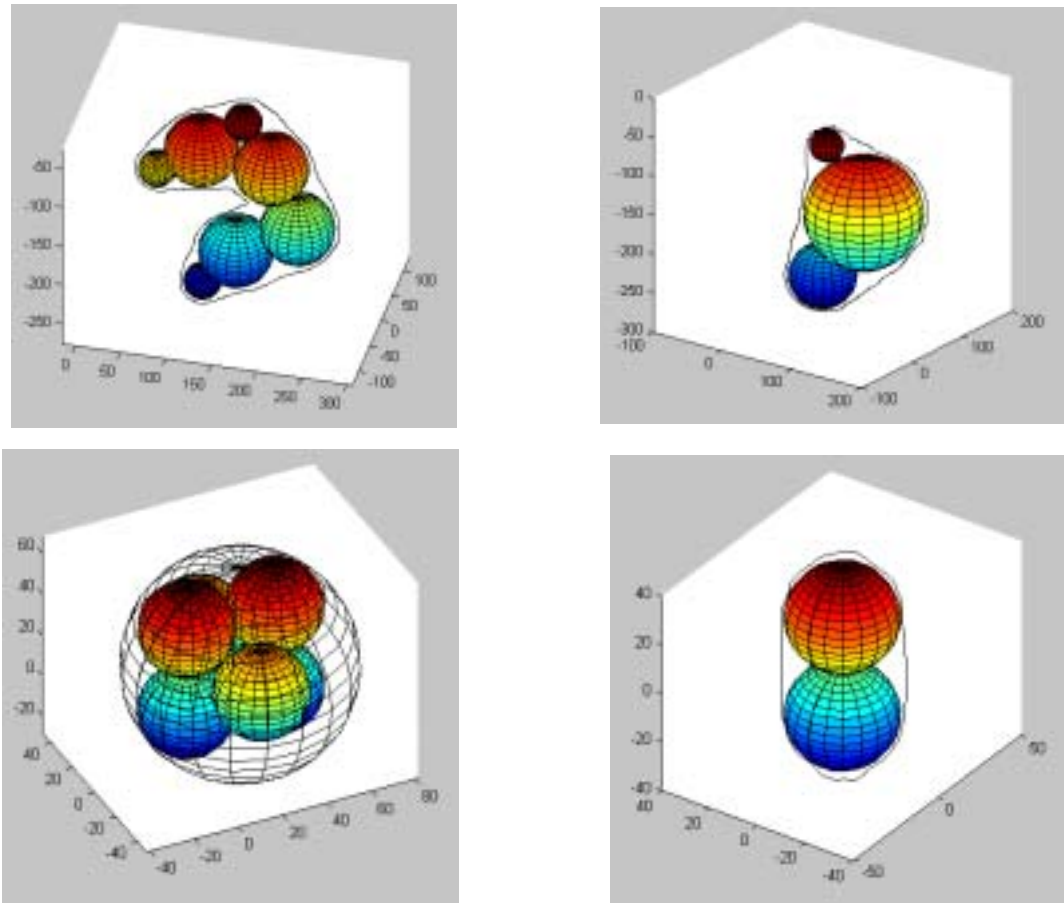| Target (figure)	Maximum section width (mm)	Helmet sizes (mm)	Number of shots	Minimum target dose	Coverage (by isodose) 50%	80%	100%
6	35	18	1	0.51	100%	97%	90%
		4	5				
8a	26	8	4	0.52	100%	97%	88%
		4	3				
8b	20	14	1	0.52	100%	96%	92%
		8	1				
		4	1				
8c	10	4	6	0.45	99%	82%	69%
8d	8	4	2	0.67	100%	97%	57%

Figure 6. Shot placement in four targets.

isodose line, the isodose line cannot cover all the points of the target. For the nodular regions or sensitive organs, the higher isodose coverage level should be specified.

- *The outstanding question from an optimization viewpoint is global vs. local optimality. How about our model?* First, the GA-based shot placement algorithm can ensure that the generating fraction is the smallest one after every shot is placed on the target. For the whole target, it also minimizes the sum of all fractions.

- *When we have several comparably optimization schemes for shot placement, how do we choose the best one?* For example, for a 10 mm-diameter sphere target, we have two comparably optimization schemes, as shown in **Table 1**. The first places one 8-mm shot and the second places six 4-mm shots. If we consider the treatment merely as a sphere-packing problem, the better choice is the first one. However, in practical treatment, we should consider the diffuse regions where no shot is irradiated. Under the first plan, inn these regions the sum of the dose value at a point is more than 1, resulting in increasing the total effective dosage; so we adopt the second plan.

- *Will there be any points outside the tumor whose dose value is greater than 1?* In **Figure 7**, though the shots have not protruded outside the target (constraint (C1)), some points outside the tumor overdose. This occurs due to the very irregular shape of the target, which is not avoidable. In this case, we should choose how to choose an optimization planning under some constraints.

Figure 7. The 100% isodose of the target in **Figure 6a**.

- *How about the robustness of our model?* For the many cases optimized thus far, high-quality dose distributions have been obtained in all cases.

Strengths and Limitations

Strengths

- Our optimization-based automated approach generates more-uniform and better treatment plans in less time than is currently used.

- The geometry-based approach is based on skeletonization ideas from computational graphics, which can speed the process of shot placement.

- The GA-based shot placement algorithm can guide the planner in selecting the number of shots of radiation and the appropriate collimator helmet sizes, it can quickly place a shot, and it can ensure global and local optimality simultaneously.

- The model parameters can be tuned to improve solution speed and robustness.

- The graphical interface is an intuitive way to demonstrate the isodose curve and the treatment effects of the planning.

Limitations

- The skeleton is a key factor for the effectiveness of the algorithm; we should seek better methods to determine it.

- Whether our model can handle very irregular targets needs to be examined.

- We use the function in Ferris and Shepard [2000] to approximate the dose calculation. Other methods of dose calculation should be examined.

- There is no guarantee that there is not a better treatment plan. Some more-intelligent algorithms, such as a neural network-based dynamic programming algorithm, could be considered.

- We have not tested our model on actual patient data.

Conclusions

From the simulation results, we know that the geometry-based heuristic with the GA optimization approach is a useful tool in the selection of the appropriate number of shots and helmet sizes. Our approach is sufficiently robust and effective to be used in practice.

In future work, we may fit ellipsoids instead of spheres, since some researchers have commented that the dose is skewed in certain directions.

References

Cho, P.S., H.G. Kuterdem, and R.J. Marks. 1998. A spherical dose model for radiosurgery plan optimization. *Physics in Medicine and Biology* 43 (10): 3145–3148.

Ferris, M.C., J.-H. Lim and D.M. Shepard. 2002. An optimization approach for radiosurgery treatment planning. *SIAM Journal on Optimization* 13 (3): 921–937. `ftp://ftp.cs.wisc.edu/pub/dmi/tech-reports/01-12.pdf` .

————. 2003. Radiosurgery treatment planning via nonlinear programming. *Annals of Operations Research* 119 (1): 247–260. `ftp://ftp.cs.wisc.edu/pub/dmi/tech-reports/01-01.pdf` .

Ferris, M.C., and D.M. Shepard. 2000. Optimization of gamma knife radiosurgery. In *Discrete Mathematical Problems with Medical Applications*, vol. 55 of DIMACS Series in Discrete Mathematics and Theoretical Computer Science, edited by D.-Z. Du, P. Pardolas, and J. Wang, 27–44. Providence, RI: American Mathematical Society. `ftp://ftp.cs.wisc.edu/pub/dmi/tech-reports/00-01.pdf`

Goldberg, D.E. 1989. *Genetic Algorithms: In Search, Optimization and Machine Learning*. Reading, MA: Addison-Wesley.

Leichtman, Gregg S., Anthony L. Aita, and H. Warren Goldman. 2000. Automated gamma knife dose planning using polygon clipping and adaptive simulated annealing. *Medical Physics* 27 (1): 154–162.

Liu, J.-F., and R.-X. Tang. 1997. Ball-packing method: A new approach for quality automatic triangulation of arbitrary domains. In *Proceedings of the 6th International Meshing Roundtable*, 85–96. Sandia, NM: Sandia National Laboratories.

Man, K.F., K.S. Tang, S. Kwong, and W.A. Halang. 1997. *Genetic Algorithms for Control and Signal Processing*. New York: Springer-Verlag.

Shepard, D.M., M.C. Ferris, R. Ove, and L. Ma. 2000. Inverse treatment planning for gamma knife radiosurgery. *Medical Physics* 27 (12): 2748–2756.

Shu, Huazhong, Yulong Yan, Limin Luo, and Xudong Bao. 1998. Three-dimensional optimization of treatment planning for gamma unit treatment system. *Medical Physics* 25 (12): 2352–2357.

Wu, J.Q. 2000. Sphere packing using morphological analysis. In *Discrete Mathematical Problems with Medical Applications*, vol. 55 of DIMACS Series in Discrete Mathematics and Theoretical Computer Science, edited by D.-Z. Du, P. Pardolas, and J. Wang, 45–54. Providence, RI: American Mathematical Society.

_____ , and J.D. Bourland. 2000a. A study and automatic solution for multi-shot treatment planning for the gamma knife. *Journal of Radiosurgery* 3 (2): 77–84.

_____ . 2000b. 3D skeletonization and its application in shape based optimization. *Computers in Medical Imaging* 24 (4): 243–251.

_____ , and R.A. Robb. 1996. Fast 3D medial axis transformation to reduce computation and complexity in radiosurgery treatment planning. In *Medical Imaging 1996: Image Processing, Proceedings of the SPIE*, vol. 2710, edited by Murray H. Loew and Kenneth M. Hanson, 562–571.

Zhang, Pengpeng, David Dean, Andrew Metzger, and Claudio Sibata. 2001. Optimization of gamma knife treatment planning via guided evolutionary simulated annealing. *Medical Physics* 28 (8): 1746–1752.

Zhou, Y., A. Kaufman, and A.W. Toga. 1998. Three dimensional skeleton and centerline generation based on an approximate minimum distance field. *Visual Computers* 14: 303–314.

A Sphere-Packing Model for the Optimal Treatment Plan

Long Yun
Ye Yungqing
Wei Zhen
Peking University
Beijing, China

Advisor: Liu Xufeng

Abstract

We develop a sphere-packing model for gamma knife treatment planning to determine the number of shots of each diameter and their positions in an optimal plan.

We use a heuristic approach to solve the packing problem, which is refined by simulated annealing. The criteria for an optimal plan are efficiency, conformity, fitness, and avoidance. We construct a penalty function to judge whether one packing strategy is better than the other. The number of spheres of each size is fixed, the total number of spheres has an upper bound, and critical tissue near the target is avoided.

Computer simulation shows that our algorithm fits the four requirements well and runs faster than the traditional nonlinear approach. After detailed evaluation, we not only demonstrate the flexibility and robustness of our algorithm but also show its wide applicability.

Introduction

We develop an effective sphere-packing algorithm for gamma-knife treatment planning using a heuristic approach, optimized by simulated annealing.
In our model, we take into consideration the following basic requirements:

1. At least 90% shot coverage of the target volume is guaranteed. This requirement is the main standard for evaluating our algorithm, or an *efficiency* requirement.

2. Minimize the non-target volume that is covered by a shot or by a series of delivered shots. This requirement is a *conformity* requirement.

3. Minimize the overlapped region of the delivered shots in order to avoid the hot spots as well as to economize shot usage. This is a a *fitness* requirement.

4. Limit the dosage delivered to certain critical structures close to the target. Such requirements are *avoidance* requirements.

The traditional model for radiosurgery treatment planning via nonlinear programming assumes that the weights of the shots conform to a certain distribution, from which the construction of the objective function is possible. To avoid the complicated computation of nonlinear programming, we devise a more feasible and rapid heuristic algorithm without reducing any precision of the outcome.

- We consider an optimal sphere-packing plan for a given number of spheres in each size, satisfying requirements 1–3. That is, in this step, we assume that the lesion part is far from any critical organ and try to find an optimal position for a fixed set of the spheres using the heuristic sphere-packing algorithm.

- We try all possible combinations of up to 15 spheres; for each, we use the above algorithm to get an optimal plan. We develop a criterion to select from the different combinations the best packing solution for our model, which is optimized by simulated annealing.

- We consider the real situation in field practice, in which the effect of a critical organ is added. Accordingly, we modify the judgment criterion so that requirement 4 is satisfied.

- Finally, to apply the above method to more general situations, we add the weights of the shots.

Though we admit that the inherent limitations of this model due to the simplification of the problem and the restriction of the hardware capacity are unavoidable, we believe that our model has successfully solved the given problem. Our algorithm is not only fast in generating solutions but also flexible in allowing parameter settings to solve more difficult tasks.

Assumptions

- Shots can be represented as spheres with four different diameters: 4, 8, 14, and 18 mm.

- The target volume is of moderate size with a mean spherical diameter of 35 mm (and usually less) [The Gamma Knife . . . n.d.]

- The maximum number of shots allowed is 15.

- The target object is represented as a three-dimensional digital map with $100 \times 100 \times 100 = 1$ million pixels.

- The volume of a object is measured by the total number of pixels in it.

- The dose delivered is above the lower bound of the effective level to kill the tumor.

Table 1. Description of the variables.

N	total number of shots
n_i	number of shots of type i
s	the sth shot used, $s = 1, \ldots, N$
(x_s, y_s, z_s)	position of the sth shot center
Position	matrix storing all the positions of the shot centers
M	average shot width
Radius	vector storing the four types of radius: $[9\ 7\ 4\ 2]$
Bitmap	$M \times M \times M$ boolean matrix storing information information from the CT/MRI image
Dose	dose delivered, a linear function of exposure time satisfying $\theta \leq \mathrm{Dose}(i, j, k) \leq 1$, where θ is the lower bound of the isodose contour
Covered	total number of covered pixels in the target volume; directly reflects the efficiency requirement
Miscovered	total number of covered pixels in the normal tissue; directly reflects the conformity requirement
Overlap	total number of overlapped pixels among different shots; directly reflects the fitness requirement
Ratio	percentage of the target volume covered
SphereInof	vector representing the number of each type of shot
SphereRadius	vector representing the radius of N shots

Background Knowledge

Gamma knife radiosurgery allows for the destruction of a brain lesions without cutting the skin. By focusing many small beams of radiation on abnormal brain tissue, the abnormality can be destroyed while preserving the normal surrounding structures. Before the surgery, the neurosurgeon uses the digitally transformed images from the CT/MRI to outline the tumor or lesion as well as the critical structures of the surrounding brain. Then a treatment plan is devised to target the tumor.

The determination of the treatment plan varies substantially in difficulty. When the tumor is large, has an irregular shape, or is close to a sensitive structure, many shots of different sizes could be needed to achieve appropriate coverage of the tumor. The treatment planning process can be very tedious and time-consuming due to the variety of conflicting objectives, and the quality of the plan produced depends heavily on the experience of the user. Therefore, a unified and automated treatment process is desired.

In our model, we reduce the treatment planning problem to an optimal sphere-packing problem by focusing on finding the appropriate number of spheres of different sizes and their positions to achieve the efficiency, conformity, fitness, and avoidance requirements.

Construction and Development of the Model

Fixed Set of Spheres

The main idea is to let a randomly chosen sphere move gradually to an optimal position.

In the beginning, N spheres are randomly positioned inside the target volume. Then one sphere is moved to a new position and we estimate whether the new location is better; if so, the sphere is moved, otherwise it remains in place. We repeat this process until a relatively good packing solution is achieved.

To implement our algorithm, we need a criterion to judge a packing solution. According to our four requirements, it is reasonable to take the weighted linear combination of the volume of those covered, miscovered, and overlapped parts as our criterion—that is, a good packing solution means less miscovered, less overlapped, and more covered volumes.

Let sphere A move to location B **Figure 1**. We restrict our consideration to just the pixels in the shaded area, which is very thin and thus has few pixels in it. The program judges which region a pixel belongs to: covered, miscovered or overlapped, and we count the pixels of each kind. We implement this idea using a function `PenaltyJudge` that returns a signed integer indicating whether the change of the packing strategy results in a better solution.
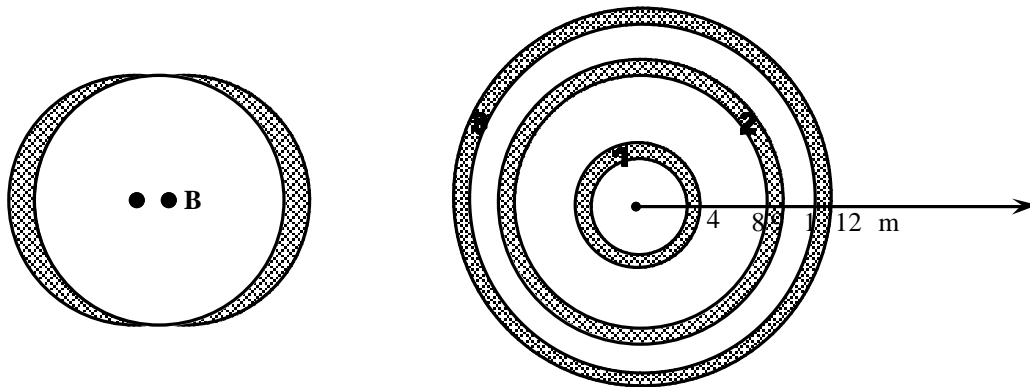
Figure 1. Sphere A moves to location B. **Figure 2.** The centers of the 18 mm spheres are set at O, the the centers of the three smaller spheres at random points in regions 1, 2, and 3, respectively.

How do we set the initial position of the spheres? Our results will be affected significantly if the starting positions are not properly set. Cramming the spheres together will not do any harm, because according to our algorithm, all of the spheres move in different directions and finally scatter through the

target volume. But there is one constraint that the initial positions must obey: Larger spheres cannot cover smaller ones. Otherwise, the smaller spheres will never move out of the larger ones, which means they are useless and wasted. Since spheres of the same size will not be covered by each other as long as their centers differ, we need to avoid only coverings between spheres of different sizes. Our technique is to set the spheres of different size in different regions of the target volume, which ensures that the spheres never cover each other.

In **Figure 2**, point O represents the center of the CT image of the target volume. We set the centers of all the 18-mm spheres at point O and center the 14-mm, 8-mm, and 4-mm spheres randomly at the tumor pixels lying in the shadowed regions 1, 2, 3, respectively. Thus, a relatively good starting status is generated.

We perturb the location of one sphere by a step (i.e., one pixel) in the North, South, East, West, Up, and Down directions. If a perturbation in one of these directions generate a better packing, we move the sphere one step in that direction. Then we choose another sphere and repeat the process. Applying this process to all of the spheres successively is one iteration. Our program generally generates a relatively good packing in about 10–15 iterations.

## Results and Data Analysis

Heuristic Method

To test the effectiveness of our algorithm, we construct a 3D target object with $100 \times 100 \times 100$ pixels through the combination of two spheres and a segment of a circle. For the effect of live simulation, we blur and distort the edge of the object through photoprocessing software so that it is very similar to the shape of a real tumor. The simulated results and the solution given by our program are excitingly good, as shown in **Table 2**.

Table 1.

Final distribution of shots from the heuristic algorithm on a simulated target.

Iterations	% covered	% miscovered	% overlapped	Time consumed (s)
0	37	39	14	—
5	75	25	8	20
10	96	11	5	40
15	96	11	5	62
20	96	11	5	83

Visualization of the Results

Plotting the resulting bitmap, we can see clearly from **Figures 3–4** the evolution of the locations of the spheres as well as the stability and robustness of our program.
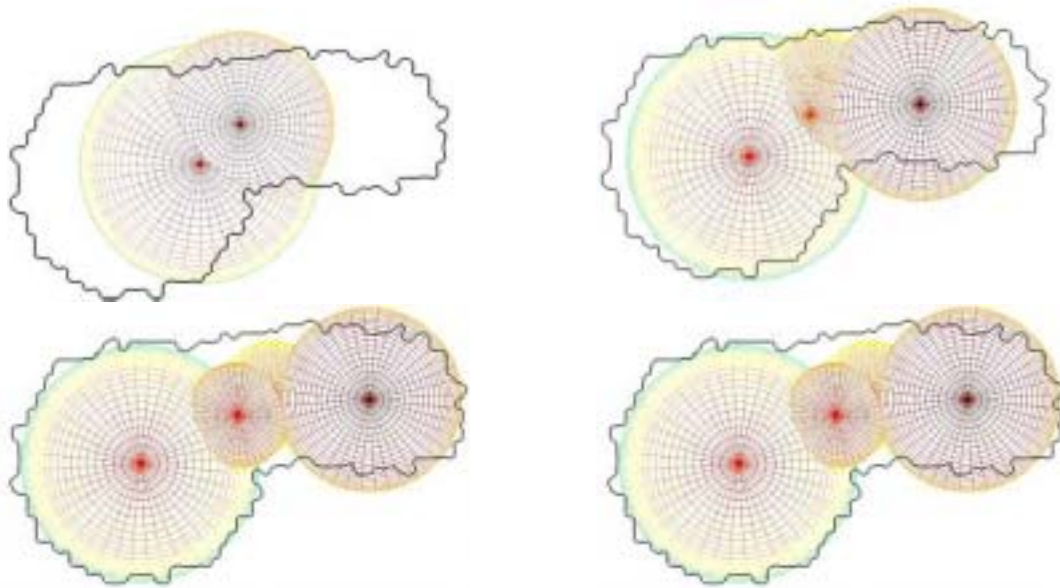
Figure 3. Distribution of spheres within the target after 0, 5, 10, and 15 iterations.
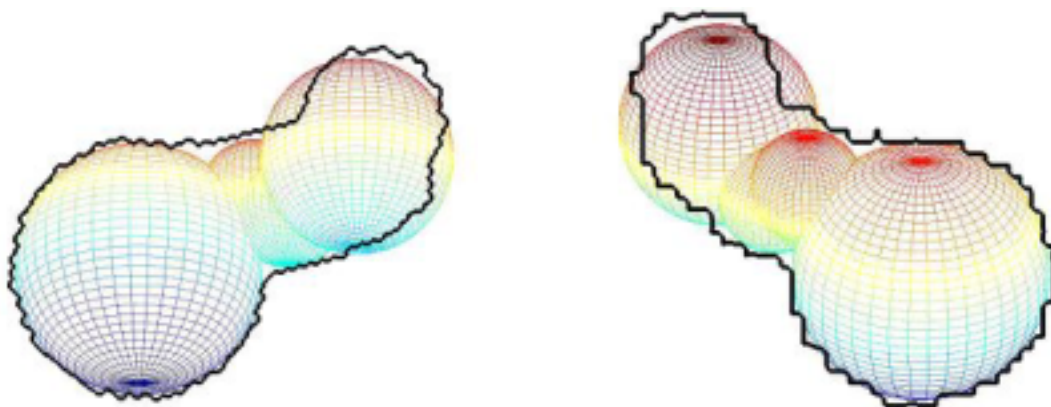
Figure 4. Three-dimensional views of final placement of spheres.

After 10 iterations, all the spheres go into a relatively stable position. Such fast and stable convergence occurs in all of our simulations. Hence, we can reasonably assume that after 15 iterations any initial packing will turn into an optimal one.

Further Development: The Best Set of Spheres

Difficulties and Ideas

So far, we have used our personal judgment about which sets of spheres to pack. A natural idea is to enumerate all combinations of the four types of spheres and find an optimal one. There are $\binom{19}{4} = 3,876$ nonnegative integer solutions to the equation $n_1 + n_2 + n_3 + n_4 \leq 15$. The runtime for our program to check them all, at 83 s each, would be 89 h, excluding the time to read the

bitmap and plot the graphs.

So, to get a near-optimal but efficient solution, we turn to simulated annealing, which we use not only to find the optimal combination of the spheres but also to determine the direction of the spheres to move in each step.

Simulated Annealing to Find the Optimal Combination

Simulated annealing (SA) is a Monte Carlo approach used in a wide range of problems concerning optimization, especially NP-complete problems, which can approximate the global extremum within the time tolerance.

SA is a numerical optimization technique based on the principles of thermodynamics. The algorithm starts from a valid solution, randomly generates new states for the problem, and calculates the associated cost function. Simulation of the annealing process starts at a high fictitious temperature (usually manipulated according to practical need). A new state is randomly chosen from the "neighborhood" of the current state (where "neighborhood" is a map defined as $N :$ State $\rightarrow 2^{\text{State}}$, $i \rightarrow S_i$ satisfying $j \in S_i \iff i \in S_j$) and the difference in cost function is calculated. If (CurrentCost $-$ NewCost) ≤ 0, i.e., the cost is lower, then this new state is accepted. This criterion forces the system toward a state corresponding to a local—or possibly a global—minimum. However, most large optimization problems have many local minima and the optimization algorithm is therefore often trapped in a local minimum. To get out of a local minimum, an increase of the cost function is accepted with a certain probability, i.e., the new state is accepted even though it is a little hotter. The criterion is

$$\exp\left(\frac{\text{CurrentCost} - \text{NewCost}}{\text{Temperature}}\right) > \text{Random}(0, 1).$$

The simulation starts with a high temperature, which makes the left-hand side of the equation close to 1. Hence, a new state with a larger cost has a high probability of being accepted.

The change in temperature is also important in this algorithm. Let $\beta_n = 1/\text{Temperature}$. Hwang et al. [1990] prove that if $\beta_n / \log n \rightarrow 0$ as $n \rightarrow \infty$, then $P(\text{NewState}_n \in \text{global extremum}) \rightarrow 1$. But in practice, we usually reduce the temperature, according to temperature$_{n+1} = 0.87$ temperature$_n$, for convenience.

We apply SA to determine both the next direction to move a specified shot and whether a shot should be deleted or not according to our judgment function. In the case of direction determination, we have

$$\%(\text{CurrentCost} - \text{NewCost}) = 2 \times \text{SphereRadius} - \text{PenaltyJudge};$$

and in the case of determining whether to delete a shot or not, we have

$$\%(\text{CurrentCost} - \text{NewCost}) = \text{RatioCovered} - 0.7.$$

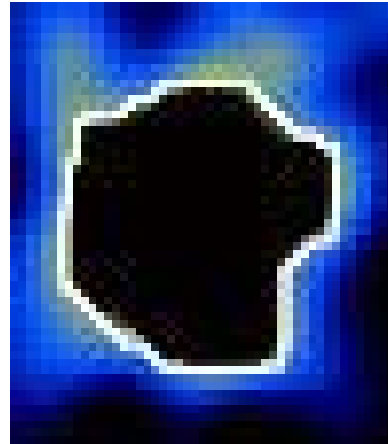After this adjustment, the results and the speed improve dramatically.

Visualization of the Results

This time, we use a tumor image from the Whole Brain Atlas [Johnson and Becker 1997]. Using 20 two-dimensional slices of the tumor, we construct a 3D presentation of it. We visualize the optimization process in **Figures 5–7**.

Using Matlab, we seek out the contour of the tumor through reading the bitmap of all the pixels. Finally, we get a bitmap of $50 \times 50 \times 50 = 125000$ pixels, which is within the capacity of our computer.
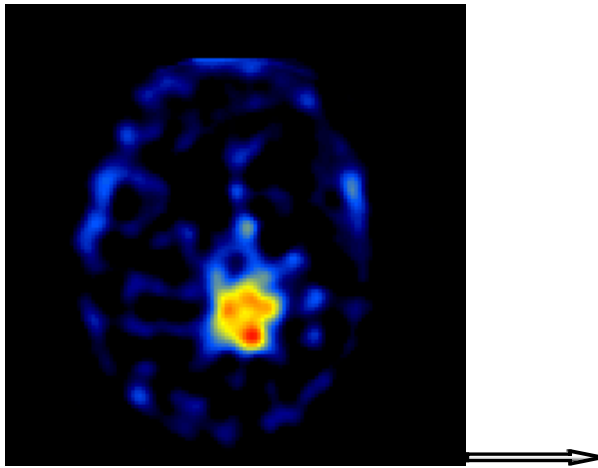
Figure 5. Sample slice of the tumor.   **Figure 6.** Contour of the tumor

Figure 7 shows the power of our algorithm.

Critical Organ

Finally, we take into consideration the existence of a critical organ. In real medical practice, the maximum dose to critical volumes must be minimized, that is, the dose delivered to any part of a critical organ cannot exceed a particular value

Thus, we modify our judging criterion to meet the avoidance requirement. In our previous algorithm, the criterion is implemented in the function `PenaltyJudge` as a weighted linear combination of the `Covered`, `Miscovered`, and `Overlapped` variables. We change `PenaltyJudge` so that if after a step of the movement, a sphere covers any part of the critical organ, the movement should not be made, even if the `PenaltyJudge` function justifies it (this kind of criterion does not differ from setting a positive value as the maximum dose that can be delivered to a critical part). We can simply give the covered critical part an infinite weight in the linear combination to achieve this goal, which is a demonstration of the flexibility of our program.

The results generated after this change do not differ significantly from the previous ones (because our heuristic algorithm also tries to avoid the protruding of the shots as much as possible), but the existence of critical organ does pose a negative contribution to the final strategy of the treatment planning.
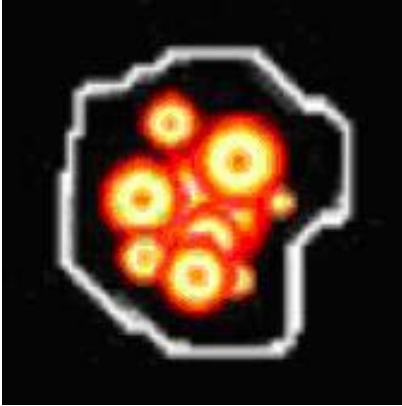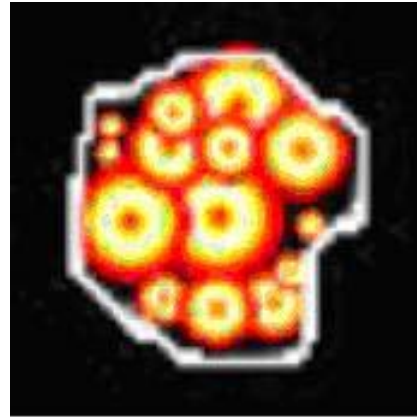
Figure 7a. Initial setting.
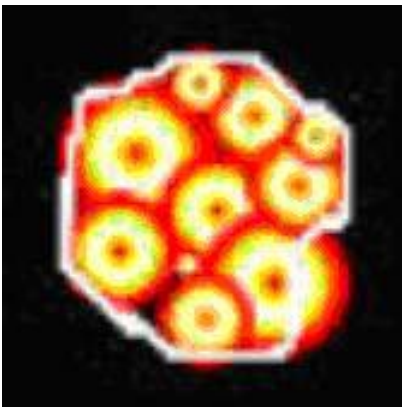

Figure 7b. The scatter process.

Figure 7c. Deletion and further scattering of the spheres.
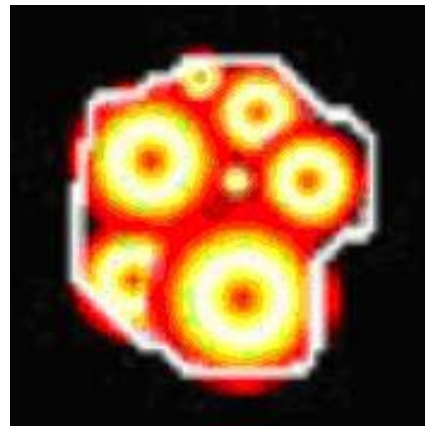

Figure 7d. Final effect; 12 shots are used to cover this large tumor.

Reoptimization

There are two aspects in the reoptimization of our model: the improvement of the quality of the final solution, and the efficiency of the algorithm.

The random starting position of the packing spheres significantly affects the performance of the solution. Although we use a technique to improve the soundness of the starting position, the starting position can still be unsatisfying, since the tumor can be of any irregular shape and size. For example, in **Figure 3**, our program sometimes generates an inferior solution; the result we present is the best from three executions.

To get out of this dilemma, for each starting position we repeat three times the search for the optimal distribution and select the best solution.

The model could also be easily modified to solve more complex situations:

- consideration of the distribution of the dose of the shots, and

- varying the the radii of the available shots according to a continuous interval.

However, with new factors or more pixels, the program slows down. To

speed it up, we can use a stepwise optimizing method—that is, first solve the problem with a coarse approximation, then refine and optimize it.

- In our initial model, we evolve a less good packing solution to a better one by pixel movements. In the modification, we make each step 3 pixels; after the packing has evolved to a stable status, we reset the step size to 1 pixel.

- We minimize the drawback of a large number of pixels by managing an image of a smaller size, i.e., an image in which one pixel represents several pixels of the original volume. We use our model to find an optimal solution for the smaller image, then return to the original data to generate a final solution.

Evaluation: Strengths and Weaknesses

Four characteristics can be used in evaluating the algorithm for planning the treatment: effectiveness, speed, flexibility, and robustness.

Since our algorithm focuses mainly on optimizing the final results to meet requirements 1-4, and the data in **Table 2** show satisfying results, our algorithm achieves the effectiveness goal. Our model also simplifies the decision of a good treatment plan to an optimal sphere-packing problem. By using the heuristic approach and the simulated annealing algorithm, we can find the optimal number of spheres of each kind and their positions in a relatively short time.

In addition, we take full consideration of various factors that affect the efficiency and safety of the gamma knife radiosurgery. By summarizing them to four requirements, we construct a penalty function that decides whether a change in the packing plan is desirable or not. Such a penalty function gives our algorithm great flexibility: If more factors are taken into consideration, we can simply add the contribution of that factor to the function. This flexibility is of great value in practice since the requirements of different patients may vary a lot.

Furthermore, the heuristic method used in our program is general. In real medical practice, when many of the assumptions in this particular problem no longer stand, we can still use our algorithm to get an optimal plan. For example, some medical literature [Ferris et al. 2003] mentions that the actual dose delivered is ellipsoidal in nature rather than spherical; we can simply modify our model to handle this situation by changing the four sphere types to ellipsoidal ones—the main outline of our algorithm needs little change.

Finally, our method is strengthened by simulated annealing, which ensures that our solution can reach the global optimum with great probability.

Though we believe that our model solves the problem, there are some limitations:

- The sphere-packing model is too simple; it fails to consider the real dose distribution and the time required for the shots to deliver enough energy.

- Due to the restriction of the hardware, our final solution to for a target consisting of 1 million pixels needs approximately 30 min on a Pentium IV PC, which means any magnification of the scale of this problem is intolerable.

Extension of the Problem

There are five factors that may affect the effectiveness of the treatment:

- How many shots to use (N)?

- Which size shots (radius)?

- Where to deliver the shots (position)?

- What's the distribution of the dose of a particular shot?

- How long to deliver shots (t_s)?

To improve our model so that it can accommodate more practical situations, shot *weights* must be added.

Our previous model mainly focuses on the first three factors, while our improvement also addresses the last two factors. We can obtain the actual shot weights distribution, since in practice it is easy to measure the relative weight of a dose at a certain distance from the shot center as well as to represent its distribution in a 3D coordination.

We fit a nonlinear curve to these measurements, using nonlinear least squares. Suppose that the function of the curve is $D_s(x_s, y_s, z_s, i, j, k)$, which represents the relative dose at pixel (i, j, k) from a shot centered at (x_s, y_s, z_s). The dose at a certain pixel of the CT/MRI image can be calculated by the function

$$\text{Dose}(i, j, k) = \sum_{(s,r) \in S \times \text{Radius}} t_{s,r} D_s(x_s, y_s, z_s, i, j, k),$$

where $t_{s,r}$ is the duration of a shot.

We make our four requirements more precise and practical by setting numerical limitations to the dose that the tumor, normal tissue, and critical part receive. These limitations, set by the neurosurgeon, vary from patient to patient.

A simple refinement is to modify the diameters in the sphere-packing problem. The diameters are no longer 4, 8, 14 and 18 mm but must be calculated using the function D_s when the specified weight of shot is known. For example, if more than 50% of the shot weight is required for the lesion part, the required diameters can be worked out from $D_s = 0.5$. (We assume that the position of the shot won't affect the distribution of shot weight—only the distance from the shot center determines the weight.) If normal tissue can receive only less than 20% of the shot weight, we calculate the diameters D corresponding to the 80% shot weight. Our conformity requirement is reduced to: The distance between the pixels of normal tissue and shot center must be greater than D.

Higher precision may be achieved using the concept of *isodose curve*: A $p\%$ isodose curve is a curve that encompasses all of the pixels that receive at least $p\%$ of the maximum dose delivered to any pixel in the tumor. The conformity requirement can be represented as the conformity of such an isodose curve to the target volume. We can also approach the shot weight problem by adjusting the amount of shot time, especially when the target is very close to the critical part. Under such circumstances, hitting the critical part is unavoidable. But we can divide the total time required for the treatment into short spans, so that the dose received by the critical part in one time span will do little harm to it while the cumulative dose can kill the tumor.

Anyhow, any improvement cannot be attained without combining real-world practice and must be balanced with the speed and efficiency requirement.

References

Johnson, Keith A., and J. Alex Becker. 1997. The Whole Brain Atlas. `http://www.med.harvard.edu/AANLIB/home.html`.

Buffalo Neurosurgery Group. n.d. Gamma knife radiosurgery. `http://buffaloneuro.com/radio/radio2.html`.

Center for Image-guided Neurosurgery, Department of Neurological Surgery, University of Pittsburgh. 2003. The gamma knife: A technical overview. `http://www.neurosurgery.pitt.edu/imageguided/gammaknife/technical.html`.

Donovan, Jerry. n.d. Packing circles in squares and circles page. `http://home.att.net/~donovanhse/Packing/index.html`.

Ferris, M.C., J.-H. Lim and D.M. Shepard. 2003. Radiosurgery treatment planning via nonlinear programming. *Annals of Operations Research* 119 (1): 247–260. `ftp://ftp.cs.wisc.edu/pub/dmi/tech-reports/01-01.pdf`.

Ferris, M.C., and D.M. Shepard. 2000. Optimization of gamma knife radiosurgery. In *Discrete Mathematical Problems with Medical Applications*, vol. 55 of DIMACS Series in Discrete Mathematics and Theoretical Computer Science, edited by D.-Z. Du, P. Pardolas, and J. Wang, 27–44. Providence, RI: American Mathematical Society. `ftp://ftp.cs.wisc.edu/pub/dmi/tech-reports/00-01.pdf`

Hwang, Chii-Ruey, and Sheu, Shuenn-Jyi. 1990. Large-time behavior of perturbed diffusion Markov processes with applications to the second eigenvalue problem for Fokker-Planck operators and simulated annealing. *Acta Applicandae Mathematicae* 19: 253–295.

Shepard, D.M., M.C. Ferris, R. Ove, and L. Ma. 2000. Inverse treatment planning for gamma knife radiosurgery. *Medical Physics* 27 (12): 2748–2756.

The Gamma Knife Problem

Darin W. Gillis
David R. Lindstone
Aaron T. Windfield
University of Colorado
Boulder, CO

Advisor: Anne M. Dougherty

Abstract

Noninvasive gamma-knife radiosurgery treatment attacks brain tumors using spherical radiation dosages (shots). We develop methods to design optimized treatment plans using four fixed-diameter dosages. Our algorithms strictly adhere to the following rule: Shots cannot violate tumor boundaries or overlap each other.

From a mathematical perspective, the problem becomes a matter of filling an irregularly-shaped target volume with a conglomeration of spheres. We make no assumptions about the size and shape of the tumor; by maintaining complete generality, our algorithms are flexible and robust. The basic strategies of the algorithms are deepest-sphere placement, steepest descent, and adaptation.

We design representative 3D models to test our algorithms. We find that the most efficient packing strategy is an adaptive algorithm that uses steepest descent, with an average coverage percentage of 40% over 100 test cases while not threatening healthy tissue. One variation covered 56% of one test case but had a large standard deviation across 100 test cases. It also produced results four times as fast as the adaptive method.

Background

Brain Tumors

The average volume of a tumor operable by radiosurgery is about 15 cm^3 [Lee et al. 2002]. We generate 3D tumor models of approximately this volume with varying physical dimensions.

The Gamma Knife

The gamma knife unit consists of 201 individual cobalt-60 radiation sources situated in a helmet. The 201 beams converge at an isocenter creating a spherical

dose distribution ("shot"). Four sizes of spheres are possible: 4, 8, 14, and 18 mm in diameter. A radiosurgery plan is used to map out shots to destroy the tumor without harming the patient. Following successful treatment, surviving cancer cells lose their ability to grow. In fact, many partially destroyed tumors shrink or even disappear in time [Kaye and Laws 1995].

The Problem

The plans should arrange radiation doses so that tumor destruction is maximized, healthy tissue is protected, and hot spots are avoided. Thus, the algorithms are subject to the following constraints:

- Prohibit shots from penetrating outside the target area.

- Prohibit overlap of shots, preventing hotspots.

- Maximize the percentage covered in the tumor, or target volume.

- Use a maximum of 15 shots.

Assumptions

- The tumor is homogeneous; it is equally productive to treat any part of it.

- The tumor is modeled discretely using a three-dimensional image.

- No assumptions are made about the shape of the tumor.

- Tumor cells are either been radiated or not; there are no partial dosages.

Problem Approach

We have divide the problem into three different pieces:

- create a variety of 3-dimensional brain tumor models,

- develop and refine sphere-packing algorithms, and

- test and compare algorithms using tumor models

Data Models

Our data consists of a $100 \times 100 \times 100$ array that represent a 1000 cm^3 space around the brain tumor. We refers to each element of the matrix as a *voxel* (three-dimensional pixel). Each voxel represents 1 mm^3 of brain tissue [Wagner 2000]. We use 1s to indicate tumor and 0s to represent healthy tissue, and we populate the arrays with tumor models as described below.

Sphere Tumor Model

Our first model is based on the simple equation for a sphere, $(x-x_0)^2 + (y-y_0)^2 + (z-z_0)^2 = r^2$, where the center of the sphere is represented by (x_0, y_0, z_0) with radius r. We fill in the voxels representing the tumor by applying the inequality $(x-x_0)^2 + (y-y_0)^2 + (z-z_0)^2 \leq r^2$ throughout the test volume.

Ellipsoid Tumor Model

The ellipsoid model uses the same principle as the spherical model. The inequality

$$\frac{(x-x_0)^2}{a^2} + \frac{(y-y_0)^2}{b^2} + \frac{(z-z_0)^2}{c^2} \leq r^2$$

represents the interior of an ellipsoid. The spherical and ellipsoid models are a basis for the mutated sphere tumor model.

Mutated Spherical Tumor Model

Tumor shapes can be modeled by unions of ellipsoids [Asachenkov 1994]. Thus, our most accurate model is created by intersecting several ellipsoids at random locations. We start with a small spherical tumor. Then we create three discrete uniformly distributed random variables U_x, U_y, and U_z, where (U_x, U_y, U_z) represents a randomly chosen voxel within the sphere. This point becomes the center of an ellipsoid that is added to the tumor. The a, b, and c parameters that define the dimensions of the ellipsoid are defined by three other random variables U_a, U_b, and U_c, uniform continuous random variables over [5, 15].

Sphere-Packing Algorithms

In practice, tumors are usually represented as a 3D image obtained from MRI (magnetic resonance imaging). We discretize the tumor and the removal spheres for processing. We explore four different methods:

- first-deepest,

- steepest descent,

- improved steepest descent, and

- adaptive.

Grassfire Algorithm

All of our sphere-packing methods employ the *grassfire algorithm* [Wagner 2000]. The grassfire method progressively marks the layers of the tumor from the outside in, analogous to a fire burning away an object one layer at a time.

For each 1-valued voxel, all surrounding voxels are surveyed. If any are 0-valued (outside the tumor), the current voxel is set to a depth of 2, which represents the boundary of the tumor. This process is repeated for every voxel in the 3D test volume, with layer numbers progressively increasing until all of the 1s in the array have been consumed. In other words, the grassfire method calculates an approximate measure of depth for each voxel in the tumor. Doing so gives an easy measure of the largest sphere that can be placed at any given point without violating the tumor boundary. If the voxel is at depth 8 or 9, then a 7-mm sphere should be used, and so on.

The basic operation of grassfire (shown in two dimensions) is shown in **Figure 1**, which shows the effect of grassfire on a circle. For readability, the boundary layer has been left at a value of 1 and the data arrays represent a much smaller area than the plots. Depth is indicated by shade; darker is deeper. The arrows show progression through initial grassfiring to the removal of a small circle from the center (just as spheres are removed from the tumor). Notice that when grassfire is applied after removal, the maximum depth is smaller than that of the original circle.

Although it is simple, grassfire provides the foundation for all of our sphere-packing algorithms.

Sphere Placement Methodology

After grassfiring the tumor model, the deepest point in the tumor is easily found. Reasonably, the deeper the point in the tumor, the more likely it is that a large radius sphere can be placed without harming normal tissue. Large (particularly 9-mm) spheres being placed in the tumor increases the coverage of the solution. Conversely, the smallest sphere (2-mm radius) is the least efficient in eradicating cancerous tissue. For the average tumor size, the 2-mm sphere removes less than 1% of the volume. Therefore, we place as many large spheres as possible before placing smaller spheres.
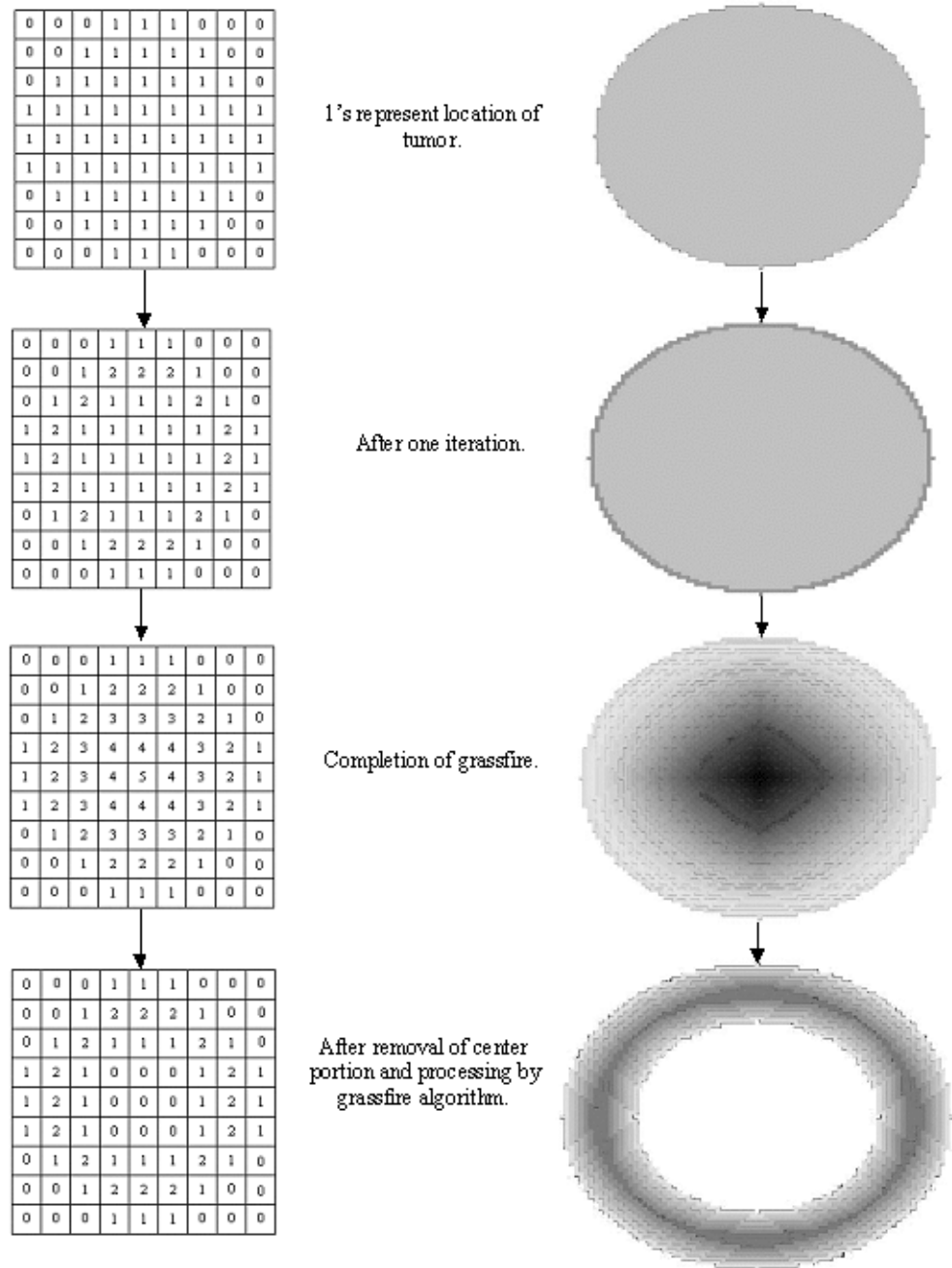
0	0	0	1	1	1	0	0	0
0	0	1	1	1	1	1	0	0
0	1	1	1	1	1	1	1	0
1	1	1	1	1	1	1	1	1
1	1	1	1	1	1	1	1	1
1	1	1	1	1	1	1	1	1
0	1	1	1	1	1	1	1	0
0	0	1	1	1	1	1	0	0
0	0	0	1	1	1	0	0	0

1's represent location of tumor.

0	0	0	1	1	1	0	0	0
0	0	1	2	2	2	1	0	0
0	1	2	1	1	1	2	1	0
1	2	1	1	1	1	1	2	1
1	2	1	1	1	1	1	2	1
1	2	1	1	1	1	1	2	1
0	1	2	1	1	1	2	1	0
0	0	1	2	2	2	1	0	0
0	0	0	1	1	1	0	0	0

After one iteration.

0	0	0	1	1	1	0	0	0
0	0	1	2	2	2	1	0	0
0	1	2	3	3	3	2	1	0
1	2	3	4	4	4	3	2	1
1	2	3	4	5	4	3	2	1
1	2	3	4	4	4	3	2	1
0	1	2	3	3	3	2	1	0
0	0	1	2	2	2	1	0	0
0	0	0	1	1	1	0	0	0

Completion of grassfire.

0	0	0	1	1	1	0	0	0
0	0	1	2	2	2	1	0	0
0	1	2	1	1	1	2	1	0
1	2	1	0	0	0	1	2	1
1	2	1	0	0	0	1	2	1
1	2	1	0	0	0	1	2	1
0	1	2	1	1	1	2	1	0
0	0	1	2	2	2	1	0	0
0	0	0	1	1	1	0	0	0

After removal of center portion and processing by grassfire algorithm.

Figure 1. Grassfire algorithm flowchart.

First-Deepest Method

The first-deepest method begins by applying the grassfire algorithm to the tumor data. We generate a list of the deepest voxels (nearly all volumes will have multiple "deepest" points after the layering process). This method simply takes the first voxel off that list and places the removal sphere at that location; the radius of the sphere used is determined from the depth value at that voxel. For example, if a voxel is 8 layers deep (and thus 8 mm deep), then a 7-mm radius sphere can be removed from that location without harming healthy tissue.

Step-by-Step

1. Grassfire the tumor data.

2. Grab one of the points at the deepest level.

3. Calculate the equation for the sphere centered at that point with the largest acceptable radius.

4. Set all voxels within the radius of the sphere to zero (effectively removing a spherical portion of tumor).

5. Reset all nonzero voxels to 1s (resetting the tumor for another grassfire run).

6. Return to step 1.

This method is very robust; when a sphere is removed, it is simply seen as a new tumor boundary, so any of the variables such as shot size, number of shots, or tumor shape can change and the algorithm still works.

Variations

We try to improve the method by looking down the list of the deepest voxels to find a more appropriate sphere center. We accomplish this by giving each voxel a score based on the depths of its neighboring points. Essentially, the algorithm tries to place the sphere at the greatest possible average depth. But doing this does not improve the total coverage; in fact, this algorithm is inferior to the first-deepest method. Placing the sphere as deep as possible reduces the depth of the next iteration, preventing more large spheres from being placed. A better strategy would be placing the sphere as shallow as possible (see **Figure 2** for a 2D example), in an effort to leave room for more large spheres.
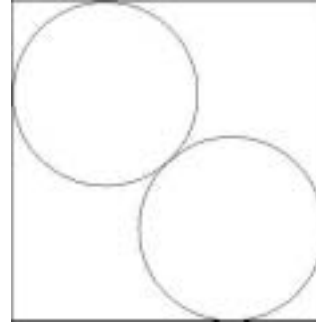
Steepest Descent Method

The method of steepest descent tries to place the largest possible sphere (as determined by grassfire) close to the tumor boundary. The steepest descent uses a scoring function to find the best location for the biggest sphere.
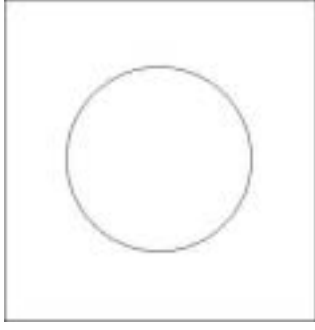
Figure 2a. A single large circle in the center prevents placement of any more large circles.

Figure 2b. If the first circle is placed far from the center, a second large circle can fit.

Starting from the deepest voxel, we calculate the gradient of the score function and proceed along the steepest path until a local max is reached, and this point is used as a sphere isocenter. This is implemented as follows:

1. Calculate the score of the deepest voxel.

2. Calculate the score of all surrounding voxels.

3. If the original voxel has the highest score, it becomes an isocenter, otherwise move to the highest scoring voxel and go back to step 1.

Scoring Function

This method is only as good as the scoring function. We have two factors, W_1 and W_2, that figure into the score of a given voxel.

The W_1 factor measures the depth of any nearby voxels; more specifically, it is an estimation of the depth-density of a sphere centered at that voxel. More rigorously defined, we estimate the W_1 at voxel (x_0, y_0, z_0):

$$W_1 \approx \frac{\iiint_{S(x,y,z)} D(x, y, z)\, dxdydz}{\text{total volume of sphere}},$$

where $S(x_0, y_0, z_0)$ is a sphere centered at (x_0, y_0, z_0).

$D(x, y, z)$ is the depth at (x, y, z), so effectively W_1 represents the average depth throughout the sphere's volume. To speed up the scoring function, we estimate this volume integral by averaging the depth values for a cube surrounding the point. The sphere is inscribed within our cube of estimation; and given that the scoring function will only be a basis of relative comparison, the level of error is tolerable.

The W_2 factor is used to make sure that normal tissue is not contained in the shot. Given the sphere size that will be used for the potential shot, we have

$$
W_2 = \begin{cases} 1, & \text{if depth } (x_0, y_0, z_0) > \text{shot radius;} \\ 0, & \text{if depth } (x_0, y_0, z_0) \leq \text{shot radius.} \end{cases}
$$

This is another place where our decision to prohibit destroying healthy tissue becomes a central part our solution. Total coverage of the tumor could be improved at the expense of healthy tissue by implementing a continuous scoring function for the W_2 weight.

Finally, the total score is given by W_2/W_1. This scoring function rewards the shot for being at a closer distance to the tumor edge (or a removed sphere, since this looks like an edge to our algorithms) while still being entirely contained within the tumor.

Improved Steepest Descent Method

The improvement on steepest descent is to allow spheres to be placed closer to the tumor boundary. The only changes lie in how the W_1 and W_2 weights are calculated in the score function.

Altered Score Function

The improved scoring function calculates the W_2 score factor in a more rigorous manner. Before, we used the depth (determined by grassfire) to determine if the shot would fit or not. The grassfire depth is actually a conservative depth estimate—there can be more distance between the voxel and the boundary than it indicates. To fit a sphere more tightly, we construct a list of the points on the boundary and consult it each time W_2 is calculated. Now,

$$
W_2 = \begin{cases} 1, & \text{if any shot voxels are in } \{(x, y, z)|(x, y, z) \text{ is on tumor boundary}\} ; \\ 0, & \text{else.} \end{cases}
$$

Adaptive Method

The adaptive method generates an initial sequence of shots using steepest descent (coverage could be improved by using improved steepest descent, but the simulations would run an order of magnitude slower). The initial sequence is then changed one sphere at a time and repacked until each shot in the sequence has been changed once. Theoretically, taking this action allows for the exchange of a large sphere for many smaller spheres, which may be more effective. It follows the idea that perhaps some spheres need to be placed poorly initially in order to allow smarter shots to be placed down the line.

For instance, consider an initial sequence of length N that starts with the following shots: { 9 mm, 4 mm, 4 mm, ... }. Using the same initial tumor, the adaptive method runs the steepest descent method, but the new sequence *must* change the first sphere, so it starts with a 7-mm sphere. On the second iteration, the new sequence keeps the leading 9-mm sphere but must change the second element to a 2-mm sphere. The third iteration starts with a 9-mm sphere, followed by a 4-mm sphere, and then changes the third sphere to a 2-mm sphere. This continues until all $N - 1$ sequences have been generated. We seek and use the sequence with maximum coverage.

Quantitative Results

Table 1.

Comparison of methods.

Method	Timing		% Coverage			
	Avg. (s)	Relative speed	Mean	SD	Min.	Max.
First-deepest	83	1	34	5.2	20	45
Steepest descent	104	1.25	38	2.9	32	45
Improved steepest descent	229	2.8	37	6.2	28	56
Adaptive	1025	12.3	40	2.5	35	44

We ran each method on the same suite of 100 test cases, except for the adaptive method, for which, because of its longer runtime we used a subset of 20 cases. **Table 1** contains a summary of the results. The maximum coverage that we could achieve was 56% (**Figure 3**).

Our algorithms work on tumors of arbitrary shape, even disjoint tumors. The result of one such pack is shown in **Figure 4**.

Qualitative Results

First-Deepest Method

As expected, this algorithm's performance is quantitatively the weakest. The maximum coverage of 45% is actually slightly better than the other methods. However, the minimum value of 20%, as well as the average of 34% are quite low compared with other methods. It also exhibits large random variations in coverage, meaning that the algorithm is equally likely to fill in a low percentage as it is to fill in a relatively high percentage of a tumor.

The method is inconsistent, yields the lowest average coverage of all methods, but it is the fastest.

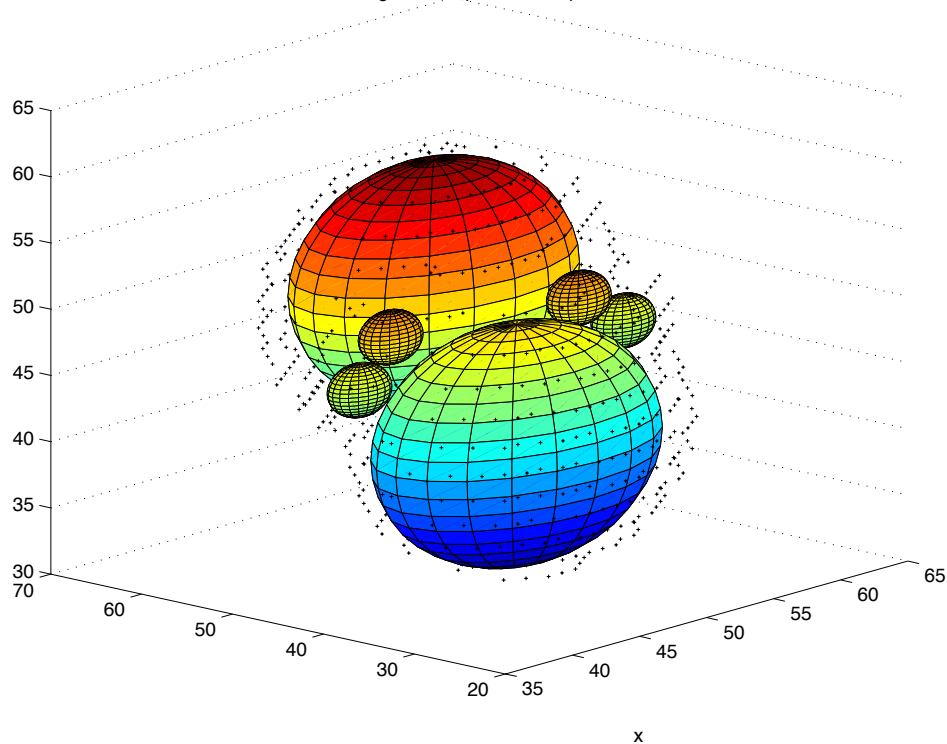Tumor # 4 –– 55.9551 % Coverage with Improved Steepest Descent Method

Figure 3. Our best result: 56% coverage.
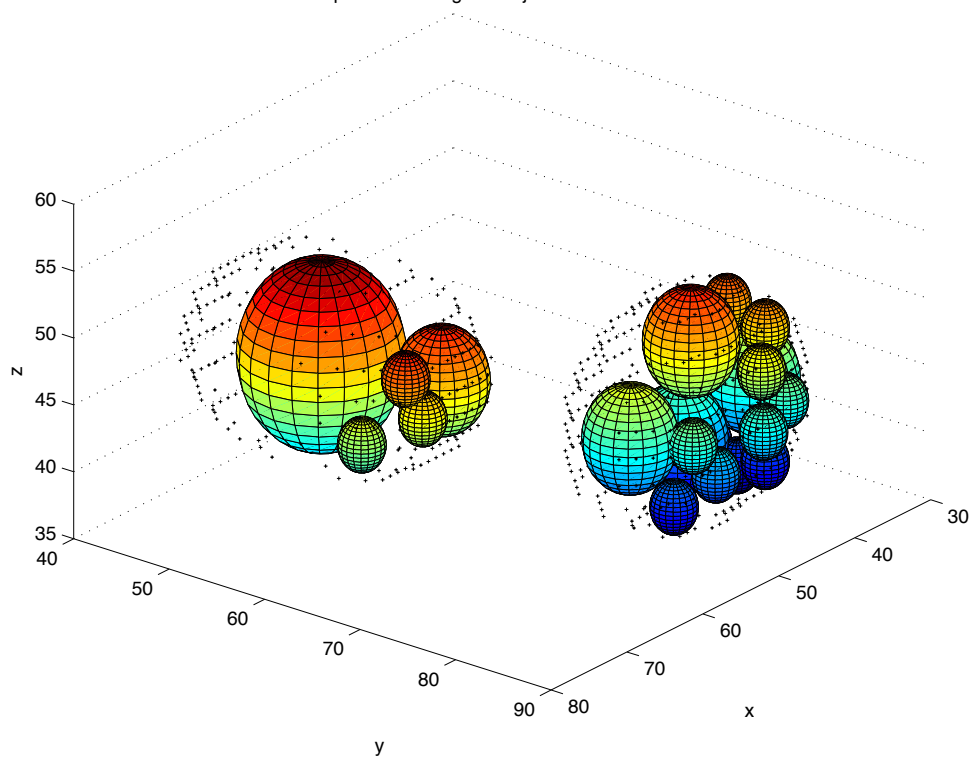
Sphere–Packing for Disjoint Tumor Growth

Figure 4. Sphere packing into two disjoint tumors.

Steepest Descent

The minimum and average coverages are significantly better than for first-deepest, and the method is much more consistent. This makes sense, because this method adapts to variations in tumor size and shape rather than using the first available isocenter for each sphere. It is fast compared to the improved steepest descent and adaptive methods.

Improved Steepest Descent

This algorithm is similar to steepest descent, except for the ability to pack spheres closer to edges and other spheres. This method does poorly on average, worse than steepest descent and the adaptive method. But it yields the best coverages—over 50% on four different test cases. Also, this method has the highest deviation of all our methods.

Adaptive Method

The average coverage of approximately 40% is the best of all four algorithms, and this method also has the lowest standard deviation. But it is the slowest and most complicated algorithm.

Conclusions

All of our algorithms have strengths and weaknesses. The first-deepest method is fast, while steepest descent is consistent in coverage. Improved steepest descent yields some of the best results in terms of coverage, while the adaptive algorithm maintains the highest average coverage and smallest standard deviation.

Weaknesses

Prohibition of hot spots and radiating healthy brain tissue prevents our algorithms from covering much of the tumor.

Strengths

Our algorithms can process any possible tumor. They are "patient-friendly"—they don't destroy anything outside of the tumor, nor do they produce spheres that intersect each other. They are also simple and robust.

Future Work

It would be nice to merge the adaptive algorithm with steepest descent to try to build up the coverage.

References

Asachenkov, Alexander, et al. 1994. *Disease Dynamics*. Boston, MA: Birkhäuser.

Aste, Tomaso, and Denis Weaire. 2000. *The Pursuit of Perfect Packing*. Philadelphia, PA: Institute of Physics Publishing.

Conway, J.H., and N.J.A. Sloane. 1988. *Sphere Packings, Lattices and Groups*. New York: Springer-Verlag.

Ferris, Michael C., R.R. Meyer, and W. D'Souza. 2002. Radiation treatment planning: Mixed integer programming formulations and approaches. Optimization Technical Report 02-08, Computer Sciences Department. Madison, WI: University of Wisconsin. `http://www.cs.wisc.edu/~ferris/papers/rad-mip.pdf` .

Kansal, A.R., et al. 2000. Simulated brain tumor growth dynamics using a three-dimensional cellular automaton. *Journal of Theoretical Biology* 203: 367–382.

Kaye, Andrew H., and Edward R. Laws. 1995. *Brain Tumors*. New York: Churchill Livingstone, New York.

Lee, J.Y., A. Niranjan, J. McInerney, D. Kondziolka, J.C. Flickinger, and L.D. Lunsford. 2002. Stereotactic radiosurgery providing long-term tumor control of cavernous sinus meningiomas. *Journal of Neurosurgery* 97 (1): 65–72.

Wagner, Thomas H., et al. 2000. A geometrically based method for automated radiosurgery planning. *International Journal of Radiation Oncology Biology Physics* 48 (5): 1599–1611.

Yi, Taeil. 2000. *A Tree in a Brain Tumor*. Gainesville, FL: University of Florida.

Editor's Note

The May 2003 issue of *SIAM News* (Vol. 36, No. 4) contains on p. 12 a photo of the University of Colorado team, which we reproduce here, together with perspectives on the MCM experience. The team members recommend dividing up roles and reveal that they used a total of eight computers during the contest. Their advisor, Anne Dougherty, also offers her perspective; she emphasizes that the contest "actually begins in the late fall," when students are recruited and training sessions are held—"to give the students time to get to know one another and to begin to form their teams."

On the same page, James Case, a SIAM judge for the MCM, gives his perspective on both MCM problems. Regarding the Gamma Knife Treatment Problem, he remarks, "Only the bravest contestants were prepared to concede that their algorithms might fail to achieve even 50% coverage."

Team members Aaron Windfield, Darin Gillis, and David Lindstone, who are members of the SIAM Student Chapter at the University of Colorado, Boulder. Their paper earned the SIAM Award for the Gamma Knife Treatment Problem. (Photo courtesy of team advisor Anne M. Dougherty.)

Shelling Tumors with Caution and Wiggles

Luke Winstrom
Sam Coskey
Mark Blunk
University of Washington
Seattle, WA

Advisor: James Allen Morrow

Abstract

We discuss a simple model for tumor growth, which results in realistic tumor shapes. We then address the question of efficient irradiation of tumors in terms of packing their volume with disjoint spheres of given radii. We develop three algorithms, based on a shelling method, which give recommendations for optimal sphere-packings. We interpret these packings as treatment plans, and we examine the corresponding radiation dosages for various qualities.

We analyze the effectiveness of our algorithms in recommending optimal dosage plans. Several problems with the algorithms are addressed. Finally, we conclude that all of our algorithms have a common difficulty covering very large tumors, and that while one of our algorithms is effective as a means of packing the volume with spheres, it does not translate into an efficient treatment plan.

Introduction

The gamma knife is a highly effective means of destroying tumor tissue. A collection of 201 beams, which send ionizing radiation produced by cobalt-60 sources, converge and deliver to a specific region a powerful dose of radiation without harming the surrounding tissue.

It is necessary to determine where the beams should converge, so the patient's brain is scanned with an MRI or CT imaging device to produce a three-dimensional image of the tumor. An optimal treatment plan is determined by analyzing this image and deriving a collection of points inside the tumor. Doses concentrated at those points are administered by the gamma knife. Selecting an optimum treatment plan can be lengthy and difficult.

We seek to automate the process of selecting an optimal treatment. We describe an algorithm to take a three-dimensional image and determine an

optimal choice for the position and size of spheres that cover the tumor as much as possible while the same time minimizing the number of spheres utilized.

The basic ingredients of our solution include:

- three tumor growth models representing three different degrees of nonuniformity;

- three sphere-packing algorithms, each representing a different spin on the concept of "shelling"; and

- testing of the algorithms against three different tumor sizes.

Exploring the Layout of the Problem

Collimators

A collimator helmet is used to direct the radiation toward a specific point in the patient's head. Cobalt-60 as a radiation source emits photons in an isotropic fashion; so, by introducing a long cylinder between the source and the target, the beams are constrained to a certain angular distribution. Over the short distance from the end of the cylinder to the target location, the radiation is confined approximately to a cylinder or column. This collimation of the radiation allows specific targeting and reduced exposure.

The collimator helmet is essentially a spherical array of cylinders, each of which directs radiation through a common point. This configuration allows 201 low-intensity beams to enter the brain and intersect in one well defined location. Since the beams are positioned around the skull evenly and are relatively weak, no normal tissue receives a high dose. However, where the beams intersect in the tumor, a huge dose is delivered (**Figure 1**). Because the collimator has only four different settings, we are physically restricted to four different dose sizes.
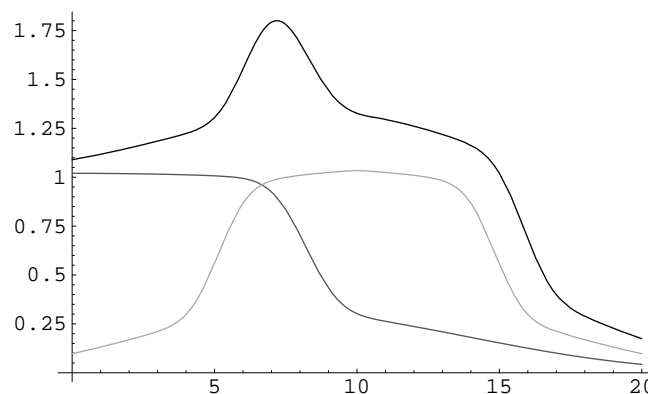
Figure 1. Radiation profile where spheres meet. The bottom two curves represent radiation profiles for individual shots (radii of 7 and 4 centered at 0 and 11) and the bold line represents the total radiation dose received.

Radiation Distribution

Because the cobalt-60 sources are evenly spaced, their intersection can be represented by a spherically symmetric radiation profile. This profile can be approximated well by error functions [Ferris and Shepard 2000]. Thus, we define the radial distribution of dose intensity to be

$$f_\rho(d) = \sum_{i=1}^{2} \lambda_i \left[1 - \text{erf} \left(\frac{d - r_i}{\sigma_i} \right) \right],$$

(1)

where λ_i, σ_i, and r_i all depend on ρ, the radius of the sphere, and d is the distance from the center of the sphere. By fitting the values of λ, σ, and r to experimental data, an accurate model for radiation intensity is generated. Ferris and Shepard [2000] give fitted values for radii of various sizes.

It is impractical to design an algorithm to optimize the placement of such intersections (called *shots*) over multiple treatments. Thus, a placement method must be developed that is both accurate and quick. By approximating the shots from collimator helmets as spheres, a much more approachable problem may be formulated: How can we pack the tumor with as many spheres as possible? By using spheres of the same radius as the beams, we agree very well with the drop-off point of the radiation distribution defined above. Thus, by packing the tumor, we can optimize the placement and number of shots.

Isosurfaces and Isodose

The constructs that define habitability within our brain space are the isodose surfaces, or *isosurfaces*. These surfaces are the level sets of the scalar field that makes up the radiation distribution in the brain space. Every point on one side of the surface has a higher dosage than any point on the other. In an ideal case, the edge of the tumor would be the isodose surface, with every point inside the tumor receiving 100% of the prescribed radiation and every point not in the tumor receiving none. However, this is infeasible, so some compromise must be reached. By comparing the regions within isosurfaces to the tumor, it is easy to see how much tumor has been cleared away, how much tumor is left, and how much brain has been sacrificed.

Digital Images of Tumors

Typically, an MRI delivers an image of the brain case, with a resolution of approximately 1 mm^3. Since the brain is about 100 mm on a side, the tumor image sits inside a $100 \times 100 \times 100$ voxel space, where each voxel represents 1 mm^3. We assume that the shape given by the imaging software is an accurate and conservative approximation of the tumor, so that if we subject voxels denoted as tumorous to doses of radiation do not damage normal brain tissue.

Problem Restatement

Given these considerations, we may restate the problem before us as follows. Given a digital image of tumor tissue, produce a list of at most 15 spheres (centers and radii) such that:

- The spheres are entirely contained within the tumor tissue.

- Each radius is either 2, 4, 7, or 9 mm.

- The spheres are disjoint (or nearly so, to avoid overdosing).

- The total volume of the spheres is as close to that of the tumor as possible.

Tumor Generation Model

We could not find images of actual tumors, so we generated our own. We created an algorithm to simulate tumor growth in time steps. This algorithm uses a cellular automaton to model cellular division [Kansal 2000]. Ideally, the lattice would have a structure similar to a biological fabric, but we take instead a simple three-dimensional grid, for several reasons:

- It is computationally convenient—not only is simulation elementary, but the output resembles a digital image without further processing.

- We are interested in studying the final shape of tumors, not their growth. Our algorithm is sufficient to produce volumes representative of tumor shapes.

Each node of the lattice represents an idealized mathematical cell. We begin by placing a single cell in the center of the space, allowing the cells to "divide" (generate a new cell) at each time step until the tumor reaches the desired size. Whether or not a cell divides depends on several factors, which vary among the three different generation methods discussed below.

In all cases, we smooth out unrealistic or undetectable holes in the tumor after it has grown to the desired size. It is theoretically possible for a tumor to reconnect with itself in a toroidal shape, but this does not happen in practice.

The Uniform Pressure Tumor

This simulation supposes that the tumor is growing in a uniformly pressurized environment. At each time step, the probability for a given cell to divide is proportional to $(1 - r/R)$, where r is the distance from the cell to the origin and R is a bound on the radius of the tumor. Since we are interested only in the final tumor shape and not its development, the constant of proportionality is essentially irrelevant. The resulting tumor shape is generally a ragged sphere.

The Varied Pressure Tumor

Suspecting that the preceding model may be too symmetric, we created a second algorithm that varies the pressure against the tumor, corresponding to the effect that the surrounding area of the brain would have on the growth of a tumor. To do this, we specify certain random points x_i as pressure points and curb tumor growth near these points. The probability for a given cell x to divide is now proportional to the product $(1 - r/R) \prod |x - x_i|/M$, where M is the maximum width of the tumor space and r and R are as before.

Tumors generated with this model are slightly more elongated and pointed than before. Some curve into a lima-bean shape around the pressure points.

The Running Amok Tumor

Newman and Lazareff [2002] postulate that once a tumor begins to jut in one direction, cells in the outcropping are more likely to receive nutrients from the surrounding brain tissue and hence are more likely to grow, whereas the less extended regions of the tumor are less likely to grow. The tumor is more likely to grow in a direction in which it has grown before; the result is a tumor that is spiny in appearance. Thus, in this third model, we remove the outside pressures and specify that more recently generated cells be more likely to divide than older ones. The resulting shape is a bulky tumor with tendrils showing recent and active growth.

Packing Spheres into Volumes

The sphere-packing problem is ages old and yet unsolved; the very problem that we are faced is NP-complete [Wang 1999].

When faced with packing rounds into a barrel, the military has been rumored to pack them as tightly as possible and then drive the barrel in a large truck over a bumpy road; doing so clears up enough space for another handful of rounds. We implement an algorithmic approximation to this idea.

The General Approach

Our plan is based on two fundamental principles:

Fit the largest spheres first. That is, we pack large spheres into the volume before considering smaller ones. The reason for this is the steep fall-off of coverage as shot radius decreases (**Table 1**). It takes twice as many 7-mm spheres to do the job of a 9-mm sphere, consuming more diametric space in the tumor and complicating the dosage plan. Since one of our stated goals is to minimize the number of doses, the principle of utilizing larger spheres first is clearly a good one.

Table 2.

Shot radius vs. coverage.

Radius (mm)	9	7	4	2
Coverage (mm^3)	3000	1300	250	12
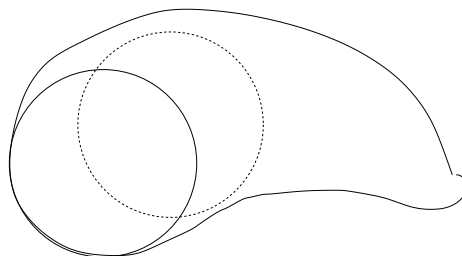
Figure 2. The sphere on the left is a better choice than the one on the right.

Spheres should hug the tumor edge. It is very likely for there to be a many-way tie for where to place the largest sphere that fits inside a given volume. But not all choices are equal—a centrally placed sphere may preclude fitting other large spheres into the volume (**Figure 2**). For example, it would be unwise to place a 9-mm shot at the center of a spherical tumor that is 16 mm in radius, as this would not allow us to place any 7-mm spheres into the tumor.

Depth-Search Algorithm

Because the tumor data is in the form of a digital image, we pack spheres into the image directly. That is, we select spherical subsets of voxels from the given tumor and consider the optimal placing of spheres (centered at voxels inside the tumor) that do not intersect one other or the edge of the tumor.)

The algorithm acts by a *shelling method* [Wagner et al. 2000], which we describe in detail. The first step is to identify the boundary of the tumor, marking the voxels on a bounding surface with value of 0. We then assign every tumorous voxel a positive value, denoting its distance from the boundary nodes, via **Algorithm 1**.

The sphere that we place inside the tumor should be as large as possible but also as close to the boundary as possible. We therefore take for the center of this sphere a point at depth r from the boundary, where r is the greatest of 2, 4, 7, and 9 available. This way, when we shell a sphere at depth r, the shelled area is along the edge of the tumor as much as possible.

In any case, our algorithm must choose the center x of the sphere from the set E_r. How this is done varies among the three algorithms.

Having chosen our candidate shell center x, we remove from the tumor the sphere centered at the center of this voxel of radius r. This translates to removing all voxels in the tumor whose coordinates are within r of the center

---

Algorithm 1 The depth evaluation algorithm

X is the set of tumorous voxels
E_0 is the set of boundary voxels
$d := 0$
while $X \neq \varnothing$ **do**
  for $x \in X$ **do**
    if x neighbors a point of E_d **then**
      move x from X to E_{d+1}
    end if
  end for
  increment d
end while

---

of the sphere.

We iteratively apply this shelling method to the volume of tumor that remains. The algorithm terminates after it has shelled 15 times, since that is the maximum number of shots allowed. However, we keep track at each stage of what percentage of the tumor has been eliminated so that fewer shots may be recommended if they are deemed sufficient.

A Hasty Algorithm

This is the simplest algorithm. Each time we must choose a center for our shell of radius r, we simply grab one at random. In some sense, this algorithm acts as a control for the next two.

A Careful Algorithm

This next algorithm improves upon the previous one in an obvious way. At each stage, we select a candidate center x from the set E_r—one that will be most beneficial toward placing the remaining spheres. Since the placement of the largest spheres has the greatest effect on the percentage of the volume, we determine which choice of center results in the largest depth by applying the shelling process to what remains of the tumor after the sphere centered at that point has been removed. We want the remaining region to have as high a depth as possible, to make it more likely that we can fit large spheres in the surrounding area.

While it would be preferable to compare all possible choices, to do so is in most cases too computationally intensive. We therefore select a number of our centers in E_r (in this case, 5), compute in each case the depth of the volume of the tumor minus the sphere centered at that point, and from these 5 pick the one whose remaining tumor has voxels with the highest depth.

A Wiggling Algorithm

Prototyping these two algorithms revealed that our Depth-Search algorithm does not always choose sphere centers as close to the tumor boundary as possible.

We developed the Wiggling algorithm as a partial solution to this problem. It rests on the theory that the depth algorithm may still work to find spheres that hug the boundary closely.

The Wiggling algorithm chooses a voxel x from E_r at random and places inside the tumor a sphere of radius r centered at the voxel. It then transports the sphere, one unit at a time, starting off in a random direction and continuing until the sphere meets the boundary as closely as possible. That is, the algorithm simply transports the sphere until it discovers that the next step would land it outside the tumor. By no accident, this method very much resembles that truck on a bumpy road.

Unfortunately, the methods of this algorithm cannot be combined efficiently with the previous Careful algorithm; any care exerted would simply be undone by wiggling.

Output

One cannot distinguish from the three-dimensional images the differences among our three algorithms. **Figure 3** shows a cut-away plot of tumor wall, together with 15 spheres selected by the Careful algorithm.

Analyzing Sphere-Placement Plans

Computing Dose Distributions

After completing calculations using discrete spheres and voxel models of tumors, we calculate the actual dose distribution from the proposed treatment plan. Using the centers of the spheres and the radially symmetric radiation functions presented earlier, we construct a scalar field in brain space defined by the formula

$$D(x, y, z) = \sum_{i=1}^{n} f_{r_i}(\sqrt{(x - x_i)^2 + (y - y_i)^2 + (z - z_i)^2}),$$

where f is the function given in **(1)** on p. 361 and (x_i, y_i, z_i) is the center of the ith sphere with radius r_i.

For all (x, y, z) in a voxel, we use the center of the voxel. Thus, all the points in the voxel get the value of D at the center, and the values of D are thereby discretized. Of course, it would be more accurate to integrate over the entire cube and use the computed value as the representative number for
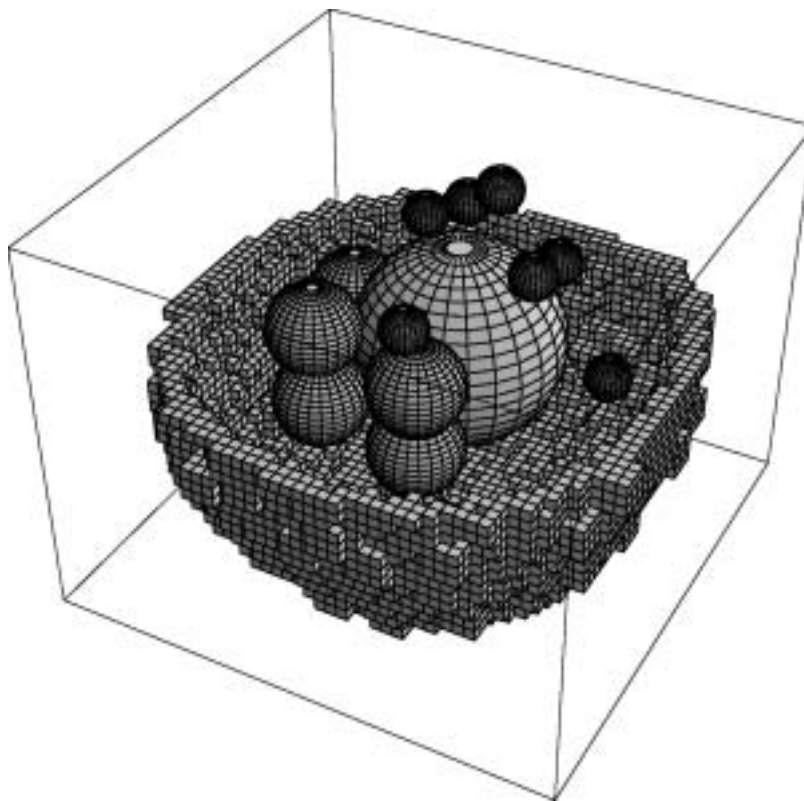
**Figure 3.** Spheres packed in a tumor by the Careful algorithm.

the voxel, but this is too computationally intensive and the accuracy gained on test cases was minimal. Using this scalar field, we can calculate isosurfaces of any value and the volume of the region contained in this isosurface. By taking various different isosurfaces, the efficiency of the spherical covering plan can be calculated. The amount of damage to the surrounding tissue is also available.

Determining the Number of Shots

Each step in our algorithm is executed in the same way whether or not there will be a subsequent shot. Hence, computing every shot and then using some set of parameters to determine the value of each successive shot enables us to compute the ideal number of shots for each tumor. Since this method is not incredibly time consuming (10–15 min for a large tumor). It is certainly feasible to run this process in the hospital and deliver a dose profile to a patient in moments.

Visualizing Dose Distribution

To facilitate visualization of dose distribution, we construct a program to slice the field of dose distribution and superimpose an image of the tumor
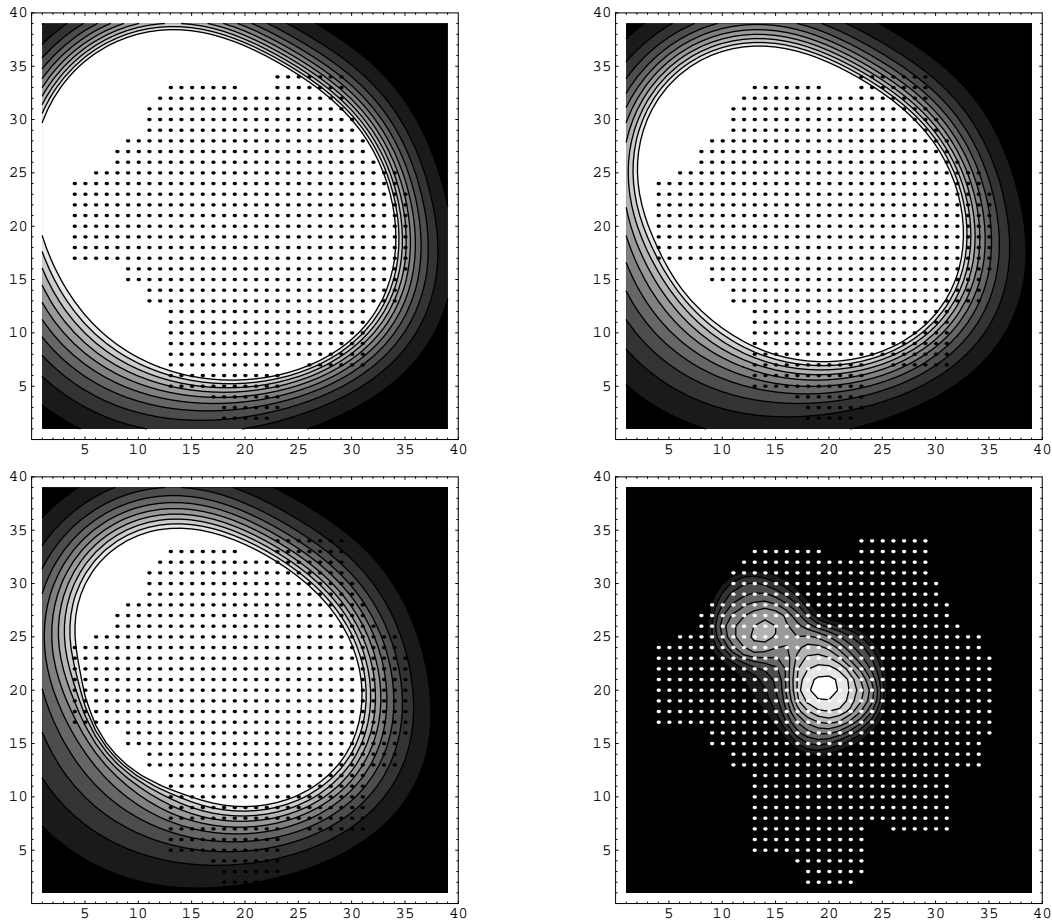
Figure 4. A single cross-sectional slice of a tumor (represented by dots). Top-left: 30% cut-off. Top-right: 50% cut-off. Bottom-left: 80% cut-off. Bottom-right: Shows only hot spots.

on it (**Figure 4**). Multiple slices make it possible to see a three-dimensional isosurface profile of the tumor. The white areas in the images of **Figure 4**, from top-left clockwise, are the regions of the tumor that receive a radiation dosage above 30, 50, 80%, and the region of potential overdosing, i.e., a region with an intensity higher than 2.5 times that of a single shot, referred to as a *hotspot*.

Applying the Algorithm

We are allowed a maximum of 15 spheres. In all of our simulations, it was possible to place 15 spheres inside the tumors, since they were of relatively high volume compared to a sphere, especially to a sphere of radius 2 mm.

From each of our three tumor-growth models, we produced 30 tumor images, 10 each of sizes 10,000 mm^3, 20,000 mm^3, and 36,000 mm^3. We then tested each of the three algorithms against all 90 tumors.

We performed two operations:

• We used the spherical dose pattern to create a scalar field of radiation expo-

sure values throughout the $100 \times 100 \times 100$ brain space. We then used this field to calculate the exposures of every cell within the modeled brain and tumor and to decide which cells survived the treatment. Using a 30% contour as our cutoff for death and survival, and further calculating the percentage exposures to other isodose cutoff values, we obtained exposure percentages for various tumor shapes and sphere-placement algorithms (**Table 2**).

Table 2. Percentage of tumor receiving 30/40/50% of shot intensity. Best results for a tumor shape and size are shown in bold.

Shape	Size (mm^3)		
	10,000	20,000	36,000
a. Hasty algorithm.			
Uniform	96/86/71	96/86/68	96/86/68
Varied	95/82/70	**96/89/70**	76/69/54
Amok	**94/87/70**	**91/82/63**	78/66/49
b. Careful algorithm.			
Uniform	96/85/69	**98/91/70**	**99/92/73**
Varied	**99/96/84**	92/82/69	**92/86/72**
Amok	94/85/64	88/79/62	**79/66/50**
c. Wiggling algorithm.			
Uniform	**99/95/82**	91/83/69	88/81/67
Varied	**99/96/84**	92/82/69	**92/86/72**
Amok	91/85/72	79/71/56	76/65/51

- We took the spherical profiles generated by the placement algorithms and estimated the radiation exposure values to all of the brain space for each generation of spherical dose pattern created by the algorithm. When the total dosage of the tumor reached a specified value, in this case 30%, the spherical dose profile of that generation was recorded. Thus, the total number of shots delivered to the patient is minimized while maintaining effective coverage of the tumor. Reducing this data gives **Table 3**. A dash means that the algorithm could not fill 90% of the volume with 15 spheres.

Evaluation of Methods and Conclusions

Difficulties Reaching 90% Coverage

Even for simple volumes, it can be impossible to cover 90% of a tumor with shots. To see this, consider a sphere of 10 mm radius. We may shell this with a

Table 3. Approximate number of shots needed to kill 90% of the tumor.
Best results for a shape and size of tumor are shown in bold.

	Volume (mm^3)		
Shape	10,000	20,000	36,000

a. Hasty algorithm.

Uniform	8	15	7
Varied	15	**10**	9
Amok	**10**	–	–

b. Careful algorithm.

Uniform	**7**	12	7
Varied	–	12	9
Amok	**10**	–	–

c. Wiggling algorithm.

Uniform	10	**10**	15
Varied	9	11	15
Amok	15	–	–

9-mm sphere, which would leave no room even for a 2-mm sphere and would still cover less than 3/4 of the volume.

Simply put, the only way our algorithms can destroy 90% of the tumors is by allowing hotspots in the tumor.

Square Lattices vs. Euclidean Distance

Even worse, no instance of our algorithm can see that it is possible to put a 9-mm shot in the 10-mm sphere. This is because the depth evaluation algorithm assigns depths to the tumorous voxels that do not entirely correspond to the physical distance between the voxels and the tumor edge. In **Figure 5** (at left), when voxels happen to differ via the coordinate axes, then the depth differential coincides with the distance between the voxels. However, in every other case the depth does not quite accurately measure distance. For example, two voxels that are diagonally adjacent differ in depth by 1, whereas the Euclidean distance between the centers of the two voxels is $\sqrt{3}$.

In many situations, the shelling method gives centers a depth that is not an accurate representation of their position inside the tumor. For example, in **Figure 5** (at right), the highlighted voxel has depth 3; so if we choose that voxel as the center of our circle, then we would place a circle of radius 3 at that point to cover the tumor. But it is clearly possible to squeeze a circle of radius 4 into the tumor. The problem is exaggerated further in three dimensions.

Our Wiggling algorithm was developed as an attempt to find a partial so-
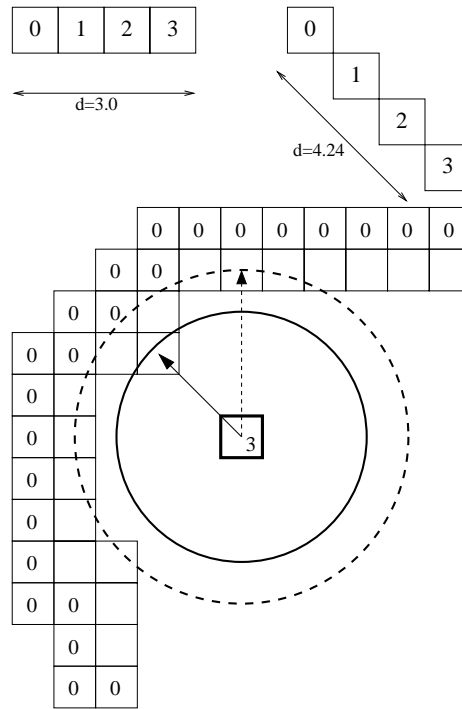
Figure 6. Left: Metric inconsistencies. Right: A schematic highlighting a weakness of our depth model.

lution to this problem. By allowing the spheres to move toward the edge of the tumor, we hoped to pack the spheres as tightly as possible.

Conclusion/Recommendation

For small or medium-sized tumors, the Careful algorithm is comparable to the Hasty Algorithm; the Hasty algorithm is preferable on time considerations.

All of the algorithms, but especially the Wiggling algorithm, have difficulty handling very large tumors, ones so large compared to the sphere sizes that it is unlikely that any combination of spheres could fill the volume of the tumor to the degree required by the problem statement.

However, for reasonably-sized tumors, the Wiggling algorithm is quite effective and works especially well toward filling in the varied-pressure tumors. This is because they bulge around the pressure points, forming pockets that are ideal for nesting spheres. When the spheres wiggle, they are more likely to settle into these regions and thus pack tightly. Furthermore, the Wiggling method runs much faster, especially compared to the Careful algorithm.

In fact, the Wiggling algorithm does such a good job of packing spheres that if we do not constrain the total number of spheres used, it tends to pack a very many, resulting in a large dosage. Furthermore, since the spheres are packed to the edge, the radiation spills out of the tumor into the surrounding normal tissue. So, while the Wiggling algorithm is a very good method of sphere-packing, it is not good for treatment planning.

To summarize:

- None of these algorithms should be used for very large tumors, which should be treated in multiple sessions.

- For moderate-sized tumors, the Hasty algorithm should be used in preference to the Careful algorithm.

- The Wiggling method is speedy and effective but does not translate well into an effective and safe treatment plan. However, we recommend it for tumors similar in shape to varied-pressure tumors, because it produces optimal plans for those.

References

Ferris, Michael C., and David M. Shepard. 2000. Optimization of gamma knife radiosurgery. In *Discrete Mathematical Problems with Medical Applications*, vol. 55 of DIMACS Series in Discrete Mathematics and Theoretical Computer Science, edited by D.-Z. Du, P. Pardolas, and J. Wang, 27–44. Providence, RI: American Mathematical Society. `ftp://ftp.cs.wisc.edu/pub/dmi/tech-reports/00-01.pdf` .

Kansal A.R., S. Torquato, G.R. Harsh, E.A. Chiocca, and T.S. Deisboeck. 2000. Simulated brain tumor growth dynamics using a three-dimensional cellular automaton. *Journal of Theoretical Biology* 203 (4): 367–382

McKernan, R.O., and G.D. Wilde. 1980. Mathematical models of glioma growth. In *Brain Tumors*, edited by D.G.T. Thomas and D.I. Graham. London, UK: Butterworth & Co.

Newman, William I., and Jorge A. Lazareff. 2002. A mathematical model for self-limiting brain tumors. `http://www2.ess.ucla.edu/~newman/LGA.pdf` .

Wagner, Thomas H., et al. 2000. A geometrically based method for automated radiosurgery planning. *International Journal of Radiation, Oncology, Biology, Physics* 48 (5): 1599–1611.

Wang, Jie. 1999. Packing of unequal spheres and automated radiosurgical treatment planning. *Journal of Combinatorial Optimization* 3: 453–463.

Wu, Q. Jackie. 2000. Sphere packing using morphological analysis. In *Discrete Mathematical Problems with Medical Applications*, vol. 55 of DIMACS Series in Discrete Mathematics and Theoretical Computer Science, edited by D.-Z. Du, P. Pardolas, and J. Wang, 27–45. Providence, RI: American Mathematical Society.

Shoot to Kill!

Sarah Grove
Chris Jones
Joel Lepak
Youngstown State University
Youngstown, OH

Advisor: Angela Spalsbury

Abstract

The goal of the model is to approximate a target volume by spherical doses (or shots) of radiation. The model that we provide satisfies several important constraints.

- The algorithm guarantees that no shot overlaps another; thus "hot spots" are eliminated.

- Each shot must also lie entirely within the target volume (to prevent harm to healthy tissue).

- The final shot arrangement is optimal in the sense that it is impossible to place an additional shot of any size without causing an overlap or breach of the target volume.

The algorithm's strength lies in deciding the best possible location for the placement of the initial shot. The remaining volume of the target area is filled by placing shots tangent to previous shots. The shots are placed in a way that guarantees as many large shots as possible are used before resorting to smaller shots, thereby minimizing the total number of doses. Our model's simplicity easily allows for adaptation when its features need to be modified to enhance its accuracy. The algorithm also is very efficient—even for an exceptionally large tumor, our program is bounded by just several million iterations, making it easily computable with any modern hardware.

We include a working computer program based on our algorithm. The software takes into account the need to protect healthy tissue while treating abnormal tissue. Our program uses digital images similar to those from MRI scans to define accurately the boundary around the target volume. This boundary then serves to prevent the normal tissues from receiving harmful levels of radiation.

We constructed data sets (sample tumors) to test our program. The performance of our algorithm on these data sets provides great confidence in its feasibility and practical effectiveness. In each case, every shot lies within the target volume without overlapping with another shot. The volume coverage had a high degree of success in each case, ranging between 86% and 91%.

In summary, our model safely allows for strategic gamma knife planning. The algorithm approaches the final shot arrangement from a geometrical perspective. It provides an efficient and effective way of planning the treatment and guarantees that several important criteria are satisfied.

Analysis of the Problem

Our task is to approximate the shape of a target volume (the brain tumor) by spherical doses (shots) of radiation. Several conditions are desirable for this approximation:

- Prohibit shots from protruding outside the target in order to avoid harm to healthy areas of the brain.

- Prohibit shots from overlapping (to avoid hot spots).

- Cover the target volume with effective dosage as much as possible, with at least 90% of the target volume covered.

- Use as few shots as possible. This is to help reduce the total amount of radiation passing through the healthy portion of the brain.

Additionally, the algorithm should be efficient enough to avoid unreasonable waiting times.

We can view the problem of formulating the treatment plan in mathematical terms. The object then is to place the least number of shots in the target volume while filling at least 90% of the volume. From a theoretical perspective, this is a sphere-packing problem; that is, to fill as much of a volume as possible with spheres.

Unfortunately, the problem of packing unequal spheres into a given volume is NP-complete [Wang 1999], making an absolute optimal solution intractable for all but the smallest target volumes. Hence, we find not an optimal solution but a solution that satisfies all the requirements while remaining of reasonable complexity.

Assumptions

- The diagnostic images are acquired from MRI scans; we assume that the resolution is 1 mm $\times$ 1 mm$\times$ 1 mm. (The actual resolution is approximately 1 mm $\times$ 1 mm $\times$ 1.5 mm [Leventon 1998].) We assume that the image can be represented as a three-dimensional array of points such that the set of points in the tumor and the set of healthy points can easily be determined.

- The mean diameters of brain tumors range from 1 mm to 40 mm [New Jersey ... n.d.]. We assume that no tumors larger than 100 mm$\times$100 mm$\times$100 mm need to be considered. At the assumed resolution of 1 mm $\times$ 1 mm $\times$ 1 mm, this gives 10^6 data points, a reasonably small amount of data.

- Each shot volume contains 100% of its potency with no leakage to outside points.

- All shots have uniform radiation density.

The Algorithm

Overall Description

The basic idea is to construct each successive sphere based on the location of previous spheres. For this reason, the choice of the initial shot or shots is very important.

The first shot placed is the largest possible shot that fits inside the target volume. Heuristics and curvature measurements of the target volume can be used to determine the exact location of this shot. For example, the first sphere could be placed tangent to the surface of the target volume in a location in which the curvature of the volume and the sphere are in close correspondence. In general, the first sphere should be placed tangent to the surface of the target volume.

The algorithm then calculates the position of the next shot by determining the location of the largest possible shot tangent to the first one. This is repeated, placing new shots tangent to the first until no more shots of any radius can be placed.

To determine if a shot of given radius and position is possible, it suffices to check each point on the surface of the proposed shot to make sure that it is fully contained in the tumor and intersects no previously placed shot.

After the volume tangent to the first sphere is full, the program begins checking points tangent to the sphere placed second. The largest possible sphere tangent to the second sphere is then placed; this is again repeated until no more spheres can be placed.

This process is continued with each sphere until no more can be placed inside the target volume. The output is a list of the centers and radii of the shots.

Definitions

We are given digital images from the MRI scans, which are converted to three-dimensional arrays of data.

Let the data set D be defined as

$$D = \{p = (x, y, z) \mid x \in \{1, 2, \ldots, N_x\}, y \in \{1, 2, \ldots, N_y\}, z \in \{1, 2, \ldots, N_z\}\},$$

where N_x, N_y, and N_z are the resolution (in pixels) of x, y, and z, respectively.

We define a function $\delta : D \rightarrow \{0, 1\}$ by

$$\delta(p) = \begin{cases} 1, & \text{if point } p \text{ is part of the tumor;} \\ 0, & \text{otherwise.} \end{cases}$$

Hence, T is the set of points in the tumor denoted by

$$T = \{p \in D \,|\, \delta(p) = 1\}.$$

We say that a point $p = (x, y, z)$ borders $p' = (x', y', z')$ if

$$(x, y, z) = (x' + \Delta_1, y' + \Delta_2, z' + \Delta_3),$$

where $\Delta_i \in \{0, 1, -1\}$ for $i = 1, 2, 3$. It is also useful to determine the set of points on the surface of the tumor. We let this set of boundary points B be defined as

$$B = \{p \in D \,|\, \delta(p) = 1 \quad \text{and} \quad \exists p' \in D \text{ such that } \delta(p') = 0 \text{ and } p \text{ borders } p'\}.$$

We represent each shot by a set of points on a sphere. Let $S_{p,r}$ denote the surface of a sphere of radius r centered at p, i.e.

$$S_{p,r} = \{p' \,|\, \lfloor \Delta(p', p) \rfloor = r\},$$

where $\Delta(p', p)$ is simply the distance between the two points and $\lfloor \cdot \rfloor$ is the floor function.

There is only a finite set R of possible radii of shots, corresponding to the set of collimator sizes. In this case,

$$R = \{9, 7, 4, 2\}.$$

Formal Specification of Algorithm

Input: The set D of data points and the function δ used to determine the target volume. From this, the set of target volume points T is determined, as well as the set of surface points B.

Output: The center and radius of each shot placed by the algorithm.

Notation:

C_i , for $i = 0, 1, 2, \ldots$, is the set representing the ith shot: $C_i = S_{p_i, r_i}$ for some point p_i and radius r_i;

n is the the number of shots placed; and i.e., $n = \max\{i \,|\, C_i \text{ is defined}\}$.

c is the index of the sphere to which new spheres will be placed tangent.

Algorithm:

1. Choose $C_0 = S_{p,r}$ such that $r \in R$ is the maximum possible and $C_0 \subseteq T$. (Details in next subsection.)

2. Let $c = 0$.

3. While $c < n$ do the following:

   (a) for every $r \in R$ (from largest to smallest) do the following:

       i. Let r' and p' be the radius and center of sphere C_c, i.e. $C_c = S_{p',r'}$.

       ii. Construct as many possible spheres $C_k = S_{p,r}$, where $r \in R$, $p \in S_{p',(r+r')}$, such that $C_k \subseteq T$ and $C_k \cap C_i = \emptyset$ for all $i \neq k$. (See details later.)

   (b) Let $c = c + 1$.

Placement of Initial Shot

Near the surface of the target volume is the most difficult area to encompass by doses of the gamma knife—hence, the first shot should be arranged to conform as closely as possible to the contour of the tumor. **Figure 1** gives an example of matching the contour.
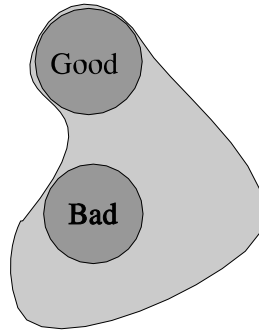
Figure 1. Placement of a good initial shot.

Measuring the curvature of the target volume is straightforward and could be used to fit the initial shot to an ideal position. Alternatively, the doctors could choose the initial position interactively based on their judgment.

A further alternative is the placement of multiple initial shots if the need arises. This could occur if the shape of the target is such that there is an obvious optimal configuration.

One additional method is the use of many runs of the algorithm with a random initial placement. The algorithm requires very little computation time, even with a large tumor size. Many runs could be made, after which the best configuration is selected. This method is also easily parallelized, allowing for a very large number of trials.

Placement of Tangent Shots

The placement of each shot following the initial sphere continues in a similar manner. The volume should be placed in contact with as many tangent points as possible in order to minimize lost volume. More specifically, choose the new $C_k = S_{p,r}$ to maximize the number of tangent points

$$t = \left| \left\{ q \in \bigcup_{i=1}^{n} C_i \bigcup B \mid q \text{ borders some element } q' \in C_k \right\} \right|.$$

Other methods may be employed, including random placement and multiple runs (similar to those mentioned above). The number of shots placed is proportional to the size of the tumor.

Analysis of Model

Worst Case Analysis

We establish a bound on the total number of points that must be checked by our algorithm. We assume a resolution of 1 mm $\times$ 1 mm $\times$ 1 mm.

For each shot S_{p_2,r_2} placed tangent to S_{p_1,r_1}, at most all of the points on the sphere $S_{p_2,(r_1+r_2)}$ must be examined. To confirm placement of the sphere S_{p_2,r_2}, each point on its surface must be checked for penetration of the boundary or intersection with other shots. We can estimate the number of points on the surface of a digitally represented sphere by its area (in mm^2). If all possible radii must be checked when placing the new sphere, then the placement requires

$$P_2 \leq \sum_{i=1}^{|R|} A(S_{p_2,r_i}) A(S_{p_2,(r_1+r_i)})$$

examinations of points, where $A(S)$ is the area of sphere S in mm^2 (rounded up to nearest integer), and $|R|$ is the number of possible radii.

We are given that the target volume is usually filled by fewer than 15 shots. Hence, we assume that 30 shots is a reasonable bound. Since 9 mm is the maximum radius and $|R| = 4$, the total number of checks necessary after placement of the initial sphere is

$$P \leq 30 P_2 \leq 30 \left(4 A(S_{p_2,9}) A(S_{p_2,(9+9)}) \right) = 30(4)(4\pi)(9^2 18^2) < 4 \times 10^7.$$

The number of checks required to place the initial sphere is assumed to be negligible, as it is bounded by the resolution of the digital image. The 4×10^7 data point examinations is also trivial for modern computers. Hence, our algorithm, even in the worst case, requires minimal computing time.

Other Strengths

- By design, this model conforms to the constraints of gamma knife treatments. That is, the model prohibits shots from protruding outside the target volume, while avoiding overlapping shots within the target volume. By placing as many shots of large radii as possible before placing smaller shots, the algorithm guarantees a minimal number of shots. In a sample implementation, our algorithm shows a coverage of nearly 90%.

- The main strength of our model is its simplicity and realistic application.

- In the model, the tumor image is transformed to a set of points, where each point represents a pixel from the MRI image. We address the boundary set to position our initial shot. The algorithm places each successive shot along contours of the target volume.

- In the final shot arrangement determined by the algorithm, overlapping shots are prohibited.

- While the shot configuration is not guaranteed to be optimal, the configuration is optimal in the sense that no shots can be added to the final configuration without overlap.

- While we assumed 0% shot gradient, our model's design addresses this issue by allowing for different shot gradients to be added easily. In short, the model can be adjusted continuously for different shot gradients at each iteration.

Limitations

- The final shot arrangement is not guaranteed to be absolutely optimal.

- A nonuniform dosage within each shot is not accounted for; however, if information is known, our program should be adapted accordingly.

- The algorithm considers only the local configuration of shots rather than the entire volume of the tumor. However, by examining only the volume tangent to a given sphere, the complexity is reduced dramatically. In practice, this limitation should affect only exceptional target volume shapes.

A Sample 2D Implementation

We create a working implementation of our algorithm in two dimensions to test its effectiveness.

The input is shown on the left in **Figure 2** as a black-and-white image describing the shape of the target volume. This image can be thought of as a

two-dimensional analog of an MRI image and is assumed to have approximately the same resolution (1 mm × 1 mm). The output of the algorithm is shown on the right in **Figure 2**, with each circle representing a shot. (Any visible overlapping of shots is only a result of roundoff error in scaling the image.)
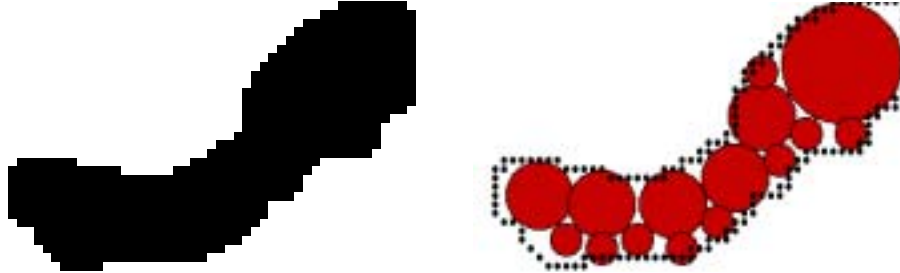
Figure 2. Sample target area and placement of 15 shots.

For a different sample area, **Figure 3** illustrates the order in which our algorithm places the shots.

The shot placement algorithm is implemented as stated but no optimizations are made in the selection process. That is, the shots are chosen by searching systematically for a satisfactory point. Nevertheless, the outcomes are successful. Over 21 samples, the minimum volume percentage achieved was 87%, the mean was 89%, and the maximum was 91%.

Although the example is only for two dimensions, the procedure is essentially the same for three—in fact, in actual implementation only the array used to represent the tumor and the definition of a sphere need to be changed.

Conclusion

The gamma knife procedure is a highly tested and extremely effective treatment for a variety of brain abnormalities. Our model works to improve the placement of the shots; we believe that with the inclusion of our model, the treatment's efficiency will increase greatly.
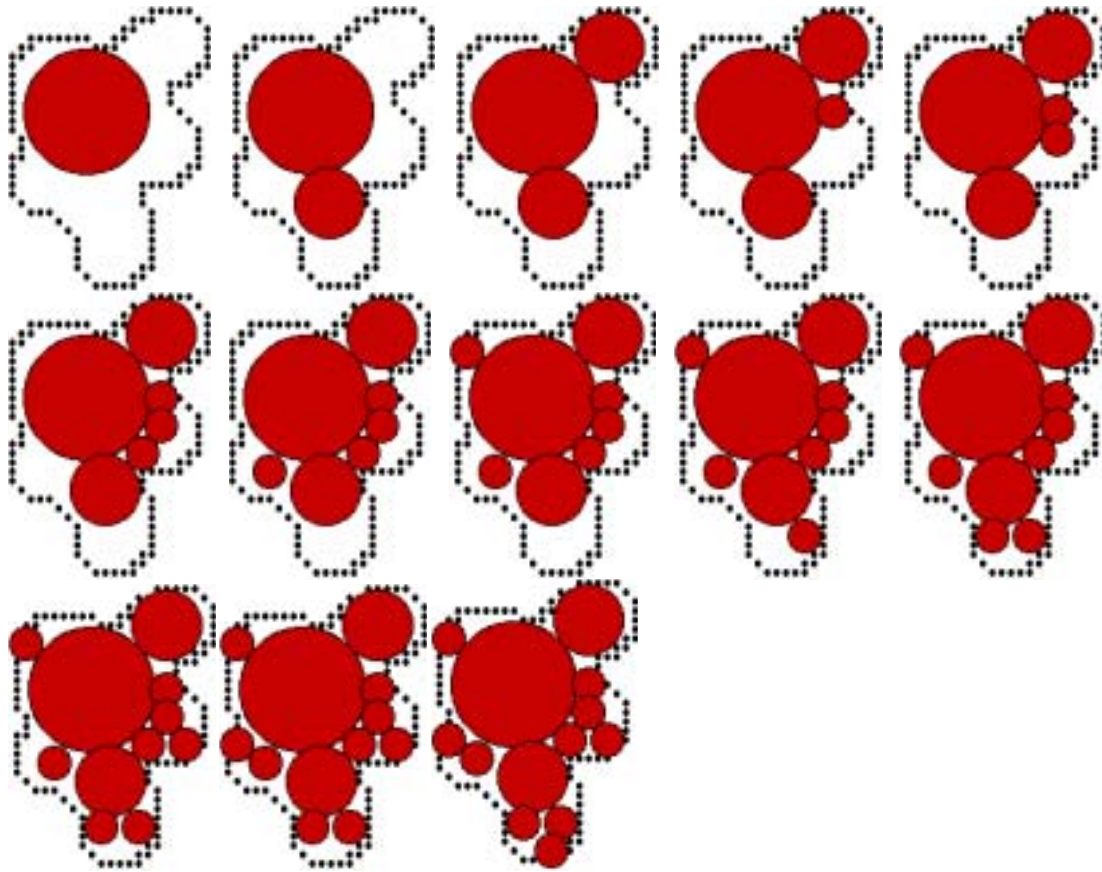
Figure 3. Sample shot sequence (13 shots).

References

Leventon, Michael E. 1998. Operating room results. `http://www.ai.mit.edu/people/leventon/Research/9810-MICCAI-Surgery/node9.html`. In Clinical experience with a high precision image-guided neurosurgery system, by E. Grimson, M. Leventon, et al. `http://www.ai.mit.edu/people/leventon/Research/9810-MICCAI-Surgery/final.html` .

New Jersey Chapter Acoustic Neuroma Association. n.d. Recent outcomes for gamma knife and FSR. `http://hometown.aol.com/ananj2/outcomes.html` .

Sutter Gamma Knife Radiosurgery Center. n.d. Frequently asked questions `http://www.suttergammaknife.com` .

Wang, Jie. 1999. Packing of unequal spheres and automated radiosurgical treatment planning. *Journal of Combinatorial Optimization* 3: 453–463.

Receiving the MAA Award at MathFest 2003 in Boulder, Colorado: Team advisor Angela Spalsbury with the team members, who are all now graduate students: Sarah Grove (applied mathematics, North Carolina State). Joel Lepak (mathematics, Michigan), Chris Jones (mathematics, Pittsburgh). (Photo courtesy of J. Douglas Faires.).